LABORATORY DESIGN-STUDIES OF THE EFFECT OF WAVES ON A PROPOSED ISLAND SITE FOR A COMBINED NUCLEAR POWER AND DESALTING PLANT

by

Vito A. Vanoni and Fredric Raichlen

W. M. Keck Laboratory of Hydraulics and Water Resources
Division of Engineering and Applied Science
CALIFORNIA INSTITUTE OF TECHNOLOGY
Pasadena, California

Report No. KH-R-14

July 1966

LABORATORY DESIGN-STUDIES OF THE EFFECT OF WAVES ON A PROPOSED ISLAND SITE FOR A COMBINED NUCLEAR POWER AND DESALTING PLANT

Final Report on a study for the Bechtel Corporation of the island site for a combined nuclear power and water desalting plant for the Metropolitan Water District of Southern California

Report by: Vito A. Vanoni and Fredric Raichlen,
Principal Investigators

W. M. Keck Laboratory of Hydraulics and Water Resources
Division of Engineering and Applied Science
CALIFORNIA INSTITUTE OF TECHNOLOGY
Pasadena, California

Report No. KH-R-14

July 1966

TABLE OF CONTENTS

LIST OF FIGURES

LIST OF TABLES

ABSTRACT

There were four major objectives to this investigation: 1) the determination of the degree of stability of the island face when constructed of armor units of various weights; 2) the run-up for a two-dimensional wave system impinging on the island face; 3) the run-up envelope on the four sides of the island in a three-dimensional model; and 4) the wave patterns caused by the effect of the island on its wave environment. Models having three different length scales were tested in the wave tank (1:50, 1:45, and 1:40) and these models are referred to as the two-dimensional models. One model was tested in the wave basin at an undistorted scale of 1:150 and it is referred to in this report as the three-dimensional model.

The first two-dimensional model was built to a scale of 1:50 and essentially corresponded to the original design proposed by Omar Lillevang, Consulting Engineer to the Bechtel Corporation. The prototype tribar weight, equivalent to the model tribar used, was 18.9 tons. This structure was stable; however, it was overtopped by waves. With an increase in the crest elevation from +30 ft. to +40 ft. some overtopping was still experienced.

The second model was built at an increased scale, 1:40. At the same time the composite slope which existed in the original design was changed so that the island face had a continuous slope of 3 horizontal to 1 vertical with the crest of the defense at elevation +40 ft. This particular model scale was chosen so that, according to the literature, the tribars would be at a condition of incipient failure for high waves. Since the same armor units were used in this model as were used in the 1:50 scale model, the increase in model scale reduced the equivalent weight of the tribars to 9.7 tons and the maximum weight of the armor rock "B" from 10 tons to 5.1 tons. The prototype structure which corresponds to this model was found to be unstable, as expected. It was observed in testing that a critical feature of the construction which contributes to the stability of the structure is the degree to which the cap-rock section is interlocked with the tribar section. The modification

made to the slope of the island face and the increased crest elevation eliminated the problem of overtopping, and the maximum run-up for a 14-sec. wave was to elevation +38 ft.

Since the model having a 1:40 length scale was unstable and that with a scale of 1:50 was stable, a third model was constructed with a model scale between these two values, a scale of 1:45. The equivalent prototype tribar weight and the maximum weight of the "B" rock for this third model, still using the same model armor units, were increased to 13.8 tons and 7.3 tons respectively by this change. The slope of the wave defense and the crest elevation were the same for this structure as they were in the 1:40 scale model, i.e., a continuous slope of the island face of 3 horizontal to 1 vertical and a crest elevation of +40 ft. This model was satisfactory both with respect to stability and to run-up. Run-up measurements were made for waves of various heights at wave periods of 16 sec., 14 sec., and 12 sec. The maximum run-up was to elevations +39 ft., +35 ft., and +31 ft. respectively for these three wave periods.

The three-dimensional model of the ocean bottom and the island was built to an undistorted scale of 1:150 with the island constructed the same as the 1:45 scale two-dimensional model. In these tests in the large wave basin the wave direction was varied as well as the wave period and wave height. The run-up envelopes obtained showed that, for comparable wave heights, the worst condition of run-up was for normally incident waves impinging on the seaward face of the island. The run-up measured for the normally incident direction was usually approximately 10% less than the run-up in the two-dimensional model for the same wave periods and wave heights. For the case of oblique wave incidence the maximum run-up was at the island corner first attacked by the wave with the run-up decreasing with distance from this corner, and this run-up was comparable to the maximum run-up experienced at normal wave incidence. However, the maximum average run-up for the oblique case was significantly less than that experienced in the case of normal wave incidence. The run-up on the shoreward face of the island for all wave directions was of the order of 1/10th of that experienced on the seaward face.

Detailed observations of the wave pattern in the lee of the island indicated that there were regions near the beach where the currents were in a direction opposite to the observed general current. From overhead photographs it was found that generally this occurred in regions where the waves which diffract around the sides of the island intersect. Measurements were made of the maximum elevation of the water surface in the region of the causeway for the case of oblique wave incidence.

CHAPTER ONE

INTRODUCTION

A. WORK AUTHORIZATION AND WORKING ARRANGEMENTS

The work covered by this report was authorized by the Bechtel Corporation Purchase Order No. 5272LA-1 dated January 14, 1966. The work to be performed is as outlined in the proposal of the California Institute of Technology (Caltech) dated December 10, 1965, with modifications outlined in a letter from the Bechtel Corporation dated January 10, 1966 and signed by William H. Wilson, Assistant Project Manager. The actual laboratory studies were carried out according to arrangements outlined in the Caltech proposal. This called for the Bechtel Corporation to furnish personnel for making the necessary modifications to equipment at the laboratory, building models and actually performing the experiments and analyzing the data. Everett Spector was the Project Test Engineer for the Bechtel Corporation during this investigation. Caltech furnished part-time services of the staff of the W. M. Keck Laboratory of Hydraulics and Water Resources and the technical supervision of the studies. The technical supervision was the responsibility of Vito A. Vanoni, Professor of Hydraulics, and Fredric Raichlen, Assistant Professor of Civil Engineering, who are the authors of the present report.

B. THE PROBLEM

The problem to be studied is outlined in the Caltech proposal as modified by Bechtel Corporation letter of January 10, 1966. The Bechtel Corporation was retained by the Metropolitan Water District of Southern California (MWD) to study the feasibility of a combined nuclear power and desalting plant to be located on an artificial island near the sea shore. The proposed island is about 1500 ft. long parallel to the coast and 1200 ft. wide. It is to be located near Bolsa Chica State Beach and its leeward face is about 2800 ft. off-shore about three miles north of the city of Huntington Beach. The

studies covered by this report are concerned with the effect of the wave environment on the island and the effect of the island on the wave patterns in the lee of the island. The detailed objectives of the study are as follows:

1. Determination of the degree of stability of the protection works proposed by the Bechtel Corporation for the exposed faces of the island and the investigation of the alternate designs with a view to improving the efficiency of the protective works.

2. Investigation of wave run-up on the exposed face of the island with a view to ascertaining the effectiveness of the proposed construction against overtopping or if necessary developing a design which will avoid overtopping.

3. Determine run-up envelopes on the four sides of the island for the design wave conditions.

4. Observe and record wave patterns around the island and between the island and the beach for several wave directions. This information will be required for appraisal of bottom disturbances around the island, of the influence of the island on sand movement or deposition at the shoreline, and of wave conditions at the shore-to-island causeway.

C. LABORATORY PROGRAM

The studies reported herein were carried out mainly at the Azusa Hydraulics and Coastal Engineering Laboratory of Caltech. Some preliminary studies needed to guide the work of the large facilities at the Azusa Laboratory were carried out in the W. M. Keck Laboratory of Hydraulics and Water Resources on the main campus in Pasadena. The studies at the Azusa Laboratory were carried out in two parts. The first part was conducted in a wave tank and covered the investigation of the stability of the island face under normally incident wave attack and the run-up of such waves. This part of the study is referred

to as the two-dimensional study. In this portion of the investigation modifications to the original design evolved from considerations of the experimental results and discussions among personnel of the Bechtel Corporation, Omar Lillevang, Consulting Engineer, and the Principal Investigators. The second part of the study involved a three-dimensional model in which the direction, height and period of the waves could be varied and is referred to as the three-dimensional study. In this series of experiments run-up on the island face was determined along with wave patterns in the lee of the island and on the beach near it.

Work on the modification of the laboratory facilities for conducting the tests started about January 10, 1966. Experiments in the wave tank on the first model of the island started about March 23, 1966, and the first experiments on the three-dimensional model were made about June 2, 1966. The experiments on both models were completed during the week of June 13, 1966.

CHAPTER TWO

EXPERIMENTAL EQUIPMENT AND PROCEDURES

A. TWO-DIMENSIONAL MODEL

1. Wave Tank and Wave Machine

The wave tank used in the two-dimensional model study is approximately 115 ft. long, 4 ft. wide, and 3 ft. deep. A schematic drawing of the tank is presented in Fig. 2.1. The tank walls are constructed of 20 gauge sheet metal and 10 gauge steelplate and are bolted to the concrete laboratory floor which forms the bottom of the wave tank. These side walls are braced at 5-ft. intervals by 2-in. x 2-in. x 1/4-in. angles connected to the top of the wall and to the floor. As shown in Fig. 2.1, a 10-ft. window of 5/8-in. plate glass extending the full height of the tank is located near the end of the wave tank where the model of the island face is installed.

The wave machine which is of the piston type is located approximately 12 ft. from the opposite end of the wave tank and is driven by a variable speed motor. The wave generator can be seen in the photograph, Fig. 2.2. The piston consists of a 1/4-in. aluminum plate which is bolted to a frame of welded structural aluminum shapes. This frame is supported on four linear ball bushings which slide on 1-1/2-in.-diameter hardened steel shafts which are located about 6 in. to either side of the tank walls. These shafts are supported on a steel frame which is independent of the wave tank structure. Both rails are adjusted so that they are in the same horizontal plane and parallel to the centerline of the wave tank.

The motor for the wave machine is a 1.5 hp electric motor with a variable speed belt drive with a speed range such that waves having periods ranging from 1.22 sec. to 7.35 sec. can be generated. The motor is also supported independently of the wave tank. This reduces the possibility of vibrations being transmitted from the motor to the wave tank and hence generating spurious disturbances on the water surface.

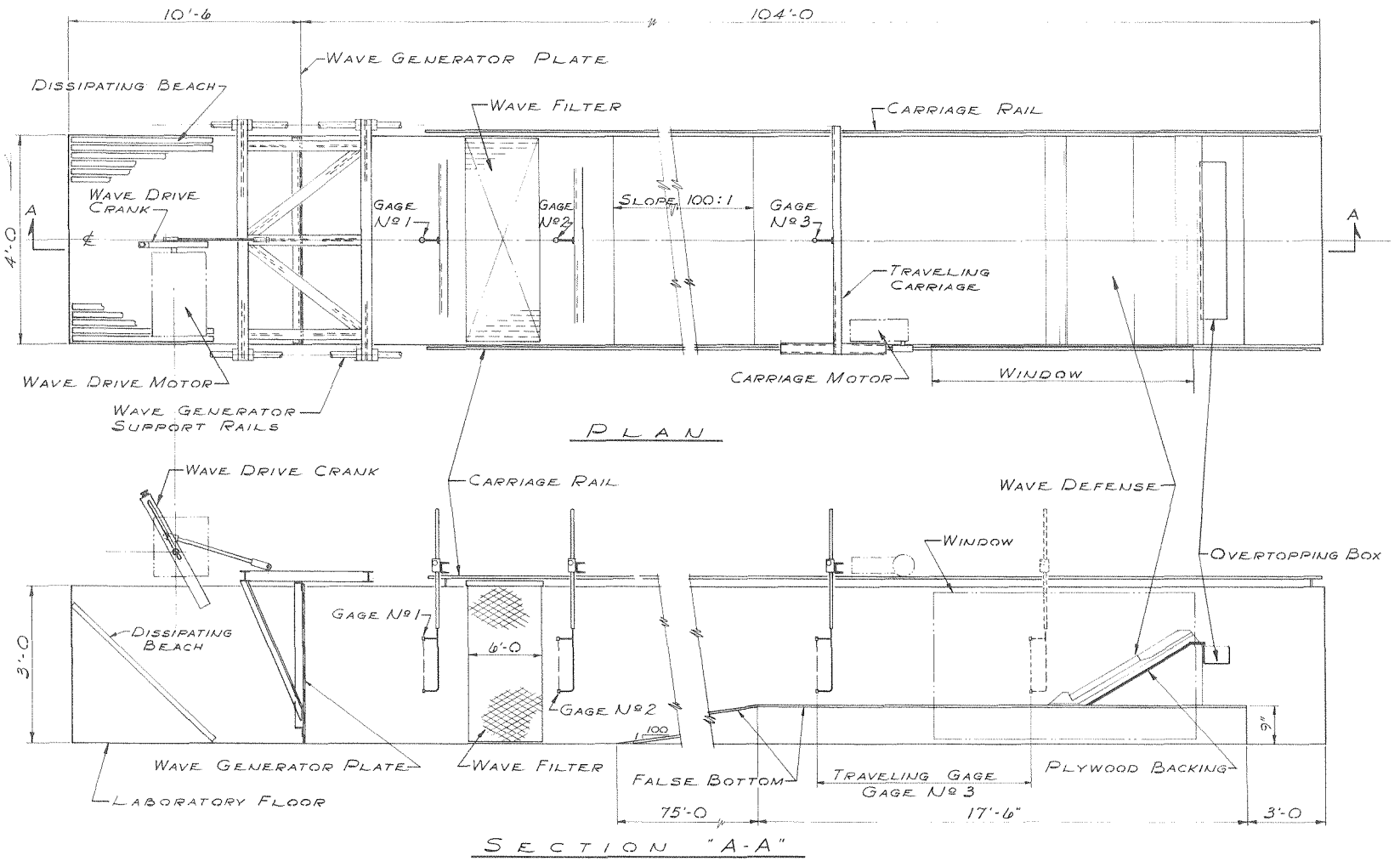

Figure 2.1 Schematic Drawing of Wave Tank

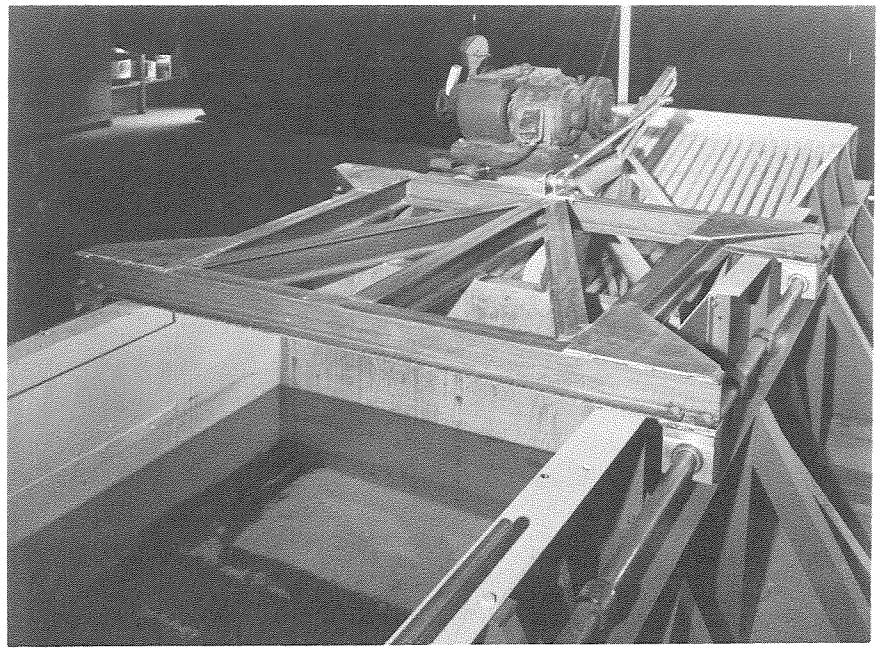

Figure 2.2 Wave Generator

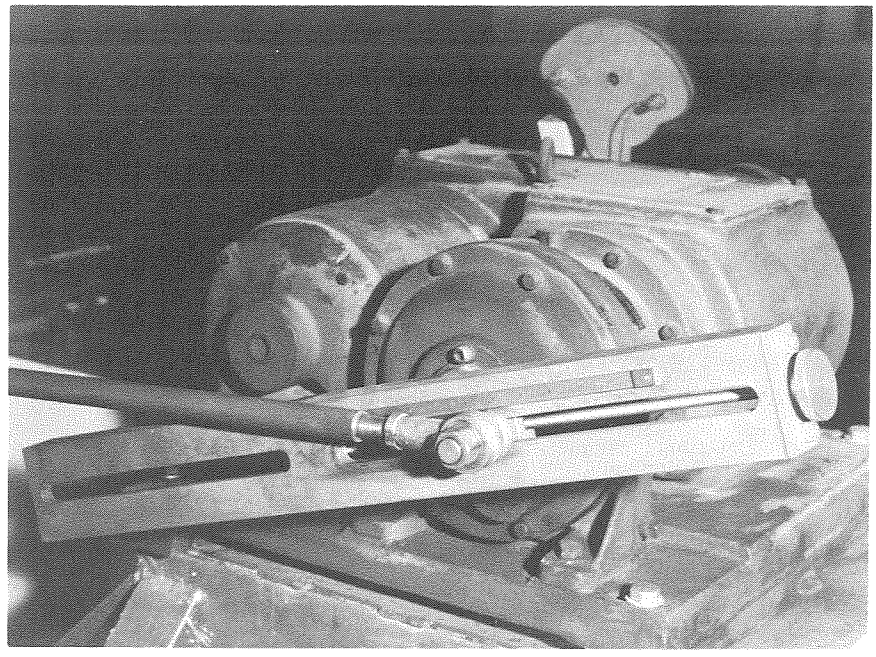

Figure 2.3 Drive Crank and Motor for Wave Generator

The drive crank attached to the motor is shown in Fig. 2.3. This crank allows the amplitude of the wave machine piston to be varied from zero to approximately 14 in., giving a total possible stroke of 28 in. The lead screw on the crank seen in Fig. 2.3 makes it possible to adjust the amplitude of the wave machine to within ±.025 in. by means of a scale attached to the crank. This fine adjustment is necessary because the ability to obtain the high waves which are of interest in this study depends strongly on making fine adjustments of the stroke of the wave machine.

An inclined beach, shown in Fig. 2.1, is located behind the wave machine to dissipate waves generated by the rear face of the piston. This beach has a slope of approximately 3 horizontal to 1 vertical and is constructed of 1-3/4 in. x 1-3/4 in. wooden strips spaced approximately 3/4 in. apart.

A wave filter is located in front of the wave machine to reduce the surface irregularities associated with waves produced by this type of generator. The filter, shown in Fig. 2.4, consists of 64 plates of expanded aluminum, 6 ft. long and 3 ft. wide. These plates are spaced approximately 3/4 in. apart and the planes of the plates are vertical and aligned in the direction of wave travel.

In order to produce the high design waves required in this study a sloping false bottom has been placed in the wave tank. The configuration of this bottom may be seen schematically in Fig. 2.1. The shape of the bottom required to produce the desired waves was determined from tests in a small wave tank at the W. M. Keck Laboratory of Hydraulics and Water Resources on the main campus of Caltech. In this small tank, the larger tank at the Azusa facility was modeled to a scale of 1:3. It was found that the design wave could best be produced by making the water depth at the model approximately one-half of that at the wave machine. Therefore, in the 115 ft. wave tank the false bottom consists of a horizontal portion approximately 17 ft. 5 in. long, in the vicinity of the model, and 9 in. above the concrete floor of the wave tank with a sloping section having a slope of 100 horizontal to 1 vertical extending 76 ft. upstream from this

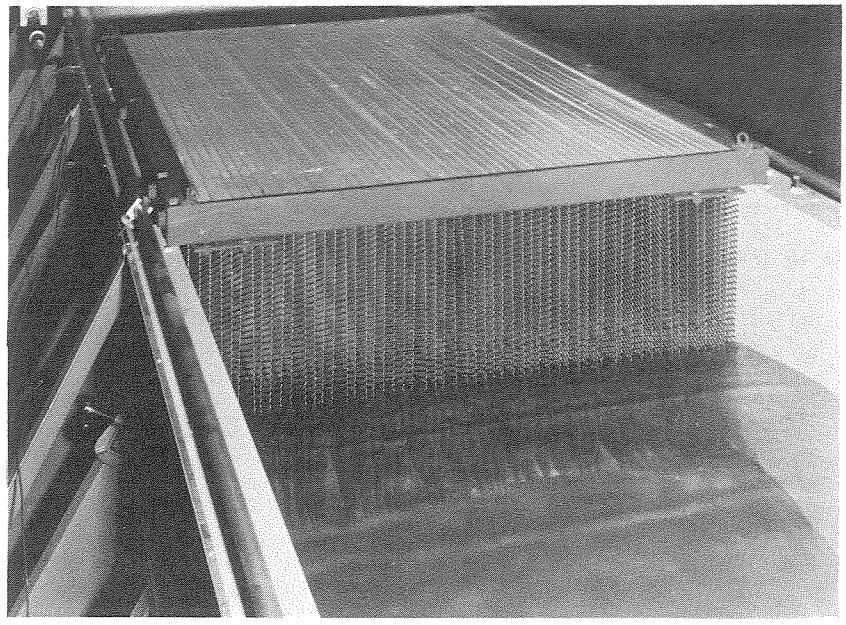

Figure 2.4 Wave Filter

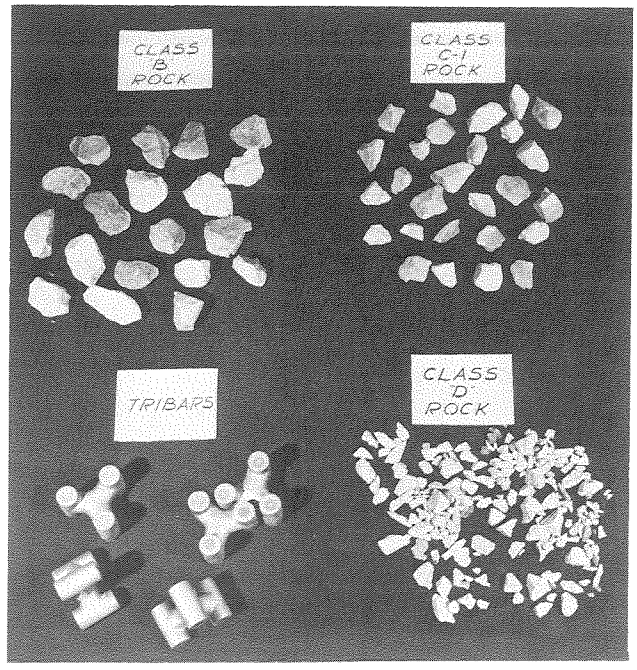

Figure 2.5 Armor Units

horizontal section and connected to the tank floor. This bottom has been constructed to tolerances of ±1/64 in. using 3/4-in. exterior plywood supported by a wooden substructure. The substructure consists of three stringers running parallel to the longitudinal axis of the flume braced laterally every 32 in. All plywood and lumber surfaces have been treated with an epoxy-based paint (Pittsburgh Aquapon) in order to water-proof the material.

Precision stainless steel rails 1 in. in diameter run along the top of the side walls of the tank. These rails can be seen in the schematic drawing, Fig. 2.1, and are attached to the flume by means of threaded studs located 30 in. apart. Using these studs both rails have been adjusted so that they are in a horizontal plane to within ± .001 ft. These rails then form the reference system for all measurements of elevation within the wave tank.

2. Model Construction

a. Wave Defense Material

The face of the island is to be armored with rock and concrete tribars (1)*. The upper surface from elevation -18 ft. with respect to mean lower low water (MLLW) to elevation +19 ft. is to be covered with one layer of tribars each individually placed. The seaward toe of the embankment and the face above elevation +18 ft. is to be armored with large rock designated as armor rock Class "B". The armor rock and the tribars are to rest on a layer of rock designated as cover rock "C-1" and the cover rock is over a layer of rock called dike rock Class "D". The rock used in this model, to represent the three kinds of rock and the model tribars are shown in the photograph, Fig. 2.5.

The specifications for the rock and tribars are given in Appendix B of a report of the Bechtel Corporation (2) to the Metropolitan Water District of Southern California and were prepared by Omar J. Lillevang, Consulting Engineer. These specifications called for tribars weighing 18 tons each and for "B" rock with individual pieces

---

* Numbers in parentheses refer to items in bibliography.

weighing between 4 and 10 tons with at least one half of the total weight of rocks to consist of pieces uniformly graded between weights of 8 and 10 tons. Specifications for "C-1" rock called for individual pieces to vary uniformly in weight, between 1 and 4 tons each. The dike rock "D" was specified as quarry run material varying in size from chips and spalls to pieces weighing 1 ton each with a reasonably uniform size distribution. The specification also required that all stone should have a specific weight of not less than 160 lbs per cu. ft. and that no stone shall have a maximum dimension that exceeds 2-1/2 times its minimum dimension.

The laws for scaling rock or other armor units which are subjected to wave forces are given by the following equations:

$$\frac{W_{r_m}}{W_{r_p}} = \frac{\gamma_{r_m}}{\gamma_{r_p}} = L_r^3 \tag{2.1}$$

$$\frac{\gamma_{r_m}}{\gamma_{r_p}} = \frac{\gamma_m}{\gamma_p} = \frac{62.4}{64.0} = 0.975 \tag{2.2}$$

$$L_r = \frac{L_m}{L_p} \tag{2.3}$$

In these equations the subscript "m" denotes model values and the subscript "p" denotes prototype values, W_r denotes the weight of the armor units, γ_r denotes the specific weight of the armor units, γ denotes the specific weight of the water and the quantity L_r is the length scale ratio, that is, the ratio of the model length L_m to the homologous prototype length L_p. Since in the model tests fresh water was used (γ_m = 62.4 lbs per cu. ft.) and since sea water exists in the prototype (γ_p = 64.0 lbs per cu. ft.) the ratio of the specific weights of the model armor units to that of the prototype units is fixed at $62.4 \div 64.0 = 0.975$.

The model rocks used to represent "B", "C-1" and "D" rock were made of a rock material with the appropriate specific weight. This material, which is used as ornaments in gardens, was obtained in large pieces and hand crushed to the required size. Specific weight determinations of 45 individual rocks used in the model to represent the "B" and "C-1" rock were made in the laboratory. The mean value of the specific weight obtained from these measurements was 158.6 lbs per cu. ft. with the smallest value being 154.1 lbs per cu. ft. and the largest 162.1 lbs per cu. ft. Using the mean value γ_{r_m} = 158.6 lbs per cu. ft. equation (2.2) yields γ_{r_p} = 162.7 lbs per cu. ft. for the equivalent specific weight of the prototype stone. The results presented herein on the stability of the rock are based on this value of the specific weight for the prototype stone. The stones were selected so as to meet the specification requirement that the ratio of the longest dimension to the least dimension not exceed 2.5.

All stones used in the model for "B" and "C-1" rock were classified according to weight. To prepare "B" stone individual rocks were separated into two groups, one having equivalent prototype weights for a 1:50 scale model ranging from 4 to 8 tons and the other with weights ranging from 8 to 10 tons. The "B" rock used in the tests was made of equal weights of the two groups of stones. The equivalent weight of prototype stone was calculated by equation (2.1) using a scale ratio L_r = 1/50 which is the scale of the first model built in the tank. Cover rock "C-1" was prepared by selecting rock having equivalent prototype weights ranging from 1 to 4 tons. The dike rock "D" was made by screening the dust out of the material left after "B" and "C-1" material had been removed. For convenience in construction of the models the armor rock "B" was painted green and the cover rock "C-1" was painted red.

Samples of "B" and "C-1" rock prepared in the manner outlined above were taken by quartering the entire stockpile of each kind of material. The weight distribution was then determined from these samples. The results of such analyses of two samples each of "B" rock and the "C-1" rock are shown on Tables 2.1 and 2.2 respectively. Column 1 of each table gives the percent of the total number of rocks

Table 2.1. Weight Distribution of Armor Rock "B" Used in Two-Dimensional Model.

1	2	3	4	5	6
Percent of total number of rocks lighter than wt in columns at right	Percent of total wt of rocks lighter than wt in columns at right	Weight of model rocks W_{r_m} grams	Equivalent Prototype Weights W_{r_p}, Tons		
			1:50 Scale Model	1:45 Scale Model	1:40 Scale Model
1. Sample No. 1 (87 rocks)					
00.0	00.0	28.3	4	2.9	2.1
10.3	5.9	35.4	5	3.6	2.6
23.0	14.8	42.5	6	4.4	3.1
32.2	22.7	49.5	7	5.1	3.6
44.8	34.0	56.6	8	5.8	4.1
73.6	67.2	63.7	9	6.6	4.6
100.0	100.0	70.8	10	7.3	5.1
2. Sample No. 2 (124 rocks)					
00.0	00.0	28.3	4	2.9	2.1
26.6	18.7	35.4	5	3.6	2.6
50.8	39.5	42.5	6	4.4	3.1
66.9	55.8	49.5	7	5.1	3.6
78.2	69.1	56.6	8	5.8	4.1
87.9	82.0	63.7	9	6.6	4.6
100.0	100.0	70.8	10	7.3	5.1

Table 2.2. Weight Distribution of Cover Stone "C-1" Used in Two-Dimensional Model.

1	2	3	4	5	6
Percent of total number of rocks lighter than wt in columns at right	Percent of total wt of rocks lighter than wt in columns at right	Weight of model rocks W_{r_m} grams	Equivalent Prototype Weights W_{r_p}, Tons		
			1:50 Scale Model	1:45 Scale Model	1:40 Scale Model
1. Sample No. 1 (106 rocks)					
00.0	00.0	7.1	1.0	0.7	0.5
44.3	29.0	10.6	1.5	1.1	0.8
44.3	29.0	14.2	2.0	1.5	1.0
56.6	40.9	17.7	2.5	1.8	1.3
68.9	55.3	21.2	3.0	2.2	1.5
87.7	80.5	24.8	3.5	2.5	1.8
100.0	100.0	28.3	4.0	2.9	2.0
2. Sample No. 2 (146 rocks)					
00.0	00.0	7.1	1.0	0.7	0.5
13.7	6.5	10.6	1.5	1.1	0.8
26.7	15.3	14.2	2.0	1.5	1.0
43.1	29.4	17.7	2.5	1.8	1.3
63.0	50.3	21.2	3.0	2.2	1.5
80.8	72.5	24.8	3.5	2.5	1.8
100.0	100.0	28.3	4.0	2.9	2.0

that is lighter than the weights listed in Columns 3-6. Column 2 gives the percent of the total weight of the rock that is lighter than the weight given in Columns 3-6. Columns 4, 5 and 6 of these tables give the equivalent prototype weight in tons for each of the three models tested. These values were obtained from the model weights by means of equation (2.1) and are based on a prototype specific weight $\gamma_{r_p} = 162.7$ lbs per cu. ft. Figs. 2.6a and 2.6b are cumulative number frequency and weight frequency curves for two samples each of model armor rock "B" and cover stone "C-1", respectively, plotted from the data of Tables 2.1 and 2.2. The two sets of curves for each rock are in terms of model weights in grams and prototype weights in tons for the 1:50 scale model. The curves for the two samples of the "B" rock differ somewhat from each other. Sample No. 1 shows that 66% of the total weight of rocks is heavier than 8 tons compared with 31% for sample No. 2. These deviations are believed to be due to sampling errors since the rock was prepared so that at least half of the total weight of the rock was made of units with equivalent weights between 8 and 10 tons each. The curves for the "C-1" rock deviate somewhat from the specified uniform distribution by having a larger fraction of large stones than required by the specification.

Fig. 2.7 shows a size-frequency curve of the material used in the model to simulate dike rock. As the curve shows this material had a median sieve size of 12.4 mm.

A drawing of the concrete tribars which are an important feature of the surface armor of this artificial island is presented in Fig. 2.8. In this study only one size model tribar was used. The table, which is an inset to Fig. 2.8, shows the common model dimension of the diameter of the leg of the tribar as well as this corresponding prototype dimension for the three model scales used in the two-dimensional tests. In addition the equivalent prototype weights which correspond to these model scales are shown.

The minimum specific weight of the concrete to be used in the manufacture of the prototype tribars has been specified by the design

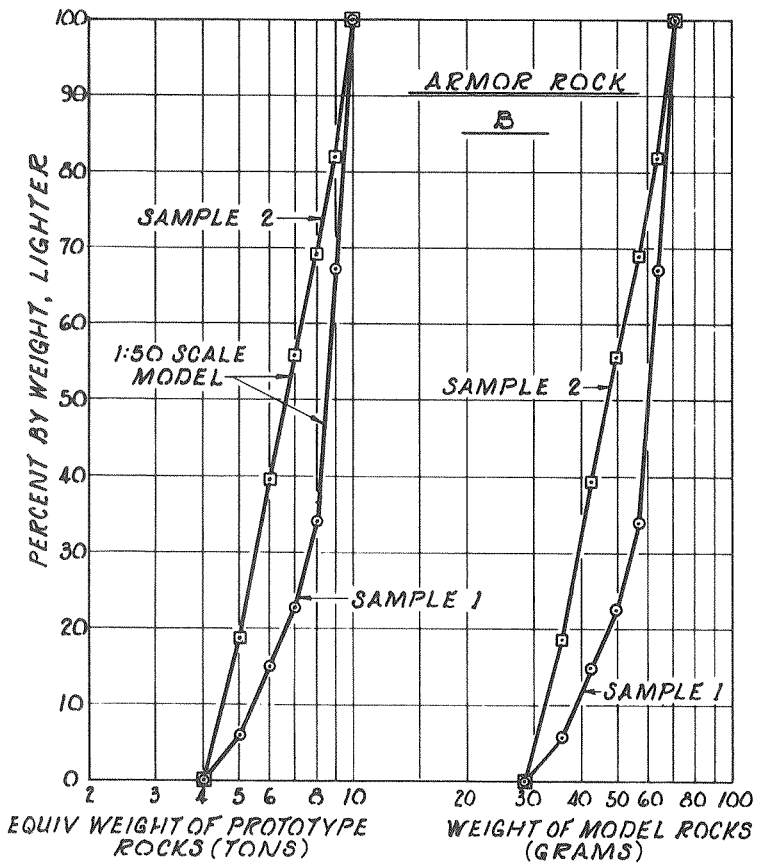

Figure 2.6a Weight Frequency Distribution for Actual Model Armor Rock and for Equivalent Prototype Rock for the 1:50 Scale Model (for Rock "B")

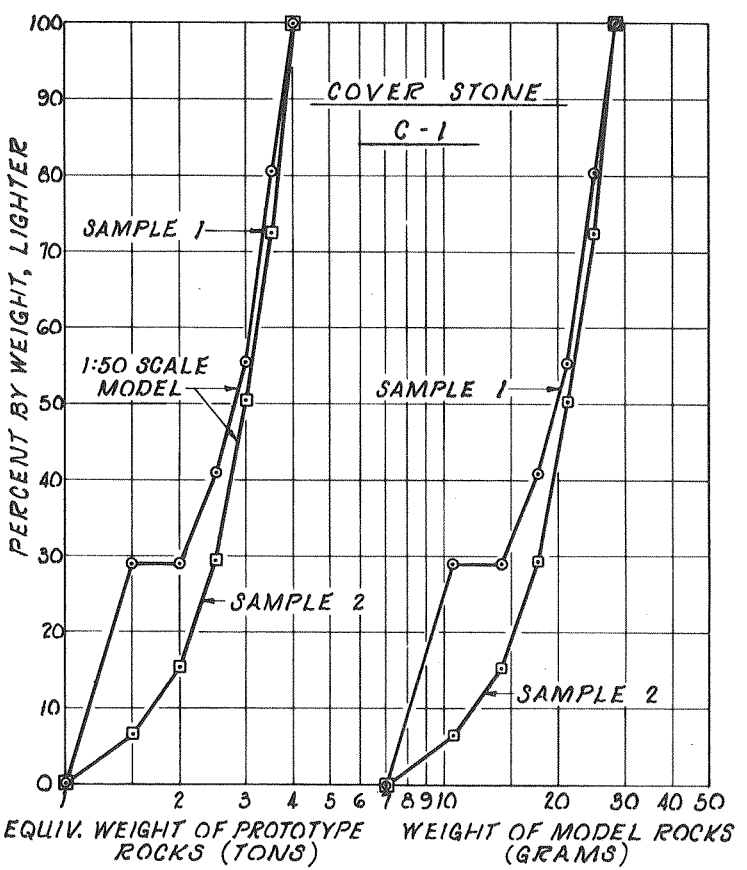

Figure 2.6b Weight Frequency Distribution for Actual Model Armor Rock and for Equivalent Prototype Rock for the 1:50 Scale Model (for Rock "C-1")

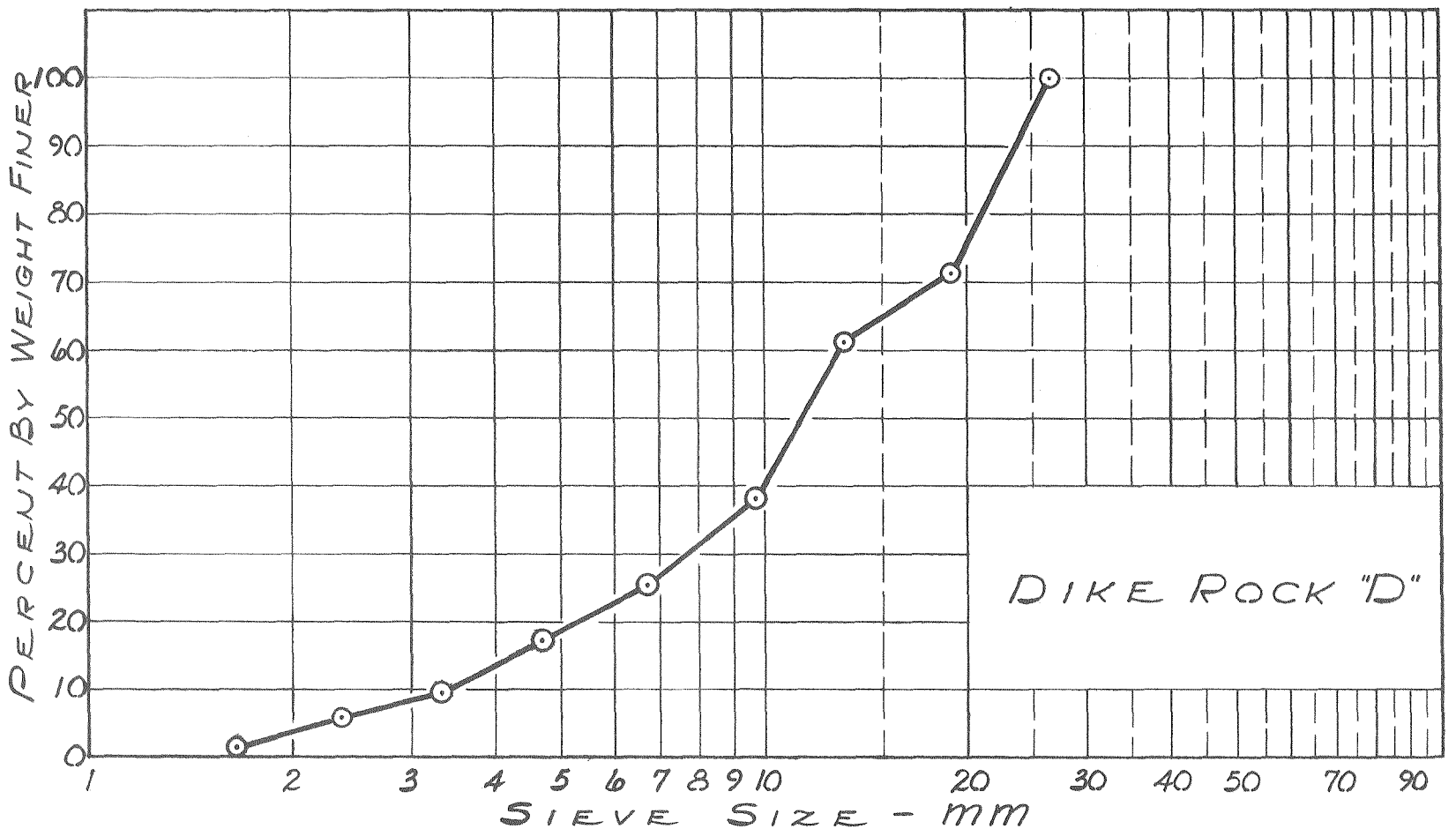

Figure 2.7 Size-Freqency Distribution of Material Used in Model to Simulate Dike Rock "D"

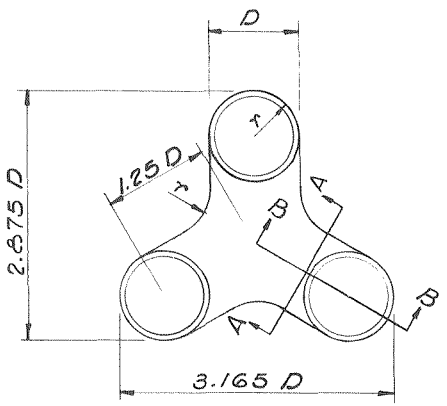

PLAN

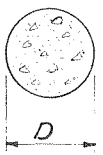

SECTION A-A

PROTOTYPE TRIBAR DIMENSIONS AND WEIGHTS CORRESPONDING TO INDICATED MODEL SCALES

MODEL SCALE	D Ft.	W* TONS
1:50	3.33	18.9
1:45	3.0	13.8
1:40	2.67	9.7

*NOTE

THIS WEIGHT IS BASED ON A SPECIFIC WEIGHT OF CONCRETE OF 146 #/ft³ AND SEA WATER HAVING A SPECIFIC WEIGHT OF 64 #/ft³

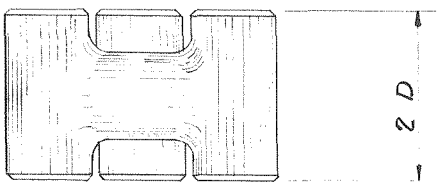

ELEVATION

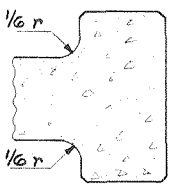

SECTION B-B

Figure 2.8 Drawing of Tribar

engineer as 145 lbs per cu. ft. From equation (2.2), this requires that the minimum specific weight of the model tribars be 141.4 lbs per cu. ft.

The model tribars were cast of an aluminum-magnesium alloy having a specific weight of approximately 168.7 lbs per cu. ft. In order to obtain the desired specific weight it was necessary to remove a portion of this alloy and replace it with a material of a smaller specific weight. To accomplish this a 29/64-in.-diameter hole was drilled in each leg of each tribar, and these three holes were then refilled with beeswax (see Fig. 2.5). The resultant average specific weight of the model tribars was 142.06 lbs per cu. ft. compared to a desired specific weight of 141.4 lbs per cu. ft. The distribution of the specific weight of a sample of the modified tribars is presented in Fig. 2.9 where the specific weight of the model tribars is plotted as a function of the percent by number lighter than a particular specific weight. The moment of inertia of these units about an axis which is parallel to the plane of two legs of a tribar and passes through its center of gravity was changed approximately 7% by this modification.

The weight distribution of the same sample of tribars used to develop Fig. 2.9 is shown in Fig. 2.10. This is a curve of the model weight of the tribars plotted as a function of the percent by number lighter than a particular weight. In computing the prototype weight of the tribar in salt water equations (2.2) and(2.1) must be applied to these values, since these tribars were cast taking into account that testing would be conducted in fresh water. The average prototype weight at a model scale of 1:50 so obtained is 18.9 tons compared to the desired weight of 18 tons. This 5% difference is due to problems arising in precision casting of units of so small a size.

b. Method of Construction of Island Faces

In placing model rock and tribars great care was taken to duplicate the result achieved in field placing. This operation was guided by Mr. Omar J. Lillevang, Consulting Engineer, who supervised some of the model construction. The dike rock "D" was placed by the handful, smoothed out with the fingers and palm of the hand and

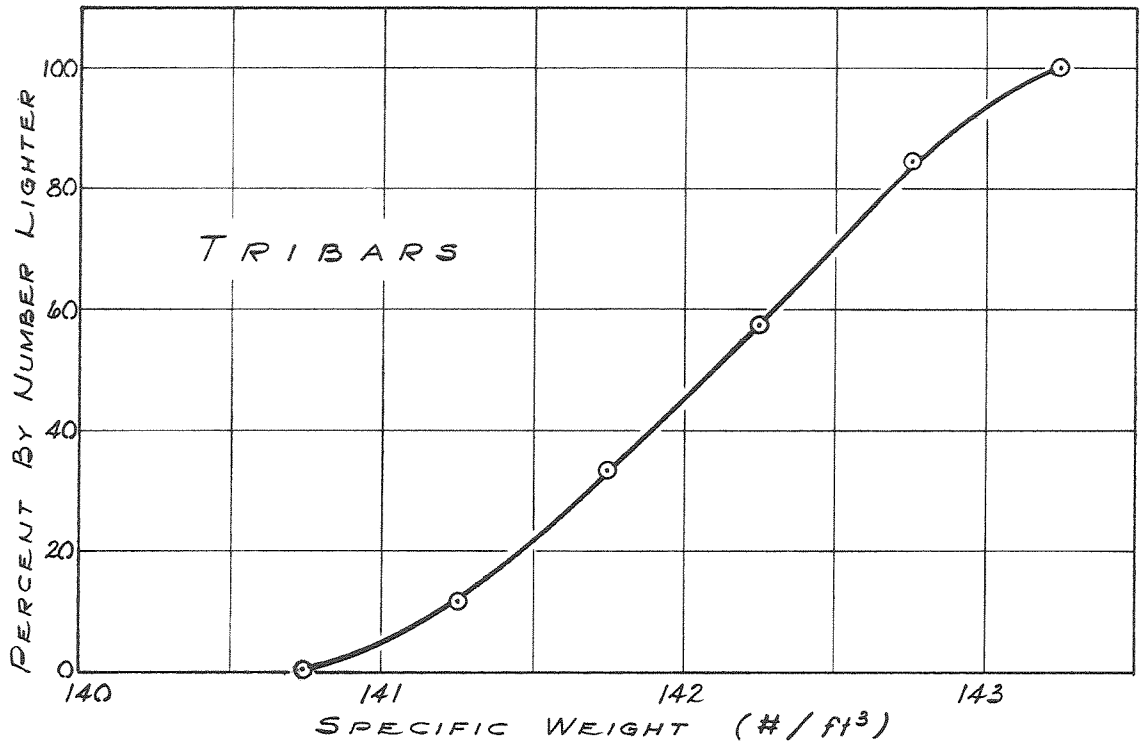

Figure 2.9 Specific Weight Frequency Distribution of Model Tribars

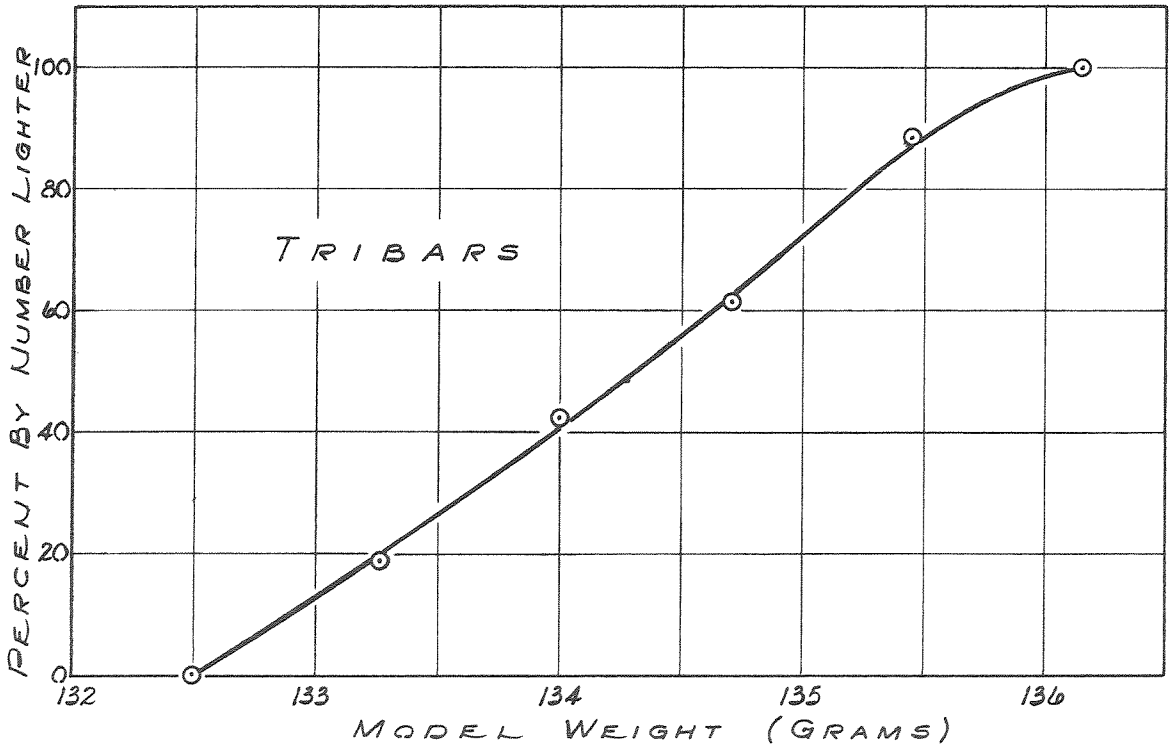

Figure 2.10 Weight Distribution of Model Tribars

then checked for grade with a straight edge. The rock was not tamped to achieve greater consolidation. The cover rock "C-1" was placed in the same manner. The armor rock "B" was placed one rock at a time starting at the lowest elevation. Rocks were selected to fit snugly in spaces between rocks already in place. If a rock was found not to fit a particular cavity it was returned to the stockpile and a more appropriate one selected. Once a rock was in place it was tested for stability against rocking by applying a slight pressure with the fingers. Under no circumstances were rocks forced into position. The upper surface of the rock facing was checked for elevation by sighting through the glass window over finish lines placed at the sides of the tank. Placing of the armor rock proved to be a very difficult and exacting task. To achieve a rock face that was uniform in texture and free from elevation irregularities required considerable time and some experience on the part of the laboratory workers. The same technique and ideas used in placing rock were used in placing tribars.

3. Instrumentation

All depth measurements and run-up measurements were made using the point gage attached to the movable carriage shown in the photograph, Fig. 2.11. This carriage moves on the precision rail system described in Chapter Two, Section A.1.

Resistance wave gages, such as shown in Fig. 2.12, were used in conjunction with a Sanborn (150 Series) direct-writing recording system to obtain time histories of the wave amplitude. Sanborn Carrier Preamplifiers (Model 150-1100AS) supply the 2400 cps, 4.5 volt excitation voltage for the gages, and in turn receive the output from the wave gages which after demodulation and amplification are displayed on a recording unit. The wave gages consist of two wire-elements, parallel to and insulated from each other, upon which the excitation voltage is impressed. As the immersion of the wires in a conducting solution is varied, their resistance changes proportionately, causing an imbalance in the full bridge circuit shown in Fig. 2.13, (the portion of the circuit internal to the recorder is shown dotted). This imbalance causes a variation in voltage drop across the gage and is recorded by the Sanborn unit as a change from the balanced position.

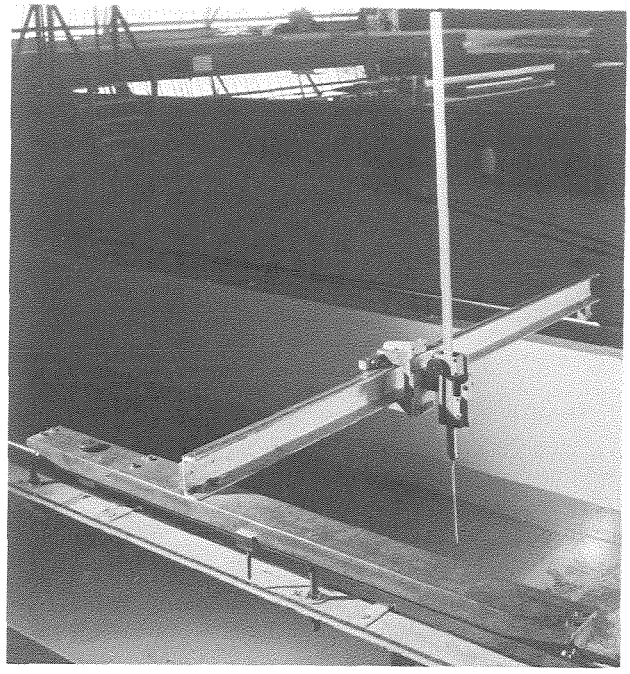

Figure 2.11 Run-Up Carriage

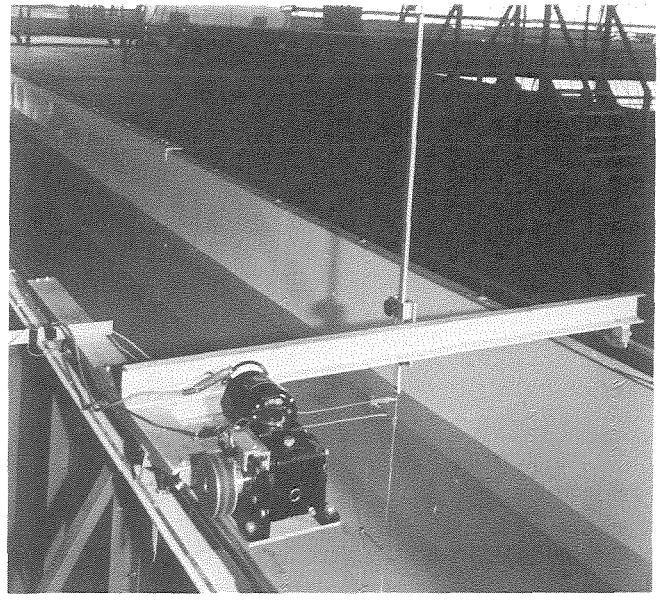

Figure 2.12 Wave Gage and Motor-Driven Wave Gage Carriage

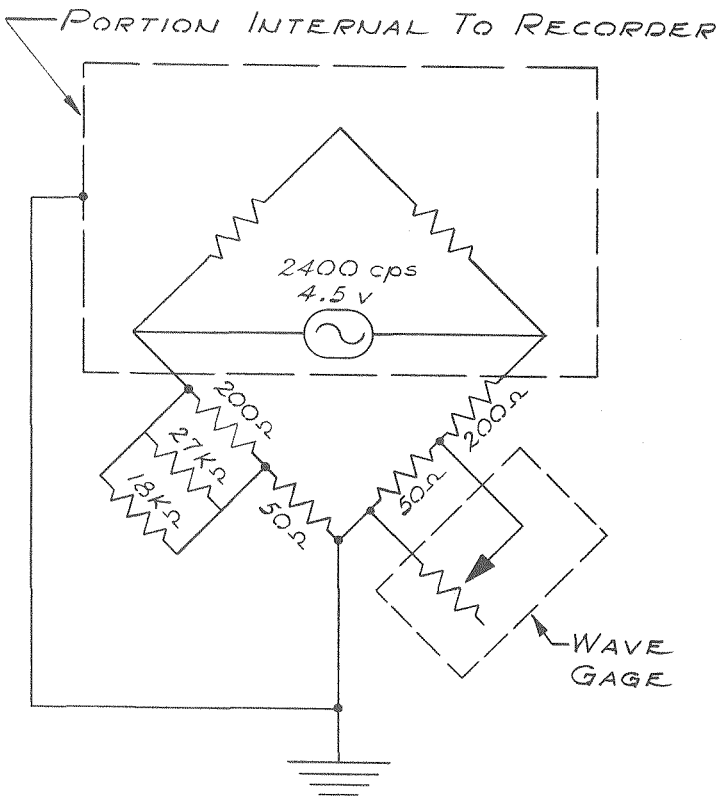

Figure 2.13 Circuit Diagram for Wave Gage

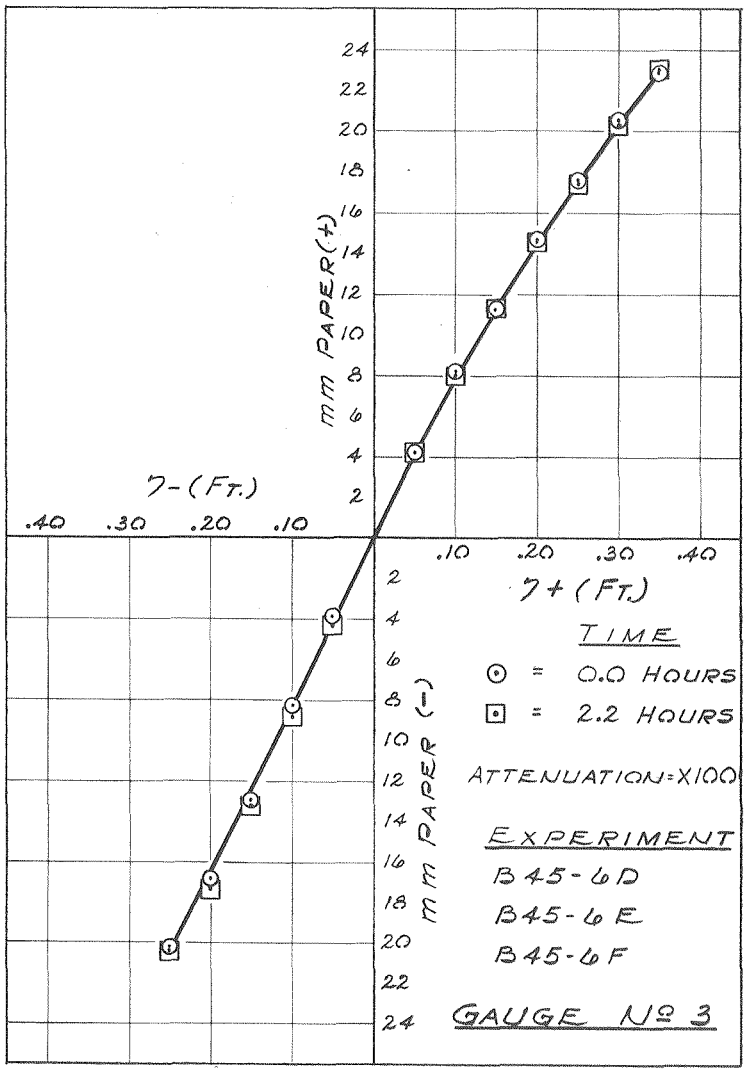

Figure 2.14 Typical Calibration Curve of Wave Gage

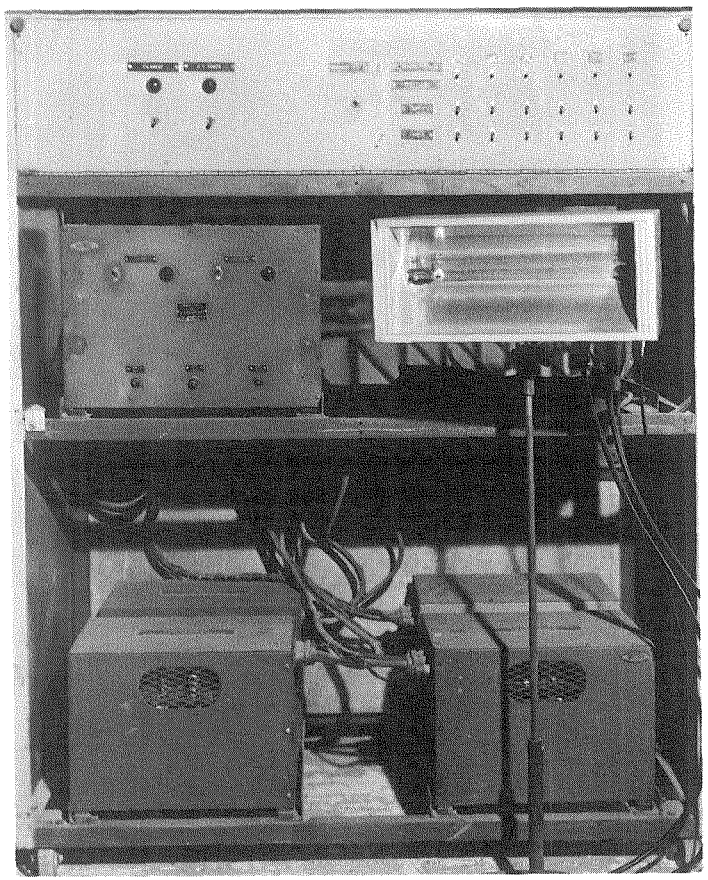

Figure 2.15a Electronic Flash Unit and High Voltage Source

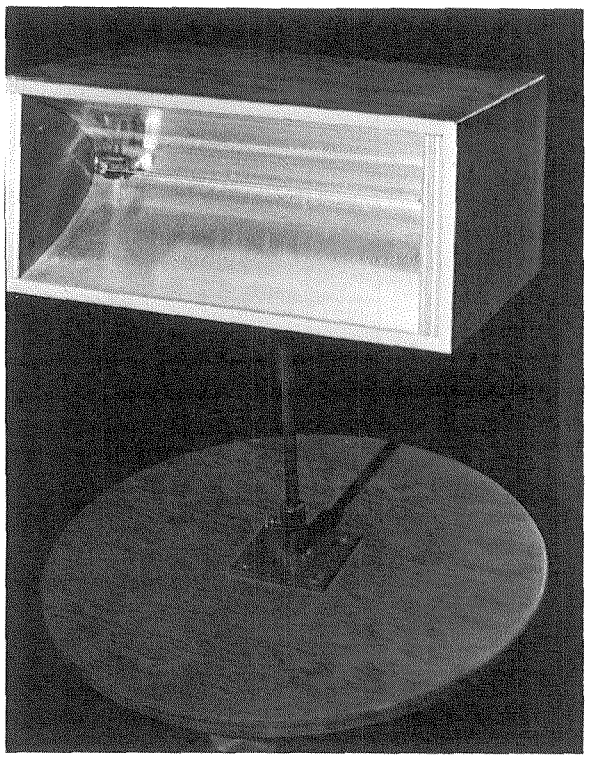

Figure 2.15b Close-up View of Flash Lamp and Support

The wave gages consist of two stainless steel wires 0.01 in. in diameter, approximately 13 in. long, spaced 1/8th of an in. apart. They are insulated from each other and stretched taut in a 3/16th-in.-diameter stainless steel frame. For ease in calibration each wave gage is mounted on an instrument holder. These details may be seen in the photograph of the wave gage and carriage, Fig. 2.12. The common plane of the wire elements is perpendicular to the direction of wave travel. A typical calibration curve of a wave gage is shown in Fig. 2.14, where the immersion or withdrawal of the gage in feet from the balanced position is plotted as a function of millimeters of deflection of the recording instrument stylus.

The wave gage used to obtain the incident wave height in the section of the wave tank with horizontal bottom was attached to the motorized carriage shown in Fig. 2.12. A rubber-tired aluminum wheel is attached to the drive shaft of a variable speed 1/15 hp D.C. motor and this wheel in turn rides on one of the rails of the wave tank thereby propelling the wave gage. The circumference of the wheel is approximately 1 ft.; hence, one revolution of the wheel moves the carriage a distance of 1 ft. In this way, the wave gage attached to this carriage can be moved longitudinally along the wave tank at a constant speed which is slow enough so that a reasonable average of the wave envelope can be obtained. A microswitch attached to the carriage is closed four times for each revolution of the wheel and produces signals which are recorded on the chart which records the wave height. In this way four equally spaced marks are produced on the chart per foot of carriage movement. In addition to this gage, similar wave gages were used to measure wave heights in two fixed locations along the tank.

All photographs in both the two-dimensional and the three-dimensional study were taken using an electronic flash-lamp system. Fig. 2.15a is a photograph of one such flash unit and the associated high-voltage electronic power supply and control console. Each unit consists of a PEK Xenon Flash Lamp 12 inches long (Type XE1-12) mounted in a parabolic reflector at the focus of the parabola. These details can be seen better in the close-up photograph, Fig. 2.15b of

one unit and its pedestal. The reflector and its associated components are mounted in a wooden case for additional protection from the high operating voltage. Eight flash lamps can be triggered simultaneously using this system.

4. Summary of Testing Procedures and Observations

With each two-dimensional model, experiments were conducted at two water depths and at several wave periods and incident wave heights. The actual conditions for these tests will be presented in Chapter Three. In this section, only a description of the procedure will be presented.

Wave measurements were made for each experiment in three different locations in the wave tank. These locations may best be seen by referring to the schematic drawing of the wave tank, Fig. 2.1. Wave records were obtained at two fixed locations; one location between the wave generator and the upstream end of the wave filter, and a second location just downstream of the wave filter. Due to wave reflections from the model, it is necessary to determine the incident wave height from a wave envelope obtained in the portion of the wave tank near the model which has a horizontal bottom. This envelope is obtained by moving the motorized carriage at a slow speed along the horizontal bottom of the wave tank from the upstream limit of the horizontal section to the toe of the wave defense. A typical wave record obtained in this manner is shown in Fig. 2.16. This figure also shows wave traces obtained at the two upstream locations. The analysis of these wave records will be discussed in detail in Chapter Three, Section A.1.

The general testing procedure for a particular prototype depth and incident wave period was the following. After construction of the wave defense as described in Section A.2.b of this Chapter, profiles of this section were obtained using the point gage and carriage shown in Fig. 2.11 and overhead photographs of the defense were taken. The desired wave machine period was set and the stroke of the wave machine was then adjusted to produce a wave of approximately one-half of the design wave height. The structure was exposed to this wave for

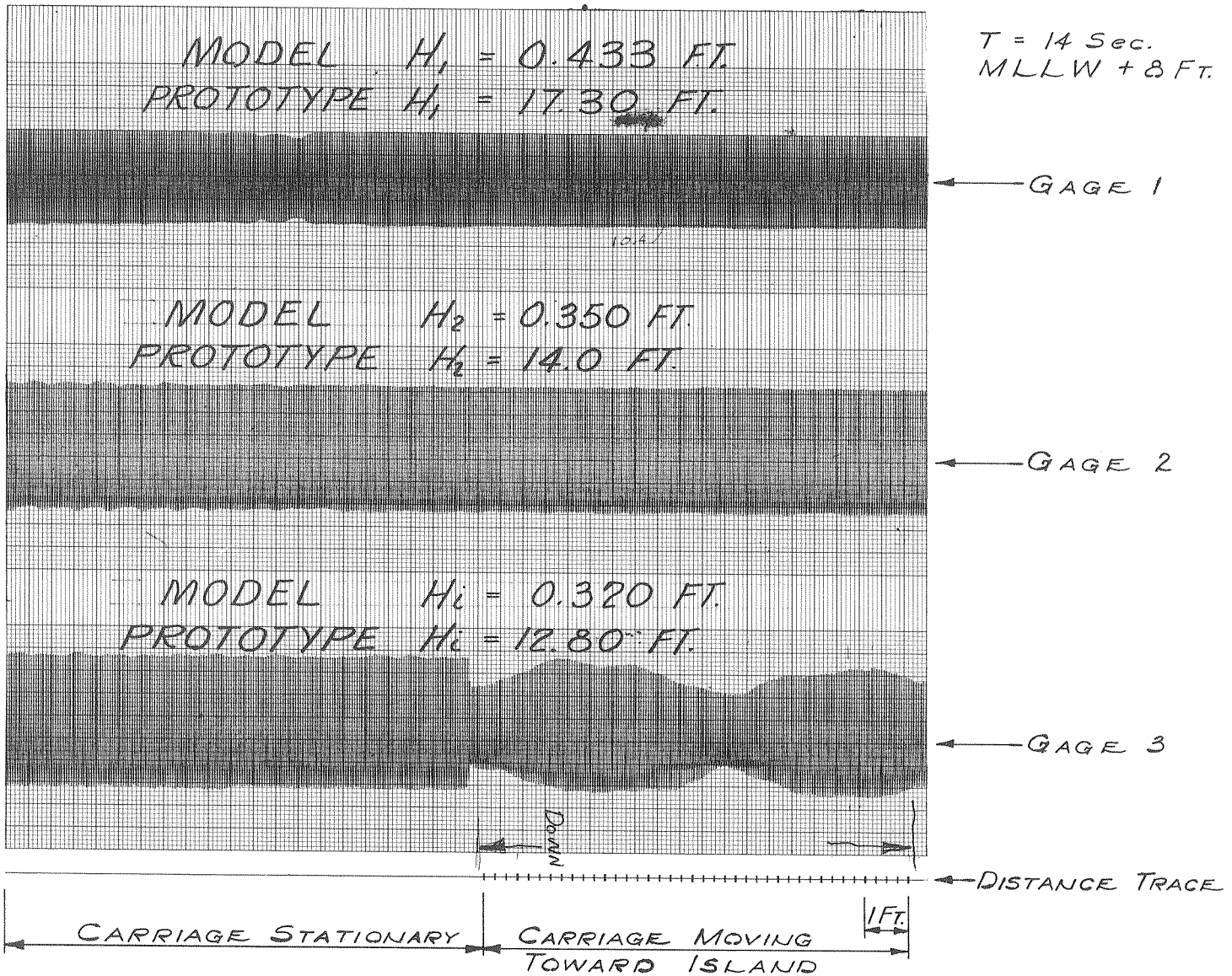

Figure 2.16 Typical Oscillograph Trace of Waves

a prototype duration of 24 hours to allow the armor elements to realistically "settle in" before proceeding with the testing. This approach was taken only preceding the first test after the structure had been rebuilt; in all other cases testing proceeded in sequence without any "settling in" period.

Due to the influence of reflections upon the incident wave a short time was usually required for the wave system to approach a steady state condition. After this condition had been reached, wave measurements were obtained at the fixed gage locations and the movable carriage was started to obtain the wave envelope. At least two traverses were made with the movable carriage for each wave condition.

At the same time as the wave measurements were being made, visual observations were made of the island face. These observations consisted of closely observing the toe rock section, the tribar section, and the cap-rock section of the face. Of primary interest was the observation of any displacement or rocking of individual elements. If an element was dislodged, its final position was recorded. Any unusual movement of elements in the island face and any unusual features of waves were also observed at this time.

Run-up measurements were made for each wave height after the wave system had reached a steady state using the movable point gage system, since it was found that the run-up obtained before the first wave reflection returned to the island face was essentially the same as the steady-state values. These measurements were made on the wave tank centerline and at not less than two locations spaced one-half ft. apart on either side of the centerline. The run-up elevation was obtained by adjusting the point gage and carriage at a particular lateral section to the position of the maximum ascent of the water surface. The lateral and longitudinal location of this point in addition to the measured elevation were recorded. Usually these measurements consisted of observing the run-up at any particular position for a number of waves so that a reasonable average could be obtained.

When overtopping was observed in the model, measurements were made of the rate of flow over the crest of the island face. This flow was collected in a galvanized sheet metal box which had inside dimensions of 36 in. long, 7-15/16 in. wide and 6 in. deep. This box was positioned as shown in the schematic drawing of the wave tank, Fig. 2.1. The flow was then determined by measuring the increase in the water depth in the box in a measured period of time.

To complete the record of visual observations and measurements, photographs were taken of the model with the condition of maximum run-up on the island face and the lowest position of the water surface on the face for each incident wave height. At the end of an experimental series a profile of the island face was obtained in addition to overhead photographs to evaluate the degree of any damage that may have occurred.

This sequence was repeated each time the wave height was changed. The maximum wave height that was attained was the maximum possible in this wave tank just prior to wave breaking in the horizontal section.

B. THREE-DIMENSIONAL MODEL

1. Wave Basin and Pneumatic Wave Generators

The three-dimensional model study was conducted in a wave basin having a length of 132 ft., a width of 88 ft., and a depth of 2 ft. The walls of the wave basin are constructed of terne plate (20 gauge) braced approximately 2 ft. on centers. The walls are bolted directly to the concrete laboratory floor. Seals between the floor and the walls and between sections of walls were made with plastic tape.

Pneumatic wave machines originally developed by the late Professor R. T. Knapp were used to generate the incident wave system in the three-dimensional model. A schematic drawing of one wave machine is presented in Fig. 2.17a, and a close-up photograph of the drive mechanism is presented in Fig. 2.17b. Four such wave machines, each 20 ft. long, were used in this study, thereby providing an incident wave crest that is approximately 80 ft. long.

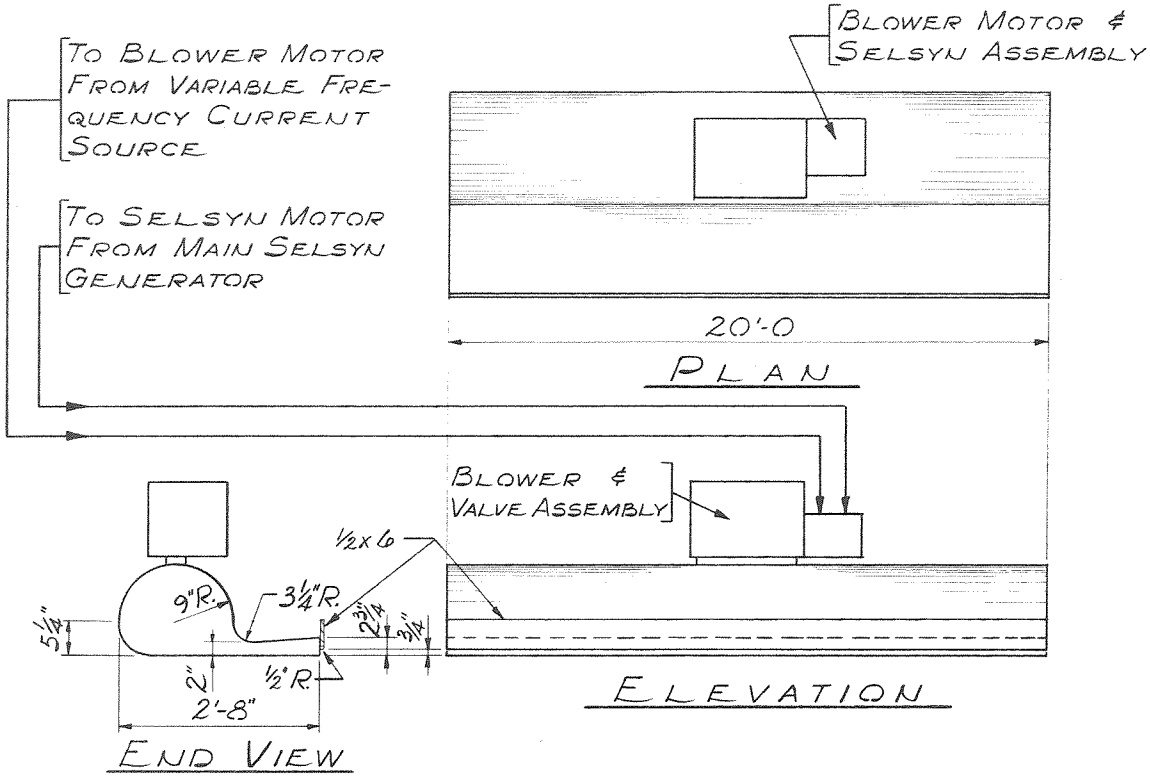

Figure 2.17a Schematic Drawing of Pneumatic Wave Generator

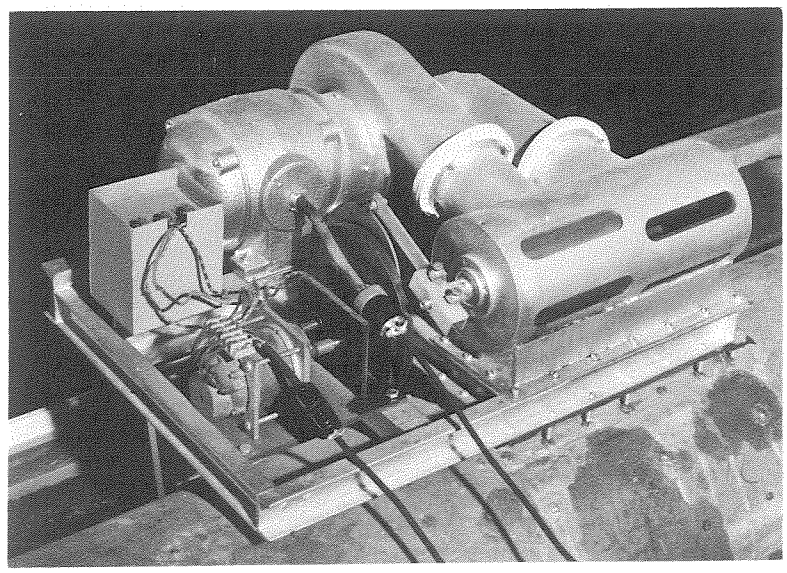

Figure 2.17b Blower Valve Assembly, and Cam System of a Pneumatic Wave Generator

Each generator consists basically of a caisson with a semi-cylindrical top in which the air pressure can be varied between positive and negative values. This caisson is connected to a water-filled diverging section approximately 11 in. long and 2-3/4 in. high. In order to improve the characteristics of the waves generated in this particular model an orifice plate has been attached to the entrance to the wave generator. This plate results in an opening of the generator to the basin 3/4 of an inch high. As the air pressure varies in the caisson, water enters and leaves the diverging section at a predetermined frequency thereby generating the wave system.

The air pressure within this caisson, and hence the amplitude of the generated wave, is varied by varying the speed of the centrifugal blower which can be seen attached to the top of the machine in Fig. 2.17b. All blowers are identical and each is driven by a 110 volt, 3 phase, 1 hp motor. The variable frequency current which drives each motor comes from a common source located in the main control console. This voltage is generated by an alternator with its separate exciter which in turn is driven by a variable speed drive through a 220 volt 10 hp. A.C. motor. Thus, as the speed of the motor drive in the console is changed, the frequency of the exciting voltage to each centrifugal blower motor changes, thereby changing the blower speed, the maximum and minimum air pressures in the caisson, and ultimately the amplitude of the wave generated.

The cyclical variation of air pressure in the caisson is obtained by means of the oscillating valve which can be seen in the photograph, Fig. 2.17b. This valve alternately connects the inlet and exhaust of the blower to the caisson at the predetermined frequency. When the inlet to the blower is connected to the caisson the exhaust is connected to atmosphere and vice versa.

The wave period is varied by varying the frequency of oscillation of the valve. Each valve is driven by a Selsyn motor through a cam and cam follower which can be seen in Fig. 2.17b. The cam is a simple disk 6-1/2 in. in diameter, mounted 2 in. off-center of the Selsyn drive shaft. In order to reduce the torque on the Selsyn motor, the cam follower is kept in contact with the cam by means of a spring

attached to the cam follower at one end and to the center of the cam at the other. The four Selsyn motors are driven from a common generator located in the wave machine console. This generator is driven by a vari-speed drive and 1/2 hp A.C. motor. Therefore, by varying the speed of this varidrive unit the rotational speed of the generator is varied and therefore the frequency of oscillation of each valve on each wave machine is varied in the same manner. In this way, the period of the waves generated by each wave machine is identical and because of the properties of the Selsyn system the phase between cam motors and hence between waves remains fixed.

In order to generate waves which approach the model at an angle, the individual wave machines are turned at an angle and staggered within the basin. When this is done a continuous wave crest can be obtained from all four machines by varying the electrical phase of three Selsyn motors with respect to one fixed Selsyn. This is accomplished at the main console through differential Selsyn generators.

2. Model Construction

a. Site Plan and Model Basin Orientation

The site plan of the artificial island and the model limits are shown in Fig. 2.18, which is reproduced from U.S.C. & G.S. Chart No. 5142. As mentioned previously, the proposed island is approximately 1500 ft. long parallel to the coast and 1200 ft. wide. The leeward face of the island is 2800 ft. off Bolsa Chica State Beach about three miles north of the City of Huntington Beach. The three-dimensional model of this artificial island and offshore topography was built to an undistorted scale of 1/150.

b. Material and Method of Construction

1) Construction of Topography

A drawing of the location of the model island within the wave basin is presented in Fig. 2.19a. The contours shown in Fig. 2.19a are the prototype contours taken from the chart, Fig. 2.18, with additional contours interpolated. The contoured bottom did not extend the full length of the wave basin as can be seen in Fig. 2.19a.

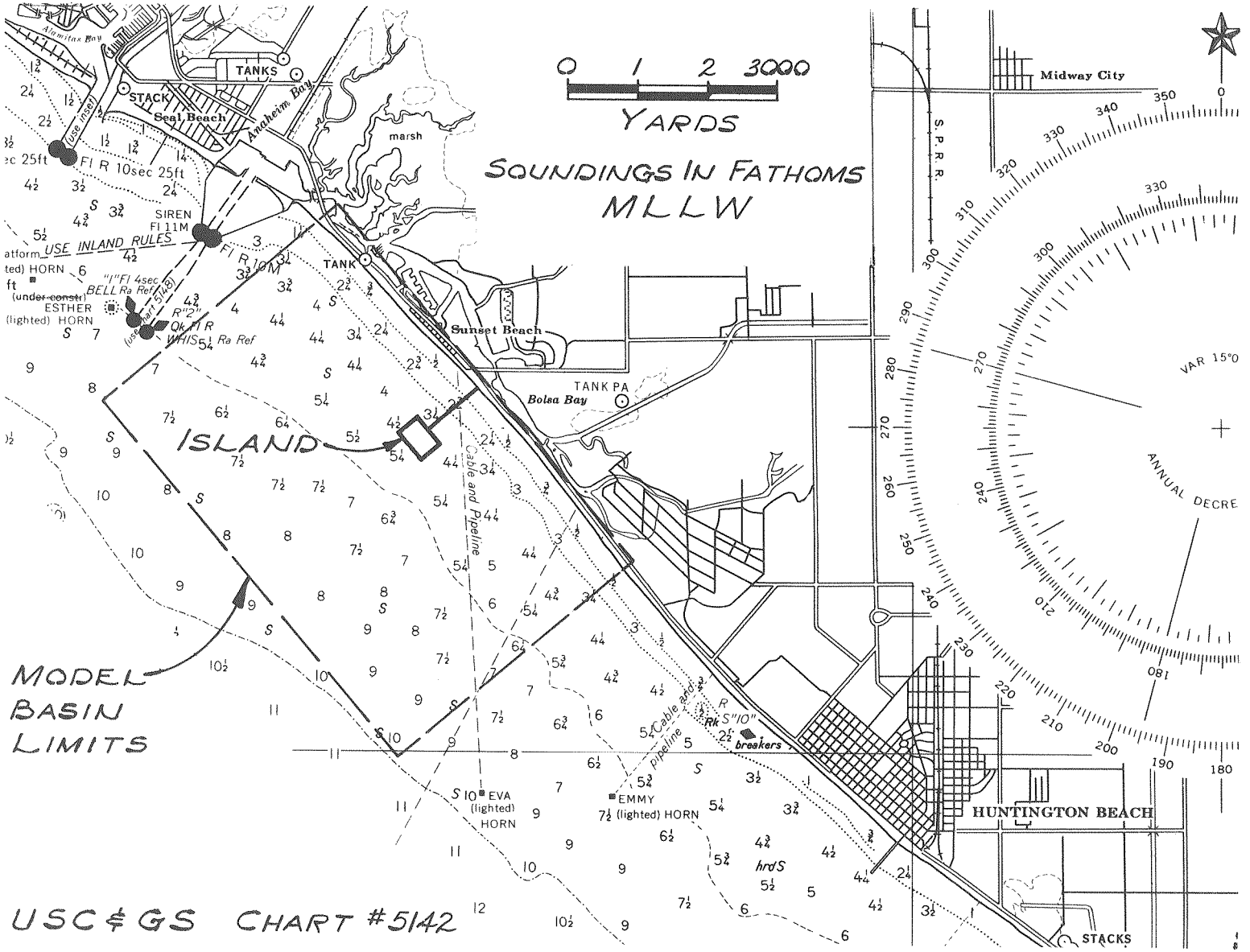

Figure 2.18 Site Plan of Artificial Island and Model Limits

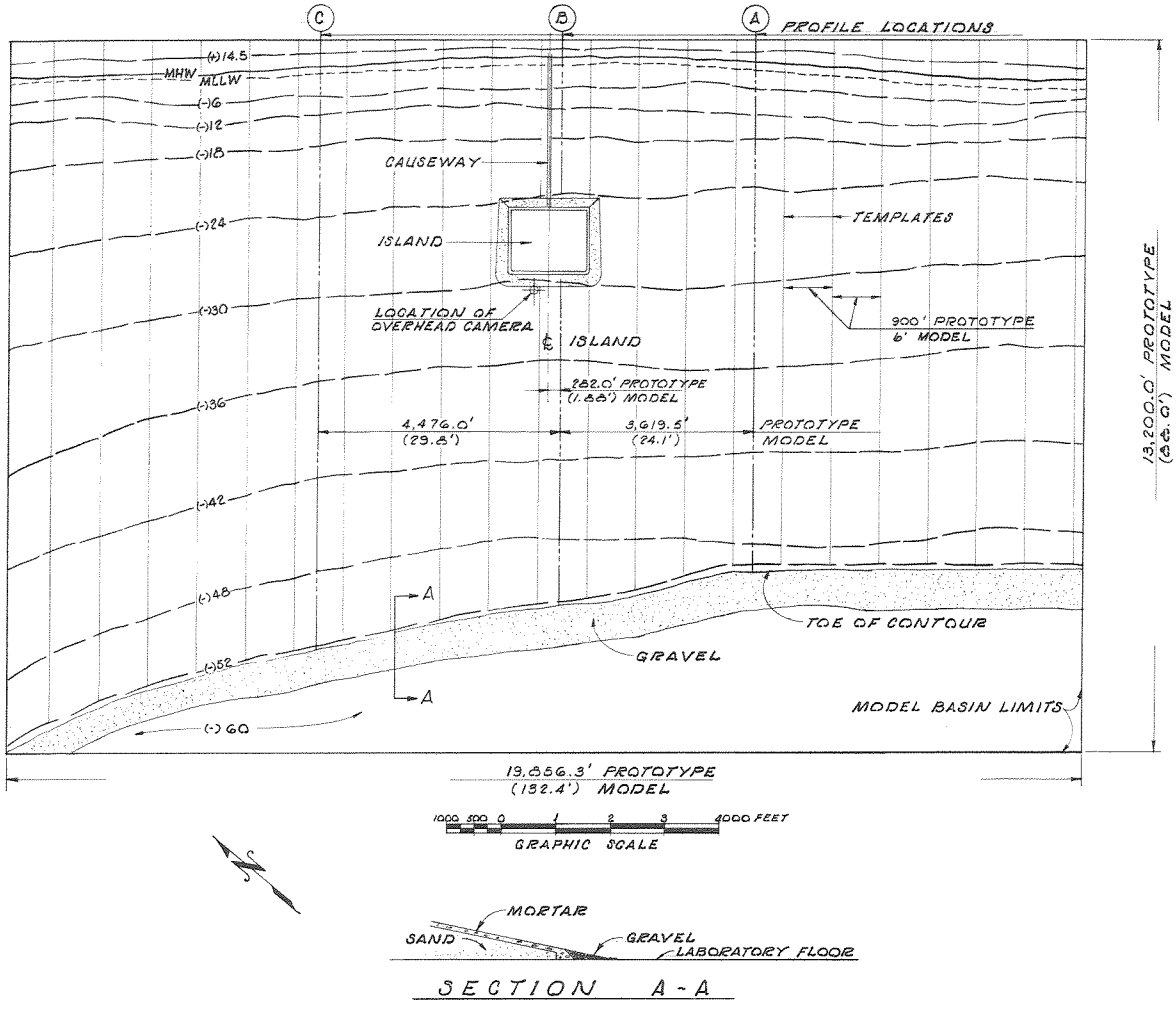

Figure 2.19a Plan View of Model Basin and Three-Dimensional Model

Figure 2.19b Three-Dimensional Model Under Construction

It was necessary to leave a level region in the wave basin so that the wave machine could be oriented in the basin on a horizontal surface. This level region is approximately at the 10 fathom contour in the prototype. Therefore, when orienting the wave machine, they must be adjusted to the direction of the refracted wave at that depth to produce the desired wave incidence at the island site.

The method of construction of the ocean bottom can be seen most readily in the construction photograph, Fig. 2.19b. In this photograph the templates are seen running perpendicular to the bottom contours. These templates are constructed of wood and are spaced approximately 6 ft. on centers. The space between the templates was filled with sand, as seen in the left-hand portion of Fig. 2.19b. The sand was wetted and compacted and then a crust consisting of cement mortar ranging from 1/4 to 1/2-in. thick was then placed on top of this compacted sand. The topography was then formed by screeding to these templates with straight edges as soon as the mortar was placed. The surface was then troweled in order to obtain a smooth surface.

Three locations are shown in Fig. 2.19a where profiles of the finished model ocean bottom were obtained. These profiles are presented in Fig. 2.20 plotted to a distorted scale. Prototype bottom elevations are also plotted in this figure for each lateral location and show relatively good agreement with the model.

2) Construction of Island

As seen in the photograph Fig. 2.19b, a rectangular wooden form was constructed of dimensions to represent the prototype island and was used to locate the island in the model. A plan view of the model island and a cross section through it are shown in Fig. 2.21. In order to construct the island face and to form a fixed plane of reference for run-up measurements, an aluminum angle frame was built on top of the wooden form. This angle frame, as seen in Fig. 2.21, consists of 2 in. x 2 in. x 1/4 in. extruded aluminum angles which are fixed to the wooden island form by means of lag bolts. These bolts have a threaded upper portion so that the four angles forming the frame could be individually leveled to bring the top surfaces of the angles into a horizontal plane. The prototype elevation corresponding to the top of the angle is +61 ft.

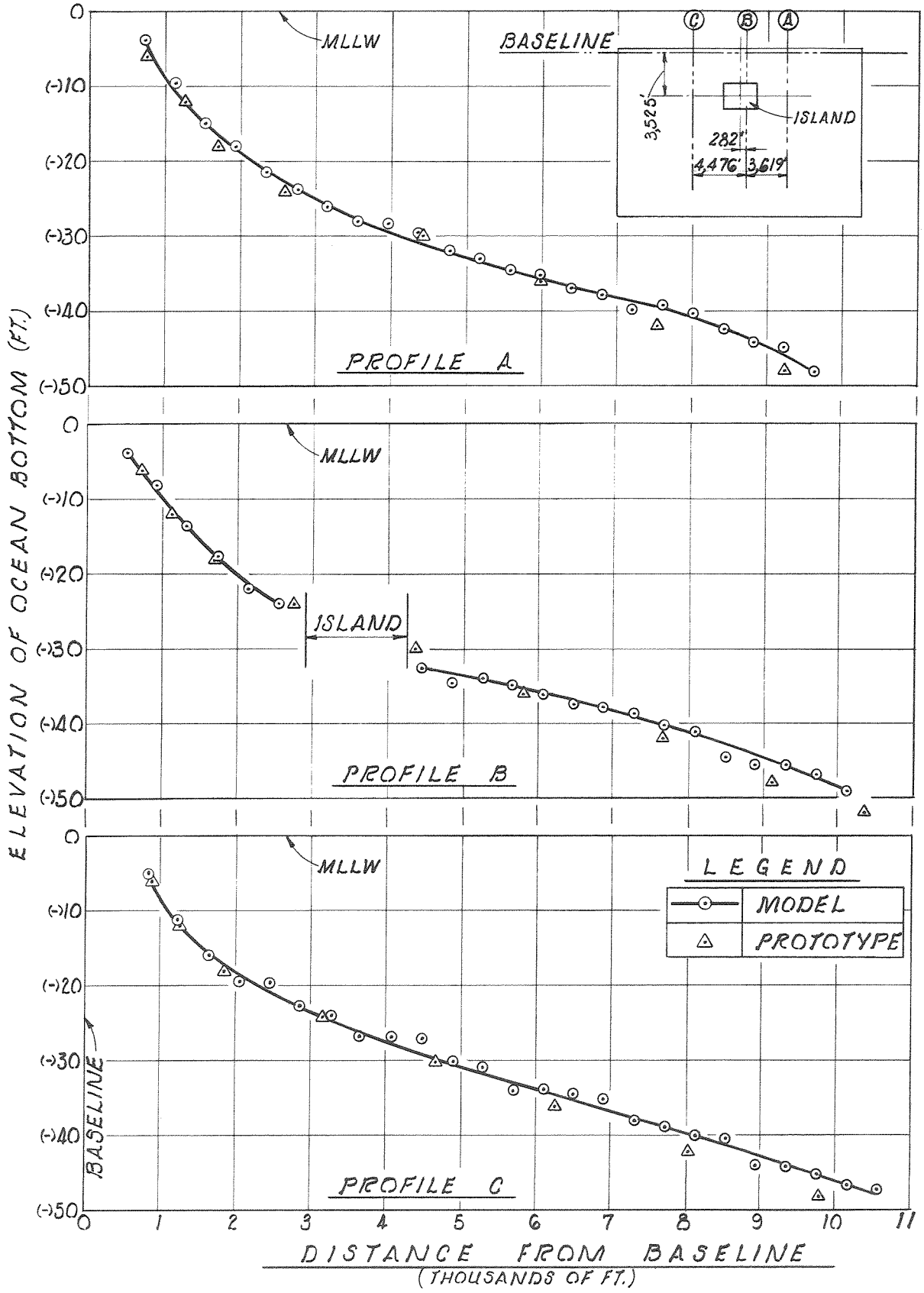

Figure 2.20 Profiles of the Prototype and the Three-Dimensional Model Ocean Bottom at Three Locations in Model Basin

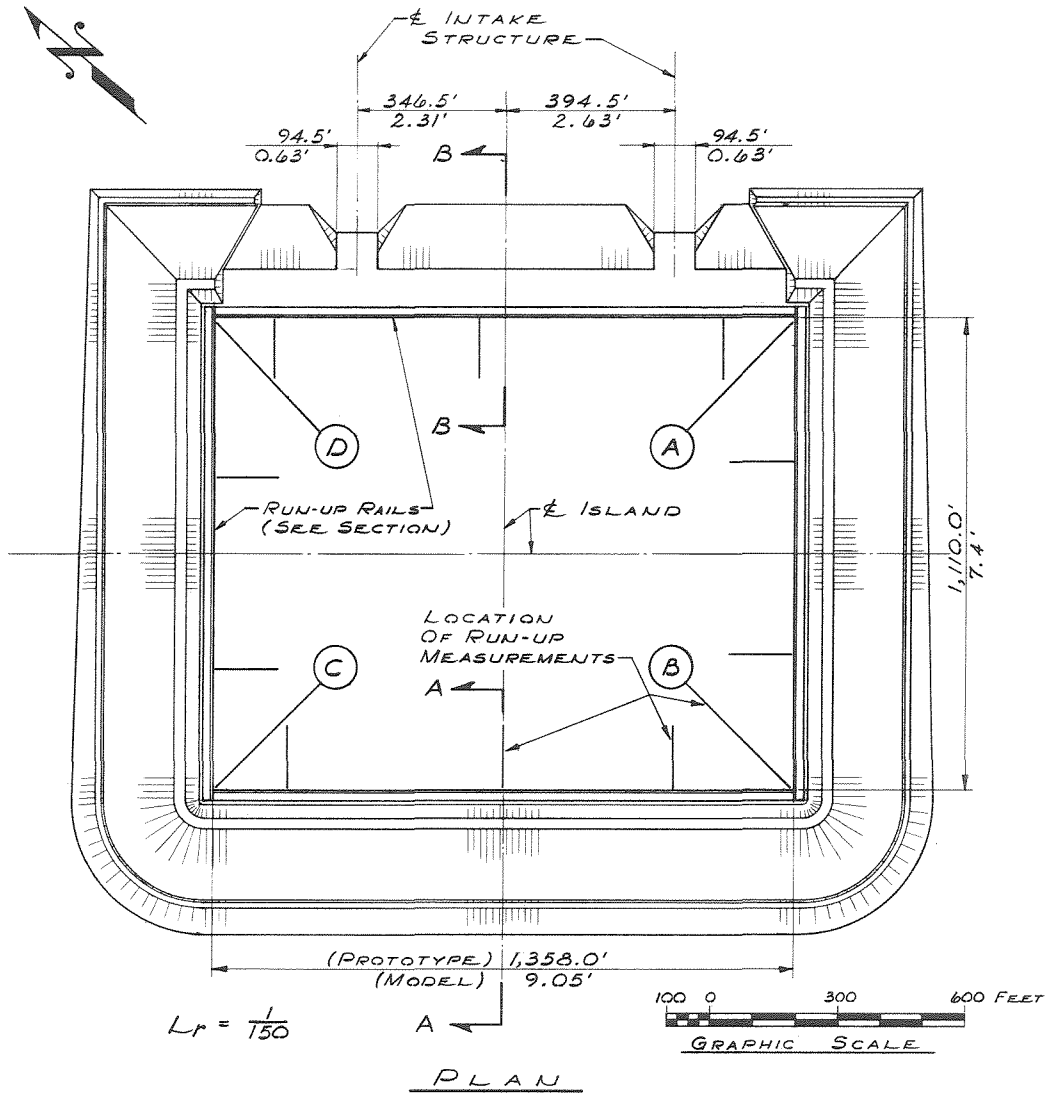

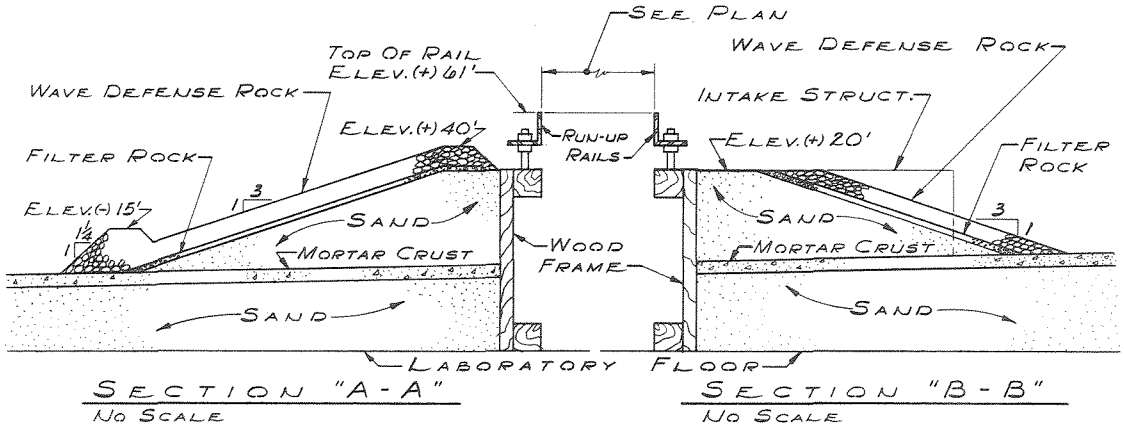

Figure 2.21 Island Configuration in Three-Dimensional Model

The lower portion of Fig. 2.21 shows the ocean bottom consisting of the mortar crust and underlying sand coming up to the wooden form. The island face is then located over this mortar crust. Sand and a filter layer were first placed around the island to form a base for the model armor facing. In lieu of using model tribars for the armor it was felt that it was reasonable to replace the tribars in the three-dimensional model with rock. This is considered to be consistent with the objectives of comparing run-up due to oblique incident waves with run-up due to normally incident waves in the wave basin. This will be discussed fully in Chapter Three, Section C.2. This rock was sorted out from gravel by sieving and retaining the fraction held between the 1/2 in. and 3/4 in. sieves. It was placed to the configuration shown in Fig. 2.21 and worked in by hand to form a relatively well-interlocked surface. The aluminum frame running along the wooden form was used as a reference surface for a template which helped in forming the final contours of the island armor.

3. Instrumentation

Resistance wave-gages similar to those used in the two-dimensional study, were used in the three-dimensional study to measure wave height. A photograph of a typical wave gage and its supporting pedestal can be seen in Fig. 2.22. The operation of these wave gages is the same as those shown in Fig. 2.12 and were also used in conjunction with Sanborn recording equipment.

Run-up measurements were made around the periphery of the island using the beam and attached point gage shown in the photograph Fig. 2.23. This beam was a 5-in. extruded aluminum channel with flanges 2-in. wide and had a point gage attached at one end. Scales were attached to each side of the aluminum angle frame and to the beam so that coordinates of the points where run-up measurements were made could be obtained.

The water depths in the vicinity of the causeway in the lee of the island, were too small to permit the use of resistance-type wave gages to measure wave height. Elevations of wave crests in this zone were measured by means of the point gage and tripod also shown in

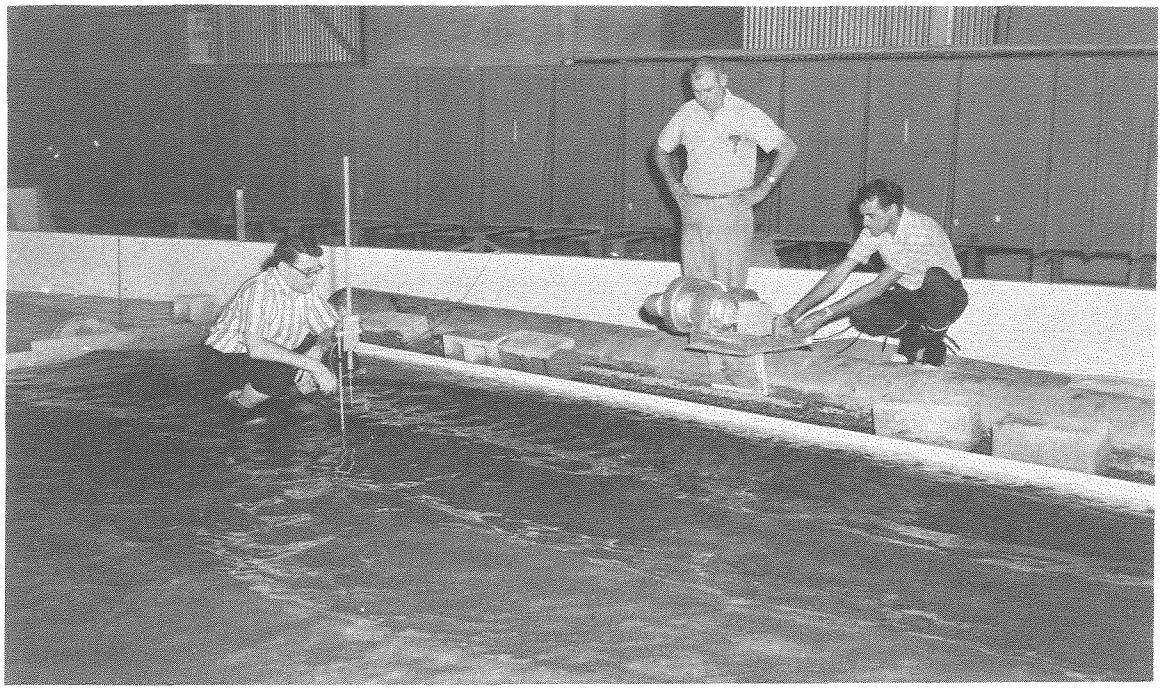

Figure 2.22 Wave Gage on Pedestal and Pneumatic Wave Generator

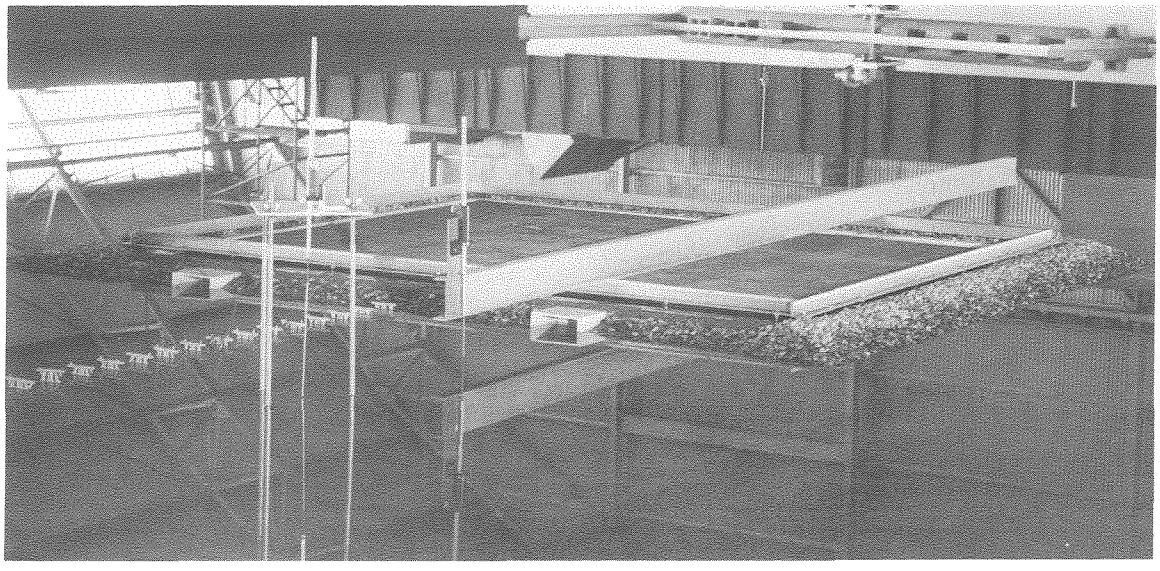

Figure 2.23 Run-Up Beam and Point Gage with Tripod Support

the photograph Fig. 2.23. The difference in elevation between the wave crest and the bottom was obtained directly with this point gage. The elevation of the bottom was obtained by measuring down from a still water surface of known elevation so that the elevation of the wave crest could then be calculated. This device provided a relatively simple method of obtaining the maximum elevation of water surface at any particular location, and it was also used in later experiments to obtain water depths at various desired points in the basin.

4. Summary of Testing Procedures and Observations

a. Wave Measurements

The locations of the pneumatic wave generators in the wave basin are shown in Figs. 2.24a, 2.24b, and 2.24c. Fig. 2.24a shows the location of the wave machines for the case of normal incidence where the wave approaches the island from azimuth 230°. In Fig. 2.24b the wave machines are oriented so that with the natural refraction, the incident wave at the island is at an azimuth of 200°, and in Fig. 2.24c the wave machines are oriented so that the wave direction at the island is at an azimuth of 240°. In each of these figures the locations of the wave gages that were used to determine the wave heights at and near the island site are indicated. The choice of these locations will be discussed more fully in Chapter Three, Section C.1. All dimensions shown are to a prototype scale. For convenience a grid based on the California Coordinate System for Zone 6 is reproduced in Fig. 2.24.

b. Run-Up

Run-up measurements were taken in the three-dimensional model at the locations indicated in the plan view of the model island shown in Fig. 2.21. These measurements were essentially the same as those made in the two-dimensional tests, and consisted of recording the coordinate locations for each run-up measurement and the measurement of the elevation of the water surface at its maximum ascent. Particular attention was given in these measurements to the determination of the run-up on the island corners for both normally incident and obliquely incident waves.

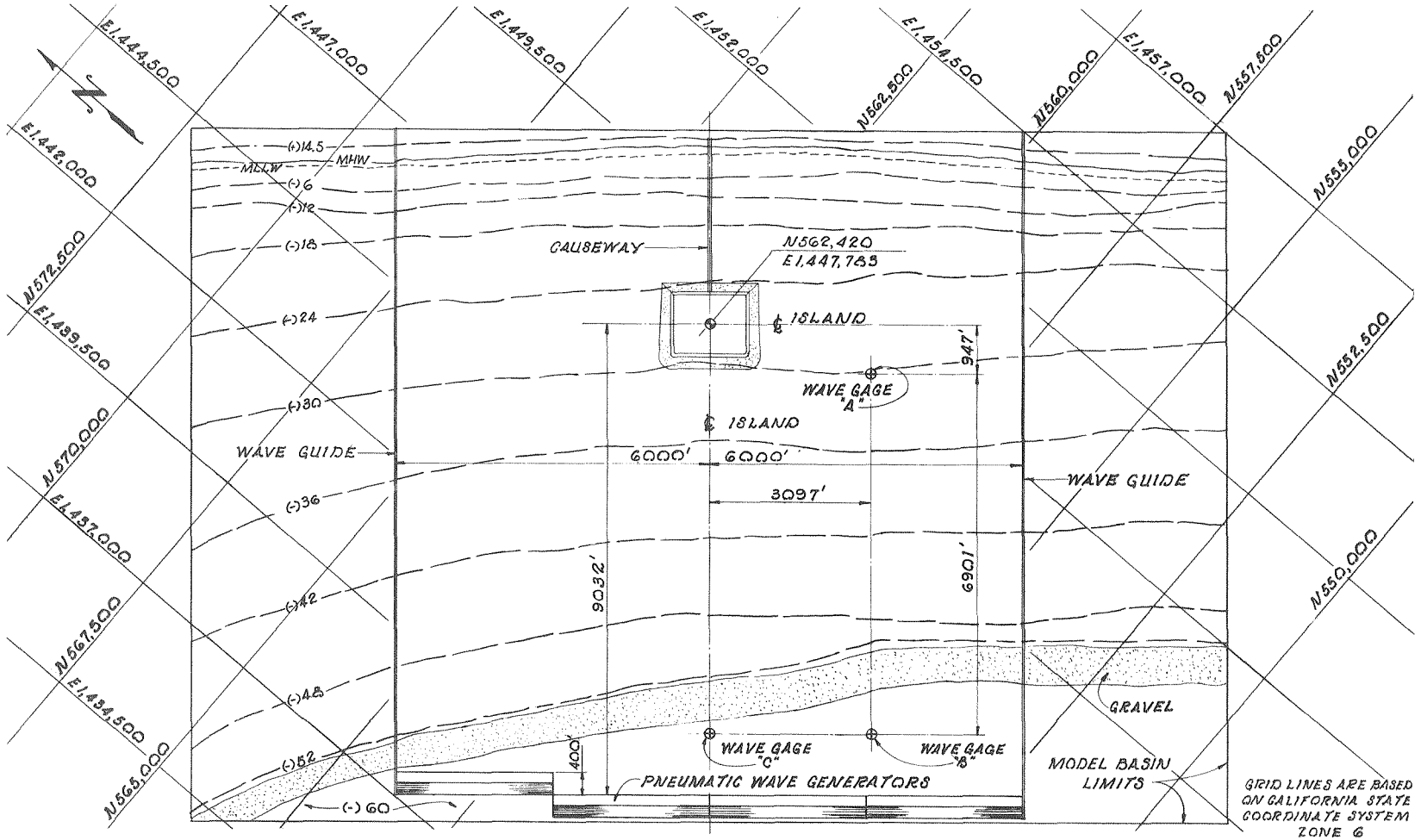

Figure 2.24a Location of Pneumatic Wave Generators for Wave Direction Azimuth of 230° at Island

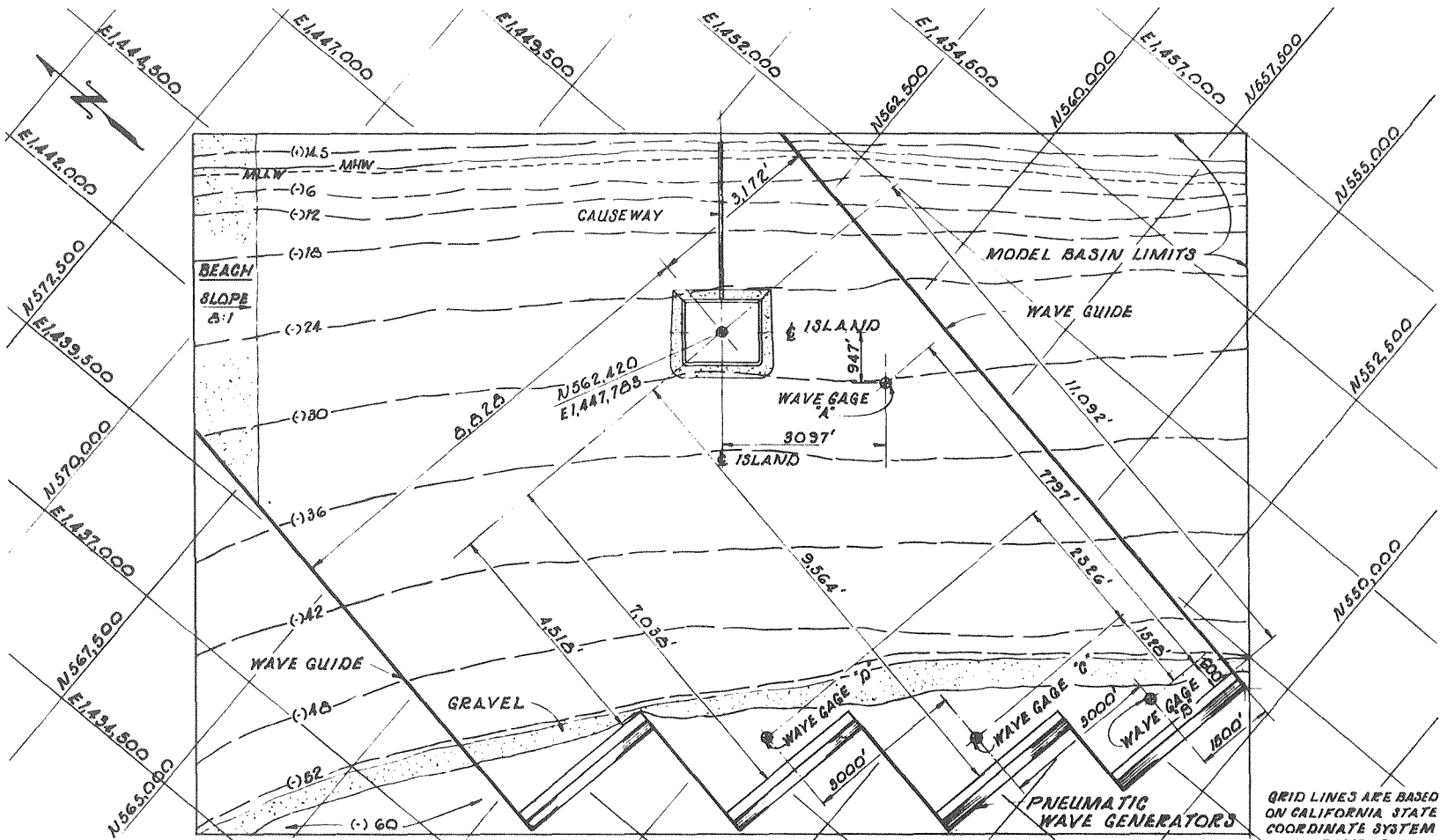

Figure 2.24b Location of Pneumatic Wave Generators for Wave Direction Azimuth of 200° at Island

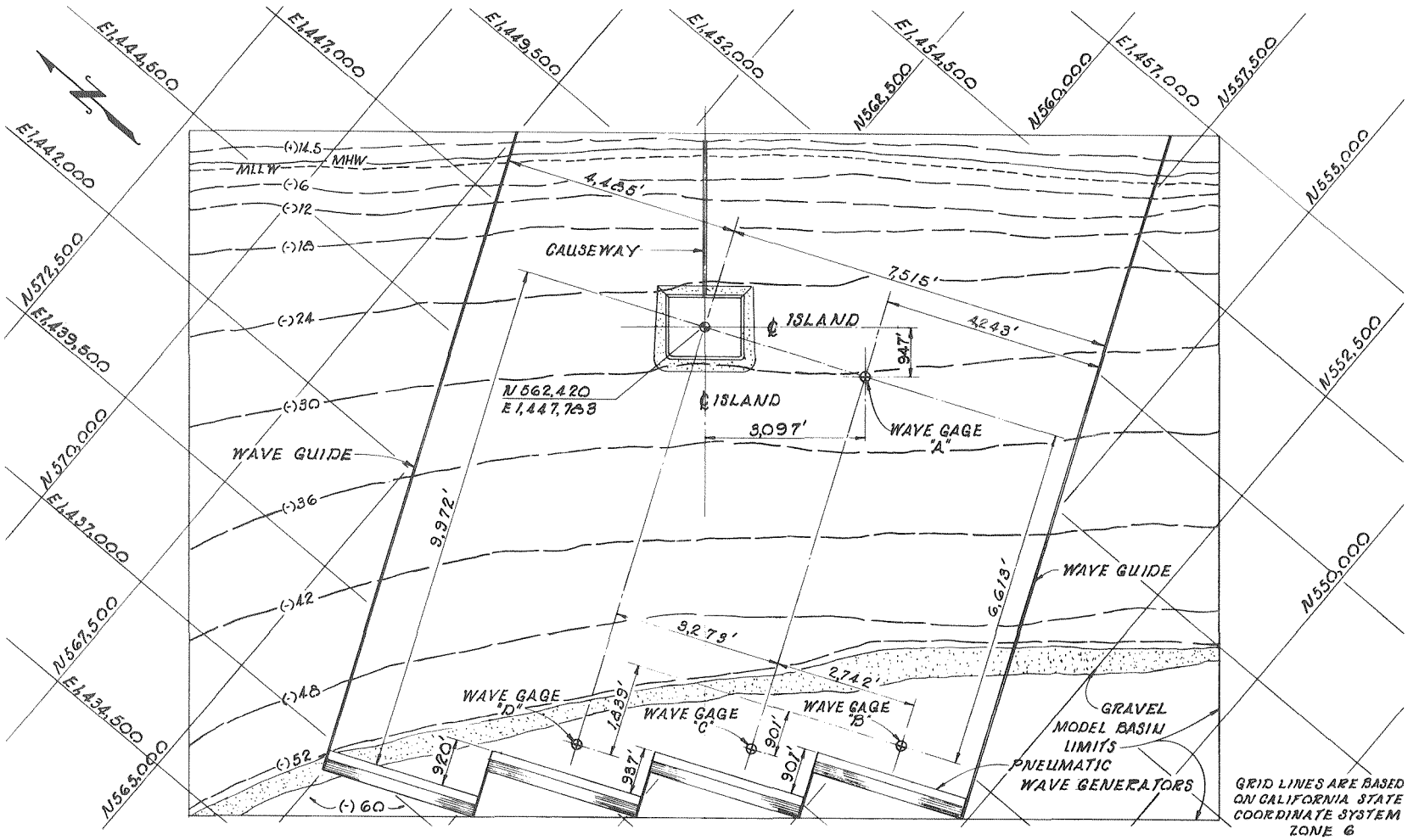

Figure 2.24c Location of Pneumatic Wave Generators for Wave Direction Azimuth of 240° at Island

c. Lee Wave System

Using the tripod support structure shown in Fig. 2.23 measurements were made in the lee of the island of the maximum water surface elevation for the cases of oblique wave incidence, i.e., the wave machine orientations shown in Fig. 2.24b and 2.24c. Wave heights were measured at nine locations along the causeway using this instrument. Similar measurements were made near the island at the intake structures using the beam and point gage shown in Fig. 2.23.

d. Overhead Photographs

All overhead photographs were taken from a camera tower located above the model basin. The photographs were taken using a 4 in. x 5 in. camera with a 90 mm lens. The plane of the 4 in. x 5 in. sheet film was located 51.7 ft. above the laboratory floor which corresponds to a prototype elevation of approximately 7750 ft. The position of the camera can be seen in Fig. 2.19a where it has been projected onto the plane of the model. The distances between the aluminum angles attached to the wooden form of the island and the distance between the intake structure shown in Fig. 2.21 provide a scale for the overhead photographs. The dimensions in this figure are given for both model and prototype to facilitate interpretation of the photographs.

e. Testing Procedure

The testing procedure for all runs excluding the preliminary runs at normal wave incidence was as follows. The wave machine period and blower speeds were first adjusted using a stop watch and electronic tachometer respectively. The phase of the wave machines was then adjusted by adjusting the differential Selsyns so that a continuous wave crest was obtained. Wave records were obtained at the various gage locations at the same time as run-up measurements were being made at the island. For the obliquely incident waves the additional measurement of maximum water surface elevation in the lee of the island was made at this time. After all

run-up measurements were obtained for the various wave heights at a particular incident wave direction, overhead photographs were taken. Wave heights were also recorded at the gage locations near the wave machines while photographs were being taken. Close-up still photographs were taken of the island corners for each incident wave direction and for conditions of both high and low tide. Still photographs were also taken of the wave system in the lee of the island. Motion pictures were taken of the wave system along all four faces of the island for these conditions.

CHAPTER THREE

PRESENTATION AND DISCUSSION OF RESULTS

A. MODEL LAWS AND WAVE ENVIRONMENT

The fundamental requirement for a satisfactory hydraulic model is for the forces which are important in determining the fluid behavior in the prototype to be important to the same relative degree in the model. These forces are: gravity forces, viscous forces, elastic forces, and surface tension forces. Since it is impossible in a practical model to properly model all of these forces a compromise must be made.

In problems dealing with water waves it is usually assumed that gravity forces are more important in the prototype than the other forces mentioned above. Therefore, in this investigation the Froude Law will govern the model-prototype relations. Since both the two-dimensional and the three-dimensional models are built to an undistorted scale, the primary modeling relationship is:

$$V_r = L_r^{1/2} \tag{3.1}$$

where the subscript r indicates the ratio of model quantities to prototype quantities; hence, V_r is a velocity ratio and L_r is a length ratio. From equation (3.1) the time scale is then:

$$T_r = L_r^{1/2} \tag{3.2}$$

Equation (3.1) results in a transfer function for unit discharge (cfs/ft) of:

$$q_r = L_r^{3/2} \tag{3.3}$$

and total discharge (cfs) of:

$$Q_r = L_r^{5/2} \tag{3.4}$$

The wave environment at the island site was determined by hindcasting studies conducted by Marine Advisors, Inc. (Ref. 2 - Appendix D) with interpretation of these data presented by Lillevang (Ref. 2 - Appendix B).

The most severe condition for wave attack at the island site is considered to be the simultaneous occurrence of high waves and high tide. Therefore, the design depth at the island is composed of the depth associated with mean lower low water level (MLLW) plus the combined effect of the highest astronomical tide level above MLLW expected at the time of the design storm and the amount of wind set-up caused by this storm. The latter two quantities are predicted to be 7 ft. and 1 ft. respectively resulting in a maximum depth at the island of 38 ft. A value for low tide of -2 ft. with respect to MLLW was used which results in a depth at the island site of 28 ft. for this tidal stage.

The design wave for the seaward and downcoast faces of the island is based on the storm of September 15-25, 1939. The period associated with the highest one-third waves of that storm was 14 sec. For an interval of 25 years the anticipated highest individual wave was calculated to be 28 ft. This is considered to be a wave which could be present at the island site if the island were not present. This concept will be discussed more fully in Section B. 2. b of this Chapter. The direction in deep water of this design wave is from azimuth 175^{o}.

Lillevang (Ref. 2 - Appendix B) has considered in his original island design that the period of this wave is known to a degree of uncertainty of ±15%. Therefore, the possibility of the design wave having a period of 16 sec., 14 sec., or 12 sec. was considered in this investigation. However, for a storm such as this, the 16-sec. wave is considered to be more unrealistic than the two smaller wave periods.

The design wave chosen for the upcoast face of the island is a 10-sec. wave with a height of 20 ft. and an azimuth direction in deep water of 270^{o} (Ref. 2 - Appendix B).

The wave environment at the island site is presented in Table 3.1 where the conditions for testing are described for both the two-dimensional and the three-dimensional models. The wave heights shown in this table are from the hindcasting predictions; the actual wave heights which would be attained with the island present will be discussed later. The direction of the waves at the island site are shown in the last column of this table, and they were obtained from refraction studies performed by Marine Advisors, Inc.

Table 3.1. Wave Environment at Island Site Used in Model Study.

Model	Tide Stage (ft)	Periods	Maximum Wave Height (ft)	Azimuth Directions of Wave	
				In Deep Water	At Island Site
Two-Dimensional	MLLW+8	16, 14, 12	28	--	--
	MLLW-2	16, 14, 12	20.5	--	--
Three-Dimensional	MLLW+8	16, 14, 12	28	230°	230°
	MLLW+8	16, 14, 12	28	175°	200°
	MLLW-2	16, 14, 12	20.5	175°	200°
	MLLW+8	10	20	270°	240°
	MLLW-2	10	20	270°	240°

B. TWO-DIMENSIONAL MODEL

1. Wave Data Reduction Procedure

As described in Chapter Two, Section A.4 the incident wave was determined from the wave envelope measured in the section of the tank having a horizontal bottom. This was accomplished in the following way.

An incident wave of sinusoidal form is assumed to approach the island. This wave is represented mathematically by:

$$\eta_i = a_i \sin (kx - \sigma t) \tag{3.5}$$

where η_i is the variable elevation of the water surface measured from the still water level, a_i is the incident wave amplitude, k is the wave number $2\pi/L$ (where L is wave length), σ is the circular frequency $2\pi/T$ (where T is wave period), and x and t represent the distance coordinate and time respectively. This wave will reflect from the island section, after dissipating some energy, and travel toward the wave generator (see Fig. 3.1a); it can be described by the following expression:

$$\eta_r = a_r \sin (kx + \sigma t + \varphi) \tag{3.6}$$

where a_r is the amplitude of the reflected wave which is different from a_i and φ is a phase angle. The wave length, L, and the wave period, T, would be the same for both waves.

Equations(3.5) and (3.6) can be superimposed, i.e., added, and if the resultant form is maximized with respect to time, the wave envelope given by the following equation results:

$$\eta_{env} = \sqrt{a_i^2 + a_r^2 + 2 a_i a_r \cos (2kx + \varphi)} \tag{3.7}$$

The maximum of Equation (3.7) is:

$$\eta_{env_{max}} = a_i + a_r \tag{3.8}$$

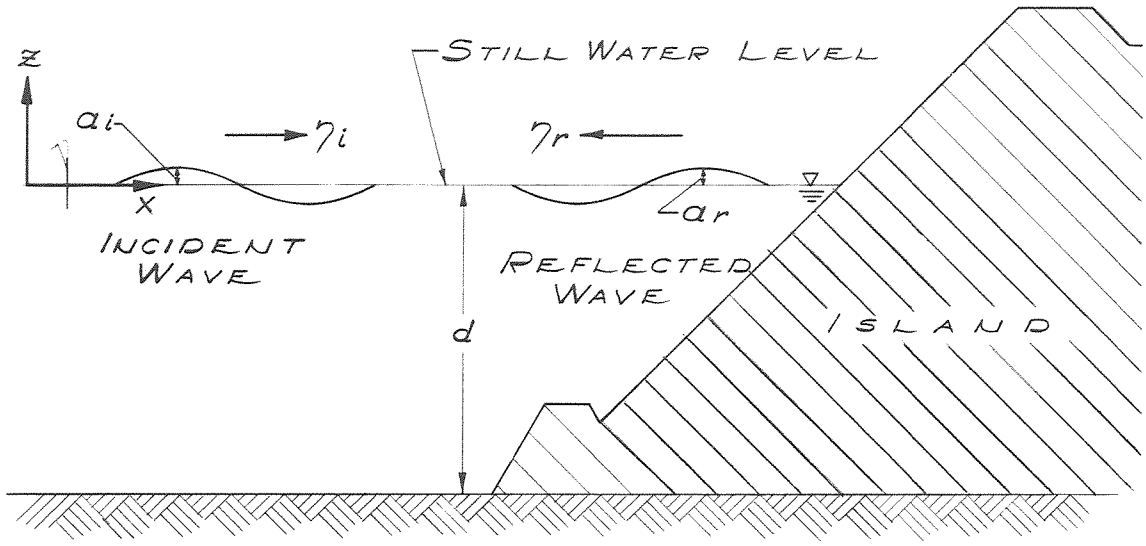

Figure 3.1a Incident and Reflected Wave System

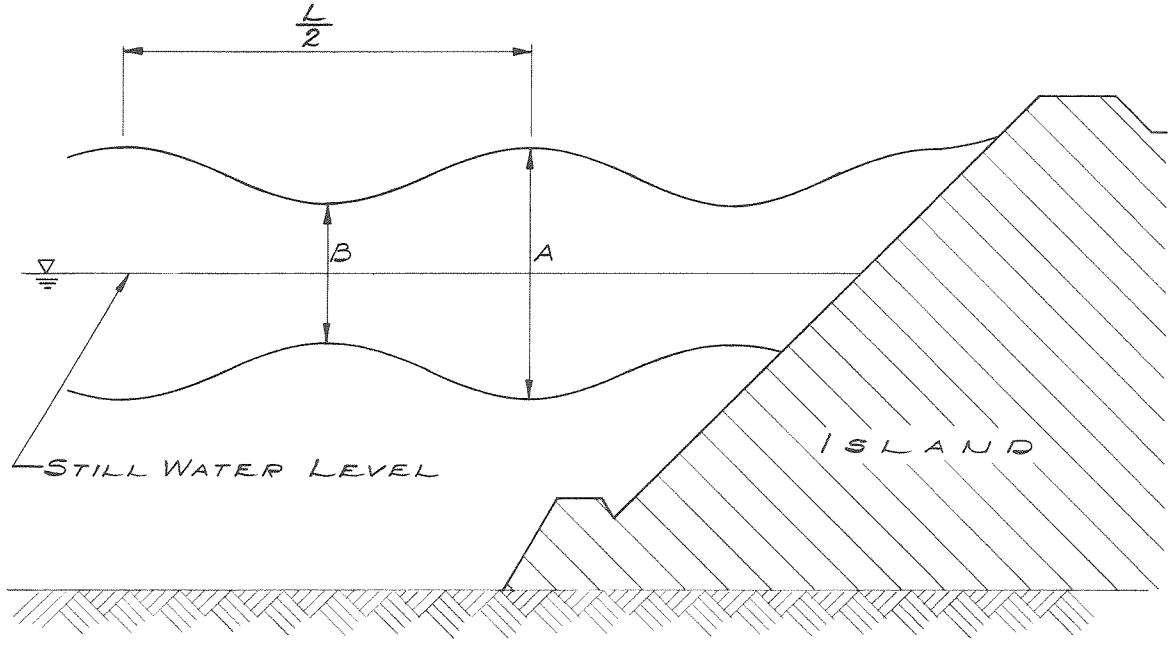

Figure 3.1b Resultant Wave Envelope

and the minimum is

$$\eta_{env_{min}} = a_i - a_r \tag{3.9}$$

or in terms of wave height, and with reference to Fig. 3.1b, equations (3.8) and (3.9) give

$$H_i = \frac{A+B}{2} \tag{3.10}$$

$$H_r = \frac{A-B}{2} \tag{3.11}$$

In the presentation of results the wave height referred to as H is the incident wave height obtained from equation (3.10).

Admittedly this method is not directly applicable to a study where the waves of interest have finite amplitudes and are the maximum possible waves in a particular depth of water. For that case the waves would no longer be sinusoidal, as shown in equation (3.5), but, for the wave lengths of this study, would approach a cnoidal wave form. To the authors' knowledge an analytical method does not exist where an envelope obtained for cnoidal waves can be reduced into its incident and reflected wave components. Therefore, due to the limited time available, the small amplitude analysis presented above was used in this investigation to determine heights of the incident and reflected waves.

Despite the shortcomings of the method, confidence in this approach can be gained from a brief discussion of the variation of the magnitude of the reflection coefficient (defined as H_r/H_i) obtained using this small amplitude wave theory. In all of the experiments conducted this varies from approximately 30% to 15%. This means that the reflected wave energy is less than 10% of the incident energy. The higher value of the reflection coefficient usually occurs at small values of the ratio of the incident wave height to the depth. In this region the small amplitude theory presented would apply. At large values of the relative wave height, i.e., the ratio of the incident wave

height to the depth, a major portion of the incident wave energy is dissipated at the island, and only a small portion of the energy would be reflected. Therefore, for this case the values of A and B shown in the envelope in Fig. 3.1b would differ by a small amount, and this method would be reasonably applicable. In fact, it is interesting to note from equations (3.10) and (3.11) that even for a value of A, 35 percent greater than B the reflection coefficient H_r/H_i defined above would only be 15 percent and the reflected wave energy would only be of the order of 3% of the incident energy.

In summary it is felt that for small values of the relative incident wave height (H_i/d) and for large values of this quantity this method used for analysis of the wave envelope gives reasonable results.

2. Results of Two-Dimensional Model Studies

a. Stability of Wave Defense

The first major objective of the two-dimensional study was to investigate the stability of the wave defense proposed in the original design. As described in Chapter Two, Section A.4 the evaluation of the stability of the structure was based on three kinds of observations. Visual observations of any movement were made during an experiment, cross-sectional profiles were obtained after the model had been built and after most series of experiments, and overhead photographs were taken before and after most series of experiments. The results of the stability investigation will be discussed in this section by summarizing the results of observations of the types described above.

Drawings of the various models which have been tested are presented in Figs. 3.2a, 3.2b, 3.2c, and 3.2d. These drawings are in terms of the prototype dimensions and show the various armor layers used and the appropriate unit weights which are represented in each model as well as the limit of the model wave defense.

The visual observations relative to stability for each series of experiments are summarized in Table 3.2 for the three sections of the wave defense: the toe-rock section, the tribar section, and the

WAVE DEFENSE ELEMENTS	WEIGHT (TONS)
TRIBARS	18.9
"B" ROCK	4 TO 10
"C-1" ROCK	1 TO 4
"D" ROCK	< 1 TON

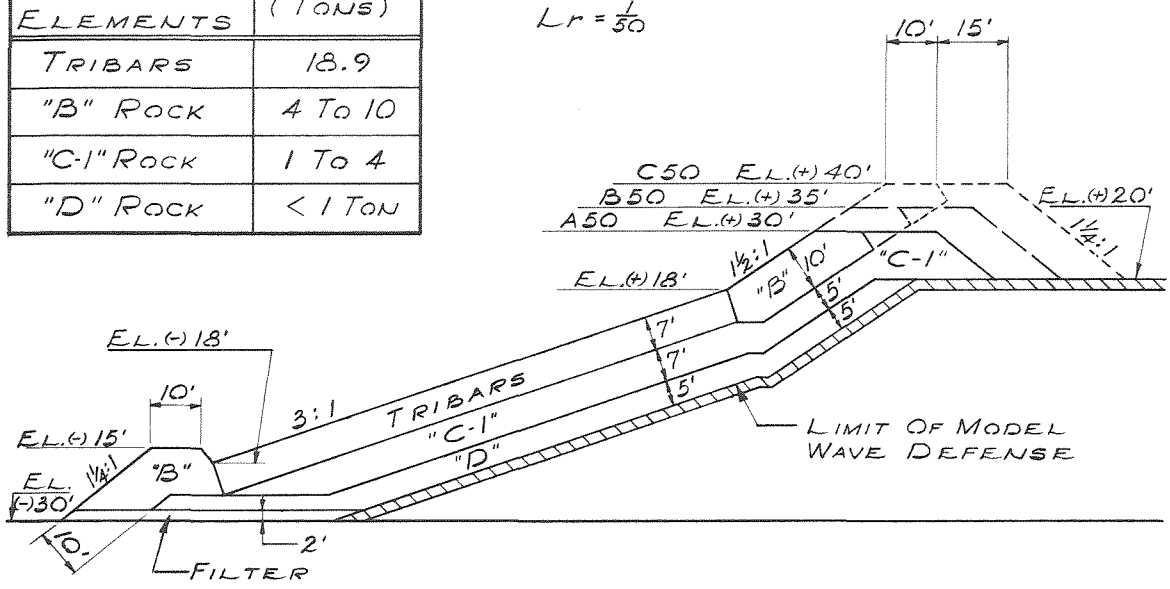

Figure 3.2a Profile of Prototype Island Face for Experimental Series A50, B50, C50 (L_r = 1/50)

WAVE DEFENSE ELEMENTS	WEIGHT (TONS)
TRIBARS	9.7
"B" ROCK	2.1 TO 5.1
"C-1" ROCK	0.5 TO 2.0
"D" ROCK	< 0.5 TON

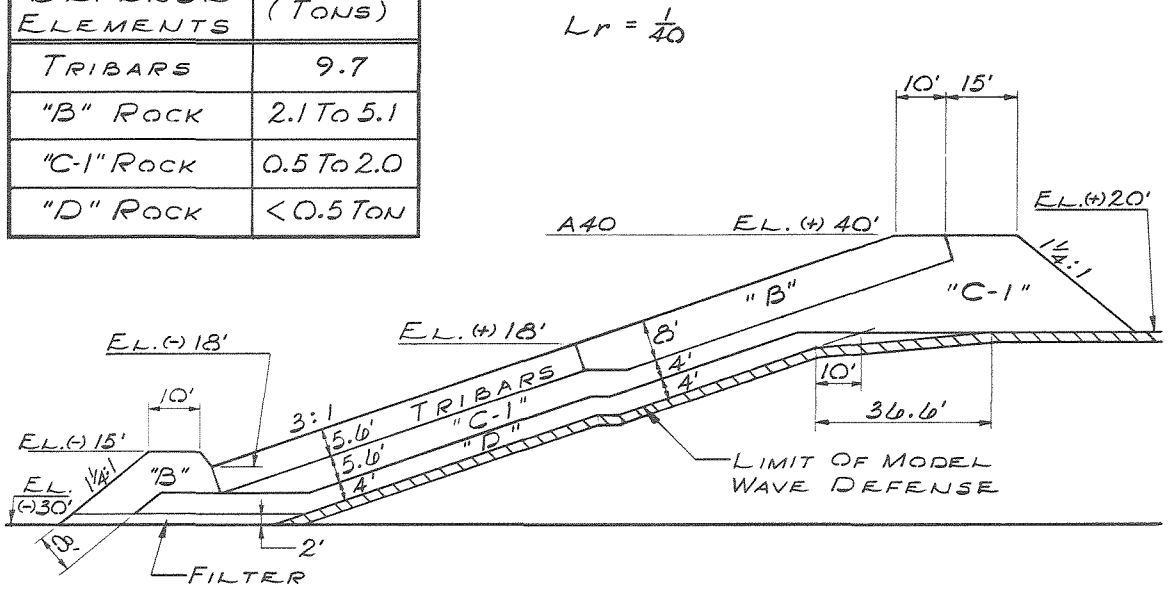

Figure 3.2b Profile of Prototype Island Face for Experimental Series A40-1, A40-2 (L_r = 1/40)

WAVE DEFENSE ELEMENTS	WEIGHT (TONS)
TRIBARS	13.8
"B" ROCK	2.9 TO 7.3
"C-1" ROCK	0.7 TO 2.9
"D" ROCK	<0.7 TON

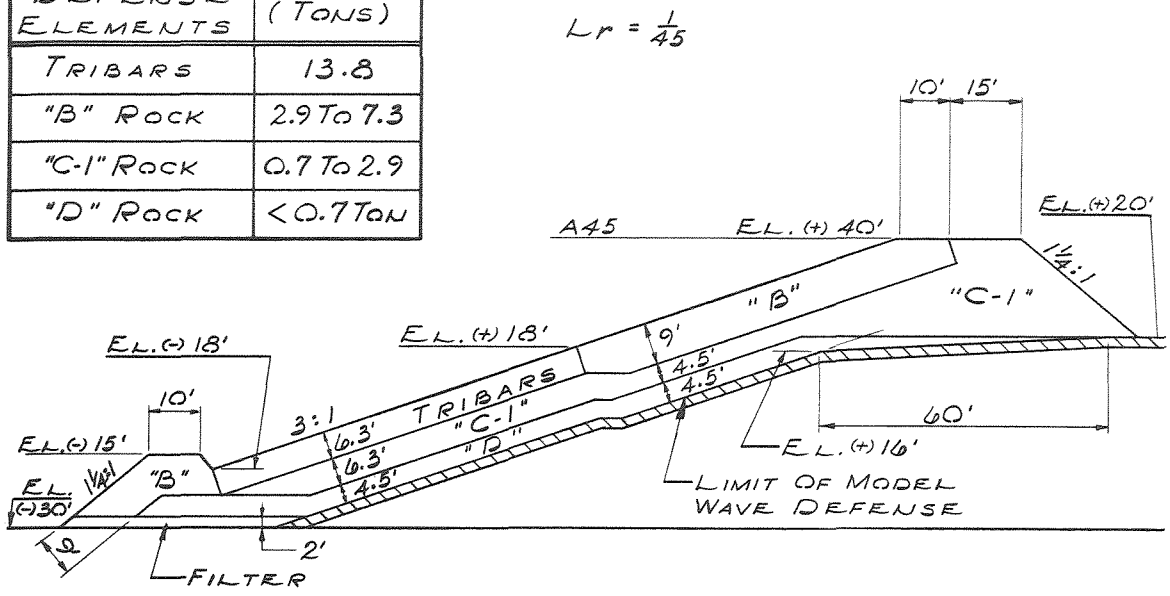

Figure 3.2c Profile of Prototype Island Face for Experimental Series A-45 (L_r = 1/45)

WAVE DEFENSE ELEMENTS	WEIGHT (TONS)
TRIBARS	13.8
"B" ROCK	2.9 TO 7.3
"C-1" ROCK	0.7 TO 2.9
"D" ROCK	<0.7 TON

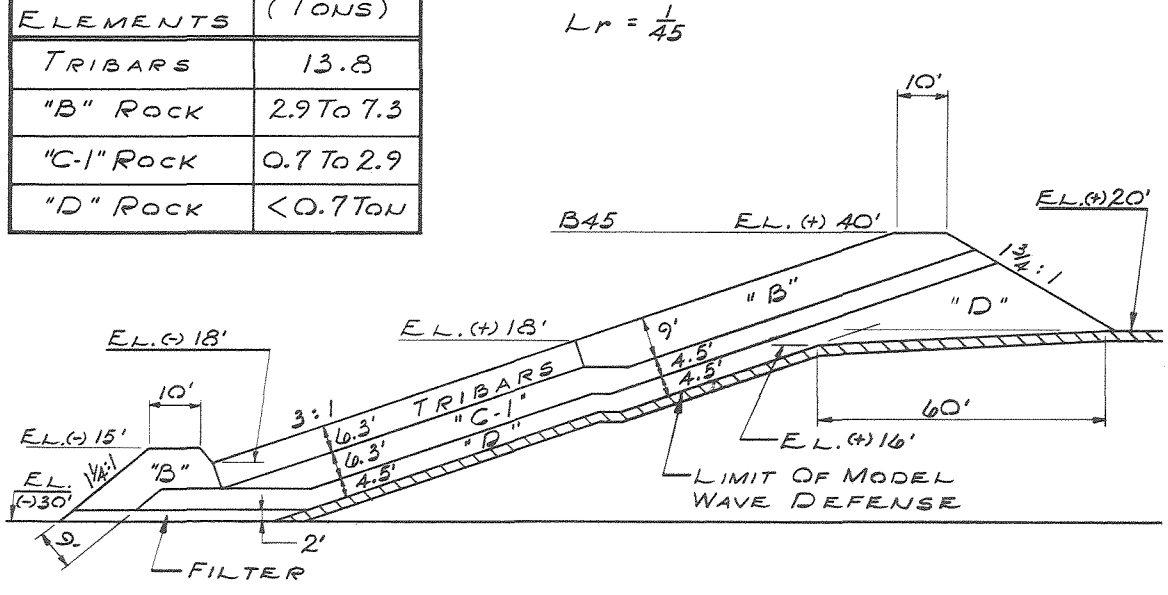

Figure 3.2d Profile of Prototype Island Face for Experimental Series B-45 (L_r = 1/45)

Table 3.2. Summary of Stability Observations in Two-Dimensional Model.

Experiment No.	T (sec)	Tide Stage MLLW± (ft.)	General Comments on Model	Summary of Observations		
				Toe-Rock	Tribars	Cap-Rock
1:50 Scale Model						
A50	14	+8	Original design	Maximum of approximately 4 to 5 rock in oscillatory movement	No observable movement	Movement due to overtopping
C50	14	+8	Crest elevation increased to +40	Minor movement	No observable movement	Movement due to overtopping
1:40 Scale Model						
A40-1	14	+8	Cap-rock not firmly interlocked with tribars	Some upslope movement of material for H/d = .618	Top row (elev +18) most vulnerable, 10 to 12 units in top row moved partially out of position and tilted in upslope direction; progressive failure of tribar face begins here; approx. 18 tribars dislodged and carried up onto cap rock by end of series.	Major problem appears to be interlocking of cap-rock with first tribar row; dislodged cap-rock first rolls upslope and then carried downslope
A40-2	14	+8	Island face rebuilt carefully so cap-rock firmly interlocked with tribars	Small movement	Rocking of one unit observed for H/d = .39; deformation of surface; general upthrust of one area and sinking of another, partial displacement of 2 units in top row; one unit 3 rows down from tribar-cap-rock interface is rotated, legs now in tilted position; violent rocking of 2 units at interface of tribar and cap-rocks.	Significant number dislodged; rock is first dislodged and then moved downslope onto tribar section; cap-rock surface rearranged.
1:45 Scale Model						
A45	14	+8	Backslope of wave defense modified	5 rocks oscillating; 1 rock dislodged and moved offshore	No observable movement	1 rock dislodged and moved down onto tribar face
B45-1	14	+8	Final model tested	4 to 6 rock oscillating throughout experiment; 1 rock dislodged and moved up to bottom row of tribars	In early experiments 2 units rocking; latter part no observable movement	Approximately 7 units rocking at higher waves; 1 rock violently dislodged, moved downslope onto tribars and then back up onto cap-rock
B45-3	16	+8	Tribar and cap-rock section rebuilt	8 units rocking; 7 rocks dislodged and moved offshore; 5 rocks dislodged and moved to bottom row of tribars	2 units rocking in early part of run; in latter part of run this motion has ceased	1 rock dislodged; 4 to 6 units rocking at large wave heights
B45-4	12	+8	Same model as B45-3	5 units rocking	No observable movement	2 units rocking
B45-4	12	-2	Same model as B45-3	6 units rocking; upon examination at end of run toe section seems to have slumped somewhat	Motion of 1 moderately rocking unit ceased in latter part of run	Run-up to elev. +14.5, tribar-cap-rock interface at elev. +18
B45-6	16	-2	Same model as B45-3	2 units rocking	No observable movement	Run-up to elev. +16, tribar-cap-rock interface at elev. +18
B45-7	14	-2	Same model as B45-3	1 unit rocking	No observable movement	Run-up to elev. +15.2, tribar-cap-rock interface at elev. +18

cap-rock section. In most cases the observations presented are themselves a summary of the observations at all wave heights for a particular wave period and tide stage. In a few cases where important events occurred the ratio of incident wave height to depth has been presented.

In the 1:50 scale model, where the tribar weight was 18.9 tons and the various rock weights are as indicated in Table 2.1 and 2.2, it was observed that there was essentially no movement of the tribars. However, there was slight movement of some cap-rock and some toe-rock. If one neglects damage due to overtopping, then it can be said that major movement in this model occurred in the toe-rock section. Due to overtopping of the structure the cap-rock section suffered considerable damage. The overtopping, and corrective procedures taken will be discussed more fully in a later section.

Since there was essentially no movement observed in the tribar section for this model scale, it was decided to increase the scale of the model to 1:40 thereby reducing the equivalent prototype weights of all elements. This particular model scale was chosen so that, according to the literature, the tribars would be at a condition of incipient failure for high waves. In addition, the original design of the island face was modified so that the defense was built on a continuous slope (3 horizontal to 1 vertical) up to elevation +40 ft. The equivalent prototype weight of the tribars was reduced to 9.7 tons by this scale change, and the equivalent weights of the rock in this model are presented in Tables 2.1 and 2.2. Table 3.2 shows that in general the motion of various elements in this model increased significantly. This is the result of the increase in model scale and consequent reduction in equivalent weights of the armor units.

The first model built to this scale (denoted by A40-1 in Table 3.2) was built without taking an extreme amount of care in interlocking the tribars and the row of cap-rock which forms the interface between the tribar section and the cap-rock section. With a wave at prototype height of 23.5 ft. this model was damaged severely. The damage appeared to be precipitated by dislodging cap-rock from the interlocking row at the tribar interface. In general in all experiments

where the cap-rock was dislodged it was first rolled upslope. In some cases this dislodged rock remained in the cap-rock section. In other cases it was moved down onto the tribar face by the backrush of the wave. With the displacement of the cap-rock, tribars were plucked out of the tribar section, starting with the uppermost row, and moved up onto the face of the cap-rock. There was also some observed movement in the toe-rock, although this was certainly small compared to that in the cap-rock.

The design of the A40-1 series was retained and the model was rebuilt and is designated as Series A40-2. A great deal of care was taken in rebuilding this model with particular attention given to the cap-rock and to the interlocking region between the cap-rock and the tribars. As was expected, this model did not show the large deterioration experienced in the A40-1 series. However, there was a significant readjustment of the cap-rock with perhaps 25 to 30 cap-rocks moving down onto the tribar section. At a prototype wave height of about 22 ft. one tribar in the second row from the rock interface was plucked from its original position, rotated and then it fell back into the space tilted on end and with this wave a few other tribars were observed to be rocking. The tribar surface which was originally plane appeared to have been deformed, i.e., some areas appeared to be at a higher elevation than previously and other areas were at a lower elevation than previously. The upper two rows of tribars were significantly disoriented with the downslope leg generally raised and the upslope leg lowered. Small motion in the toe-rock was also observed during this run.

In order to increase the equivalent size of the tribars and rock elements over those for the 1:40 scale model, the model scale was reduced to 1:45. This increased the equivalent prototype weight of the tribars from 9.7 to 13.8 tons and increased the equivalent rock weight in accordance with Tables 2.1 and 2.2. The tests with this model showed that the increase in weight of tribars was sufficient to insure stability of the tribar section. Except for some very minor and isolated rocking the tribars were stable. This model was tested completely for waves with three prototype periods: 12 sec., 14 sec.,

and 16 sec., and for the condition of high tide (MLLW+8 ft.) and of low tide (MLLW -2 ft.). In all of the test runs there was some slight to moderate rocking motion in the toe-rock section. For some cases a small number of toe-rocks were dislodged. Due to the run-up on the cap-rock section at high tide there was a readjustment of the cap-rock which was apparent during the run.

These visual observations, for the models with the three different scales, can be summarized as follows. In all cases there was some slight movement observed in the toe-rock section; in some experiments toe-rock was actually dislodged, but generally motion was limited to light to moderate rocking of individual elements. For the two smaller scale models, the tribar weights of 18.9 tons and 13.8 tons were considered to be sufficient for stability. However, when the tribar weight was reduced to 9.7 tons (1:40 model scale) there appeared to be serious movement in this section. Some movement and readjustment of the cap-rock was observed for models with all three scales; however, significant displacements of the cap-rock were observed only for the model built to a scale of 1:40 in which the armor units had the least equivalent prototype weights.

The second method of observing stability was by obtaining initial and final profiles of the wave defense using the point gage and carriage arrangement shown in Fig. 2.11. It should be realized, before discussing the results, that this type of measurement is quite difficult, due to the size of the individual armor units compared to the size of the point gage and the profiles obtained are at best simply averages.

Profiles obtained at three lateral locations along the wave defense are presented in Fig. 3.3 for the A40-2 series of experiments. The profiles shown were obtained on the centerline of the wave defense and 0.5 ft. to either side (20 ft. to either side in the prototype). Three profiles are shown for each lateral location: the design profile, a profile taken after construction, and a profile taken after experiment A40-2B. After that experiment the structure had already been exposed to a prototype wave of height equivalent to 12.3 ft. for

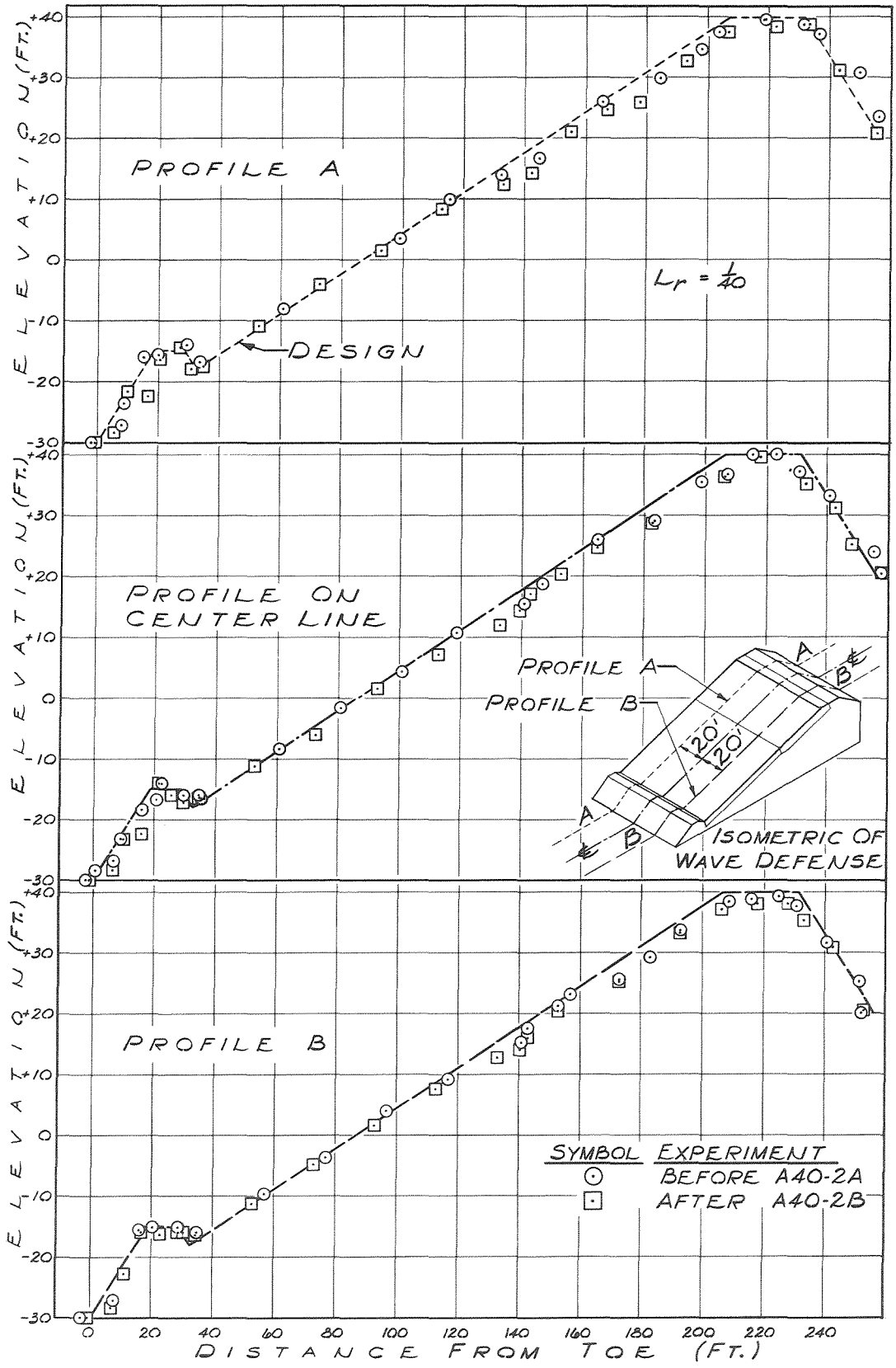

Figure 3.3 Island Profiles in Two-Dimensional Model (L_r = 1/40)

approximately 22 (prototype) hours. It is seen that for these rather small waves there are displacements in the tribar face movements of at most 2 ft. vertically. The toe section on the flume centerline and at one lateral station are also readjusted. The back face of the wave defense at the two locations has also tended to be displaced vertically downward from 2 ft. to 4 ft.

A similar set of profiles is presented in Fig. 3.4 for the 1:45 scale model. In this case four profiles are shown at the same lateral locations as that in Fig. 3.3; due to the change in model scale the lateral profiles are now 22.5 prototype ft. off-center. The four profiles are: the design profile, a profile after construction, and two profiles taken at two different times during the course of testing. It should be noted that, due to experimental error, the toe section of the model was not built exactly to the specifications.

It is seen in Fig. 3.4 that on the centerline at one location the tribar section has changed by approximately 1 ft. from the original profile and at the lateral section, primarily in the region of the cap rock, the change has been at most 2 ft. This is not considered at all serious, considering the duration of time that this structure has been exposed to wave attack. (The durations for these profiles shown are summarized in Table 3.3.) The change in the profile between

Table 3.3. Prototype Wave Exposure in Two-Dimensional Model (Series B45)

Experiment	Wave Period T (sec.)	Tide with respect to MLLW (ft.)	Equivalent Prototype Duration t (hrs)
B45-3A to A45-3O	16	+8	58.5
B45-3P to A45-3T	16	+8	19.7
B45-4A to A45-4I	12	+8	34.9
B45-4J to A45-4S	12	-2	36.2
B45-5A to A45-5I	14	-2	35.3
B45-6A to A45-6J	16	-2	37.5
		Total	222.1 = 9.25 days

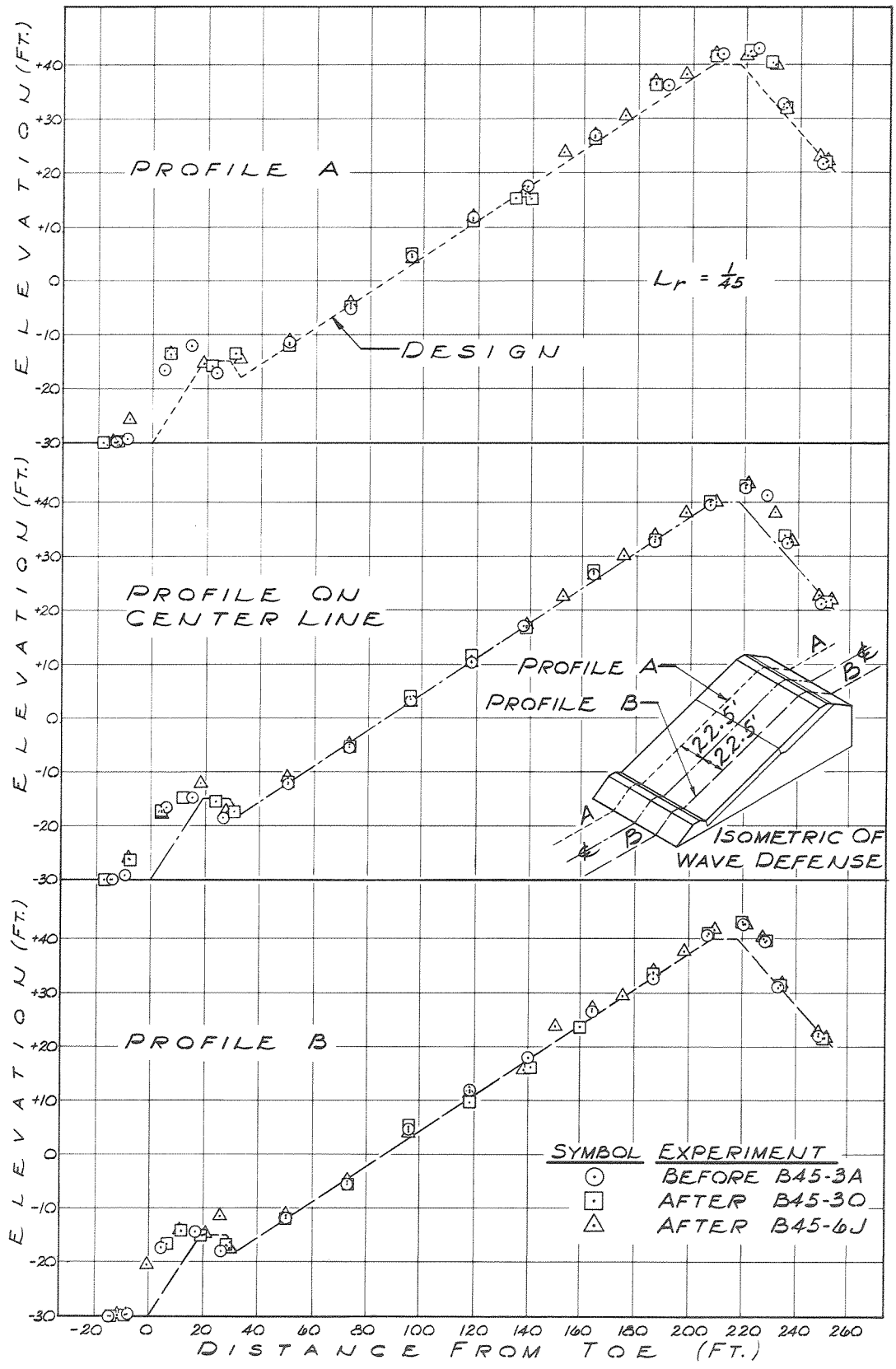

Figure 3.4 Island Profiles in Two-Dimensional Model (L_r = 1/45)

Series B45-3A and Series B45-3O represent a prototype wave attack of 58.5 hours (2.44 days) duration. During this interval of time the structure was exposed to prototype wave heights ranging from approximately 5.6 ft. to 22.2 ft. The last profile represents the cross section after run B45-6J. From Table 3.2 it is seen that this represents an added wave attack duration of 163.6 prototype hours (6.8 days) and represents exposure to waves ranging in period from 12 sec. to 16 sec. for both the case of high and low tides. The wave heights during this period of time ranged from a minimum of about 7 ft. to a maximum of approximately 22 ft.

Therefore, comparing the results shown in Fig. 3.3 to those shown in Fig. 3.4, the displacement of the profile from the original profile for the 1:45 scale model was perhaps slightly less than that indicated for the 1:40 scale model. However, the difference in times of exposure is significant. The duration of the tests of the model with the smaller scale (1:45) was ten times as long as that of the model with the larger scale (1:40).

The results of this type of observation can be summarized as follows. Although small displacements were observed in the 1:45 scale model (tribar weight 13.8 tons), the time of exposure and the range of wave heights was significantly greater for this model than for the case of the model having a scale of 1:40 (9.7 ton tribars). Therefore, this comparison indicates also that the prototype defense having a 13.8 ton tribar is more stable than that having a 9.7 ton tribar.

The third method of evaluating stability was from overhead photographs of the wave defense taken before and after a series of experiments. In Fig. 3.5a the wave defense is shown after construction and in Fig. 3.5b it is shown after experiment A40-1C. The serious damage to the wave defense is evident in Fig. 3.5b. This photograph shows the tribars that have been dislodged and moved up onto the cap-rock section and the portion of the cap-rock which has been dislodged and moved down the slope onto the tribar section. The upper rows of tribars away from this area of complete destruction have been

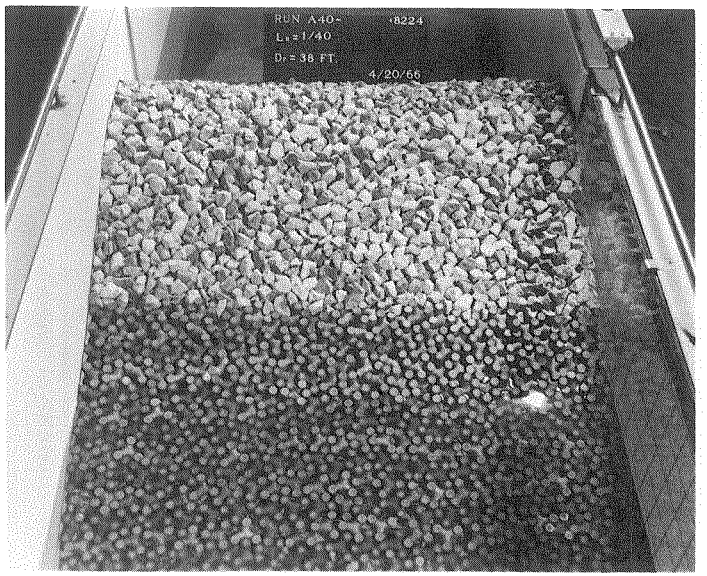

Figure 3.5a Photograph of Island Defense in 1:40 Scale Model Before Testing (Series A40-1)

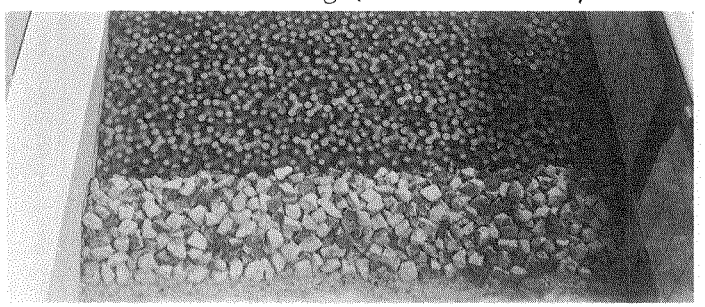

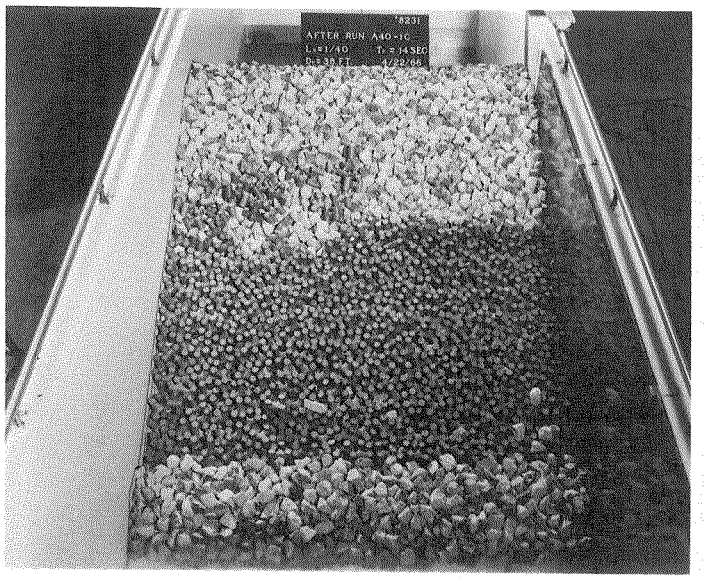

Figure 3.5b Photograph of Island Defense in 1:40 Scale Model After Testing (Series A40-1)

rotated and reoriented. In addition cap-rock has been moved down the slope onto the tribar section.

Overhead photographs of the wave defense are presented in Figs. 3.6a and 3.6b for the A40-2 series. Unfortunately photographs were not taken after construction for this model. However, a photograph is shown in Fig. 3.6a of the wave defense after it had been exposed to a wave with a height equivalent to 12.1 ft. for a period equivalent to 22 prototype hours. Fig. 3.6b shows this same model after it has been exposed to prototype waves of a 14 sec. period and heights ranging from 1.6 ft. to 22.3 ft. for a prototype duration of 66 hours (2.75 days). The cap-rock movement and rearrangement is evident in this figure as well as some reorientation of the tribars in the first tribar row at the cap-rock-tribar interface. Careful study of these two photographs will show some tribars primarily in the upper row which have been reoriented and tilted.

Similar photographs for the 1:45 scale model are shown in Figs. 3.7a, 3.7b, and 3.7c. Fig. 3.7a is an overhead photograph showing the model after construction and Fig. 3.7b is a photograph of the model after being exposed to waves ranging in height from 5.6 ft. to 22.3 ft. for approximately 68.2 prototype hours. A final overhead photograph from this series is presented in Fig. 3.7c taken after Run B45-6J. The structure at that time had been exposed to waves at the three periods, at both high and low tide and a full range of wave heights for a prototype time of 222.1 hours (9.25 days). The feature that is significant in these photographs is the apparent lack of change of the tribar orientation with this long exposure to wave attack. Comparing these photographs to Figs. 3.5 and 3.6 the rearrangement of tribar face for the case representing the 9.7 ton tribar is quite evident.

In summary, these photographs tend to indicate that the model with the 9.7 ton tribars is apparently much less stable than the model with the 13.8 ton tribars.

From the combination of visual observations, cross-sectional profiles, and overhead photographs the following criterion for tribar

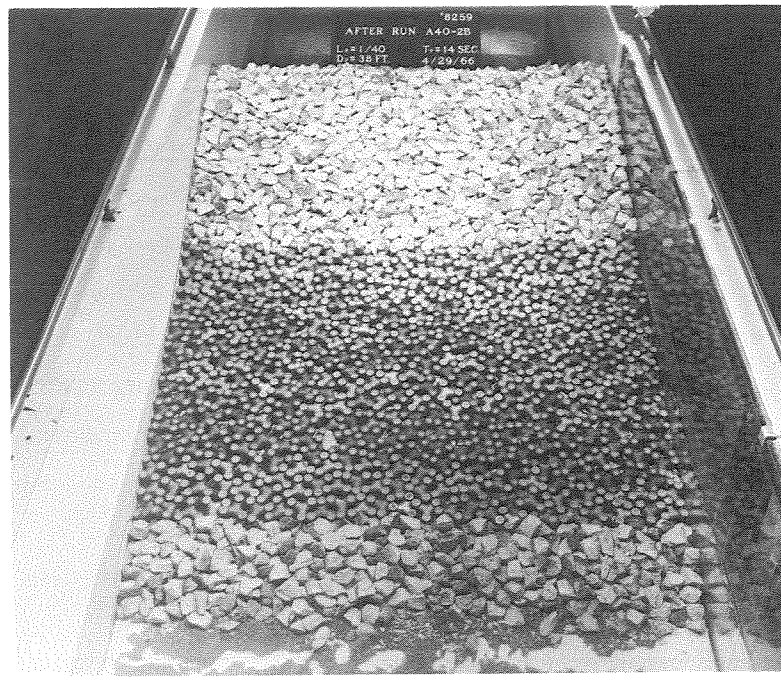

Figure 3.6a Photograph of Island Defense in 1:40 Scale Model After 22 Hours (Prototype) of Testing (Series A40-2)

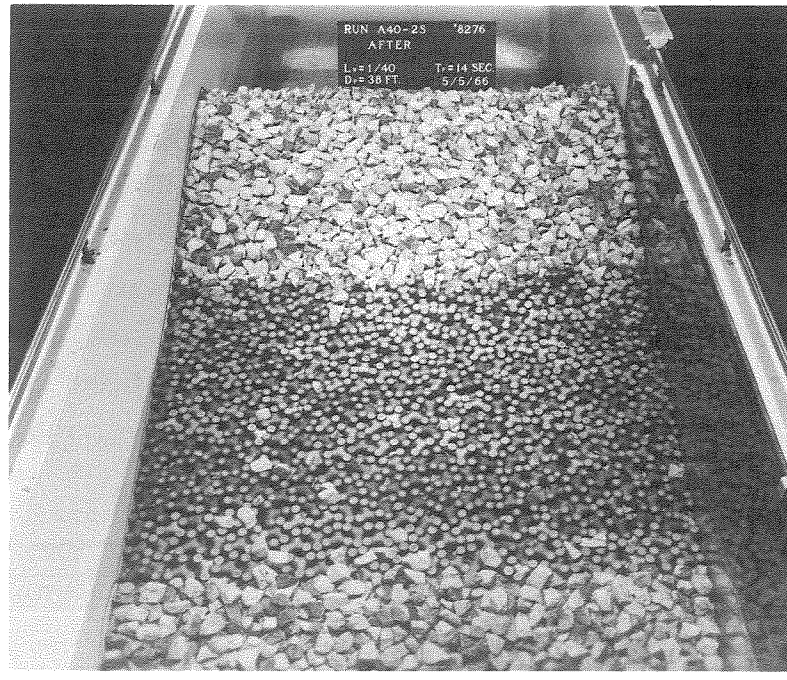

Figure 3.6b Photograph of Island Defense in 1:40 Scale Model After additional 66 Hours (Prototype) of Testing (Series A40-2)

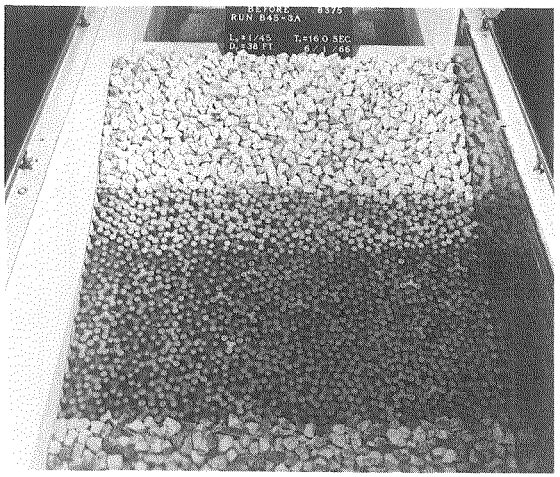

Figure 3.7a Photograph of Island Defense in 1:45 Scale Model Before Testing

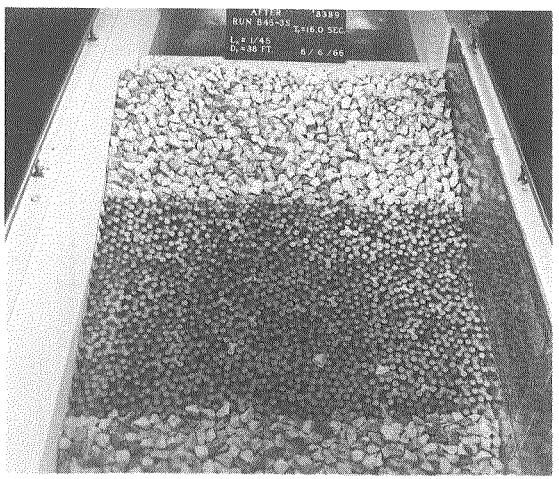

Figure 3.7b Photograph of Island Defense in 1:45 Scale Model After 68.2 Hours (Prototype) of Testing

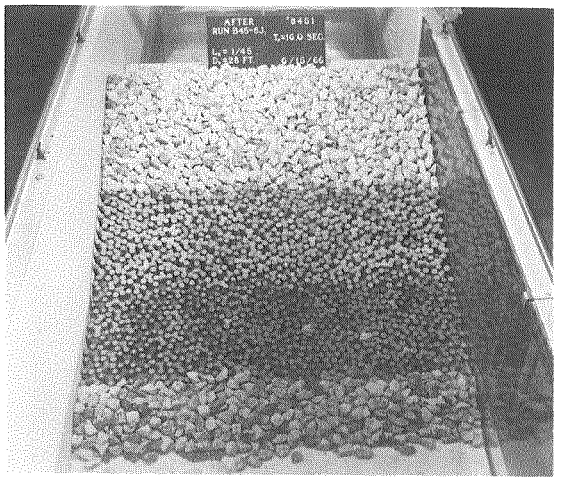

Figure 3.7c Photograph of Island Defense in 1:45 Scale Model After 154 Hours (Prototype) of Additional Testing

stability has evolved. The tribars are considered to be unstable if there is a significant displacement of individual units and a rearrangement and/or destruction of the tribar section of the island face. From the above discussion it is apparent that the island faces consisting of 18.9-ton tribars and 13.8-ton tribars are stable. However, the 9.7-ton tribar section is certainly unstable.

In the 1:45 scale model some rocking was observed in the toe-rock and some general readjustment of the cap-rock section was evident (see Figs. 3.7a, 3.7b, and 3.7c). In order to make the complete wave defense equally stable, i.e., the cap-rock face experiencing only minor readjustments, it may be considered reasonable to increase the size of the armor rock compared to the equivalent prototype rock weights represented in the 1:45 series of tests.

It was evident in all models tested that the most vulnerable area for wave defense destruction was at the interface between the tribars and the cap-rock. This was especially evident in the comparison of the A40-1 series and the A40-2 series. Therefore, the cap-rock in this section must be interlocked with the tribars with a great deal of care to obtain a stable system. In other words, the stability of the wave defense is a function not only of the size of the individual elements but the degree of interlocking of these elements.

It is of interest to compare the experimental results on stability of armor units described above with that found in the literature. These comparisons will be made on the basis of the Hudson formula (Ref. 3),

$$W_r = \frac{\gamma_r H^3}{k_D (S_r - 1)^3 \cot \alpha} \tag{3.12}$$

in which W_r is the weight or armor units in lbs that will be stable under the attack of waves of height H ft., γ_r is the specific weight of the unit in lbs per cu. ft., S_r is the ratio of specific weights of the armor units to that of the water, α is the angle of the plane of the armored face with the horizontal and k_D is a numerical coefficient obtained by experiment. In the tests of the three models all quantities in equation (3.12) except k_D are known so that values of k_D can be

calculated and compared with values recommended for use in the literature. This comparison is made for tribars in Table 3.4. In the calculations the specific weights of prototype tribars and of sea water were taken as 146 and 64 lbs per cu. ft. respectively and cot α was taken as 3. The prototype wave height used, in accordance with equation(3.12), is the wave height that would exist if the structure were not present.

Table 3.4. Tribar Stability Factors, k_D.

Model Scale	1:50	1:45	1:40
Equivalent prototype wt of tribars, W_r, Tons	18.9	13.8	9.7
Prototype wave height H ft.	28	28	28
k_D	13.4	18.4	26.2

The literature (Ref. 3) states that incipient failure will occur with $k_D = 27$. It is seen that the results of the present tests agree closely with this value.

b. Run-Up

Run-up is defined as the vertical distance that water will rise above still water level on the face of a structure due to wave attack. The nomenclature to be used in this phase of the study is shown in Fig. 3.8. The quantity R is used to denote the run-up distance as shown in Fig. 3.8; run-up elevation ($R_{elev.}$) refers to the elevation above MLLW of the highest point to which the water will rise on a structure.

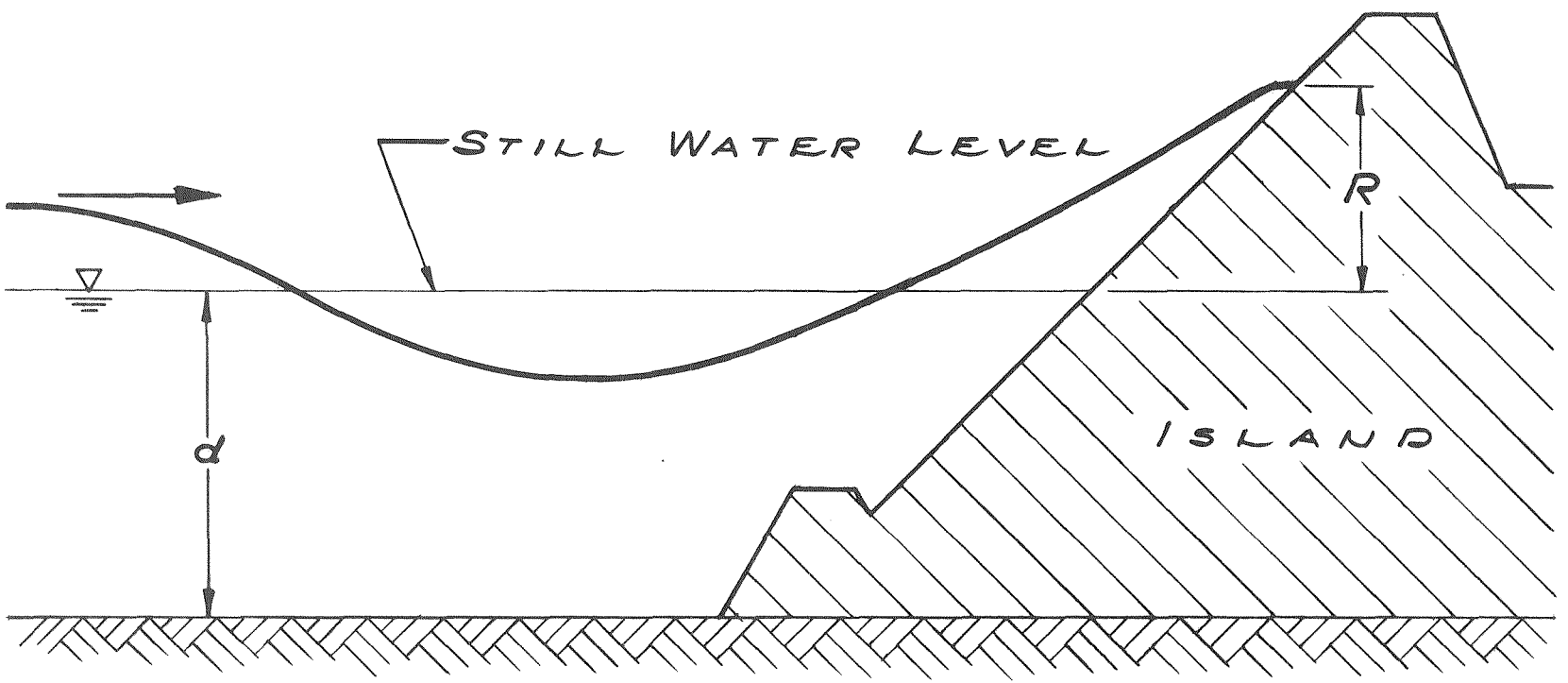

Figure 3.8 Definition Sketch for Run-Up.

In the two-dimensional model study determination of run-up was the second major objective. The design criterion required that overtopping for waves having periods of 16 sec., 14 sec., and 12 sec. be eliminated by the wave defense to prevent damage to facilities on the island. As mentioned previously, these wave periods result from considering the hindcasting studies of Marine Advisors, Inc. (Ref. 2 - Appendix D) where the period of the highest 1/3 waves for the design condition is 14 sec. and the uncertainty of ±15% in this period as described by Lillevang (Ref. 2 - Appendix B).

Run-up on the face of the island is shown in the photographs of Figs. 3.9 and 3.10. Each of these figures is a series of photographs showing the same wave advancing onto the structure (1:45 scale model) and running up the face. Both figures are for the case of a prototype wave of a 16-sec. period and for the condition of high tide (MLLW+8 ft.). The sequence in Fig. 3.9 is for a prototype wave height of 17.4 ft. and shows a wave of a rather smooth profile advancing toward the structure. The three photographs on the right in this sequence are particularly interesting because they show the crest of the non-breaking wave, advancing up the structure to an elevation of +29.8 ft. Fig. 3.10 is a similar sequence for a wave with equivalent prototype height of 20.7 ft. or approximately 3.3 ft. higher than the one in Fig. 3.9. The run-up elevation in this case is +38.3 ft. or 8.5 ft. higher than in the sequence shown in Fig. 3.9. It is interesting that the run-up has increased more than 2.5 times the increase in wave height. This wave is more peaked than the lower wave and in the three pictures on the right in this sequence, appears almost to be a spilling breaker.

The results of the run-up tests on the model corresponding to the original design are presented in Fig. 3.11. In this figure the elevation of run-up in feet is plotted against the prototype wave height in feet with the profile of the wave defense plotted to a distorted scale on the right. The run-up results from two models are shown in Fig. 3.11: the first model denoted as the A50 series had a crest elevation of +30 ft. (the original design) and the second model, C50 series, had the same configuration as the original design but the crest elevation was increased to +40 ft. It is seen that a wave of height 8.4 ft. will cause

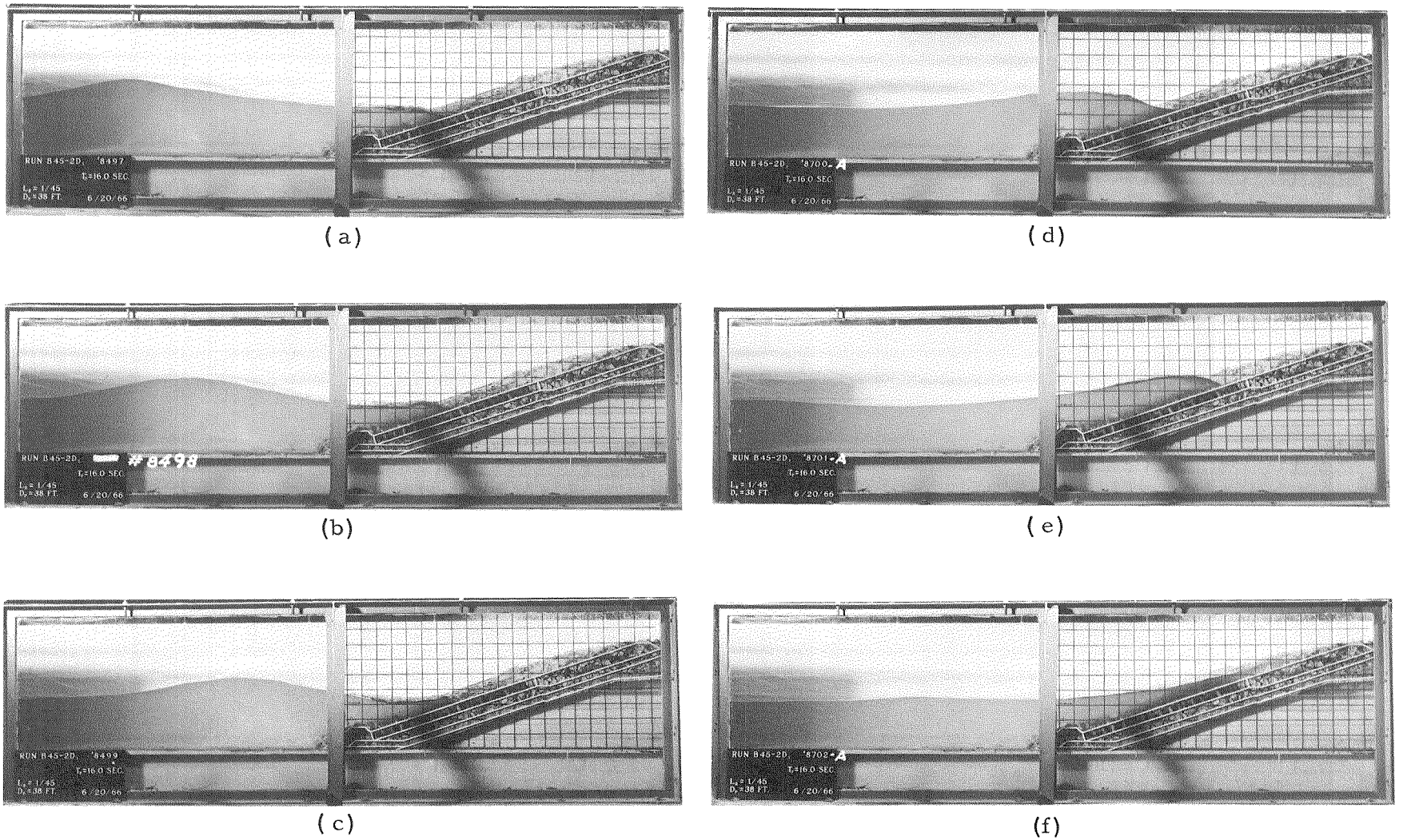

Figure 3.9 Sequence of Wave Advance in 1:45 Scale Model
H = 17.4 ft., R_{elev} = +29.8 ft., T = 16 sec.,
MLLW +8 ft. (grid spacing is equivalent to 10 ft.)

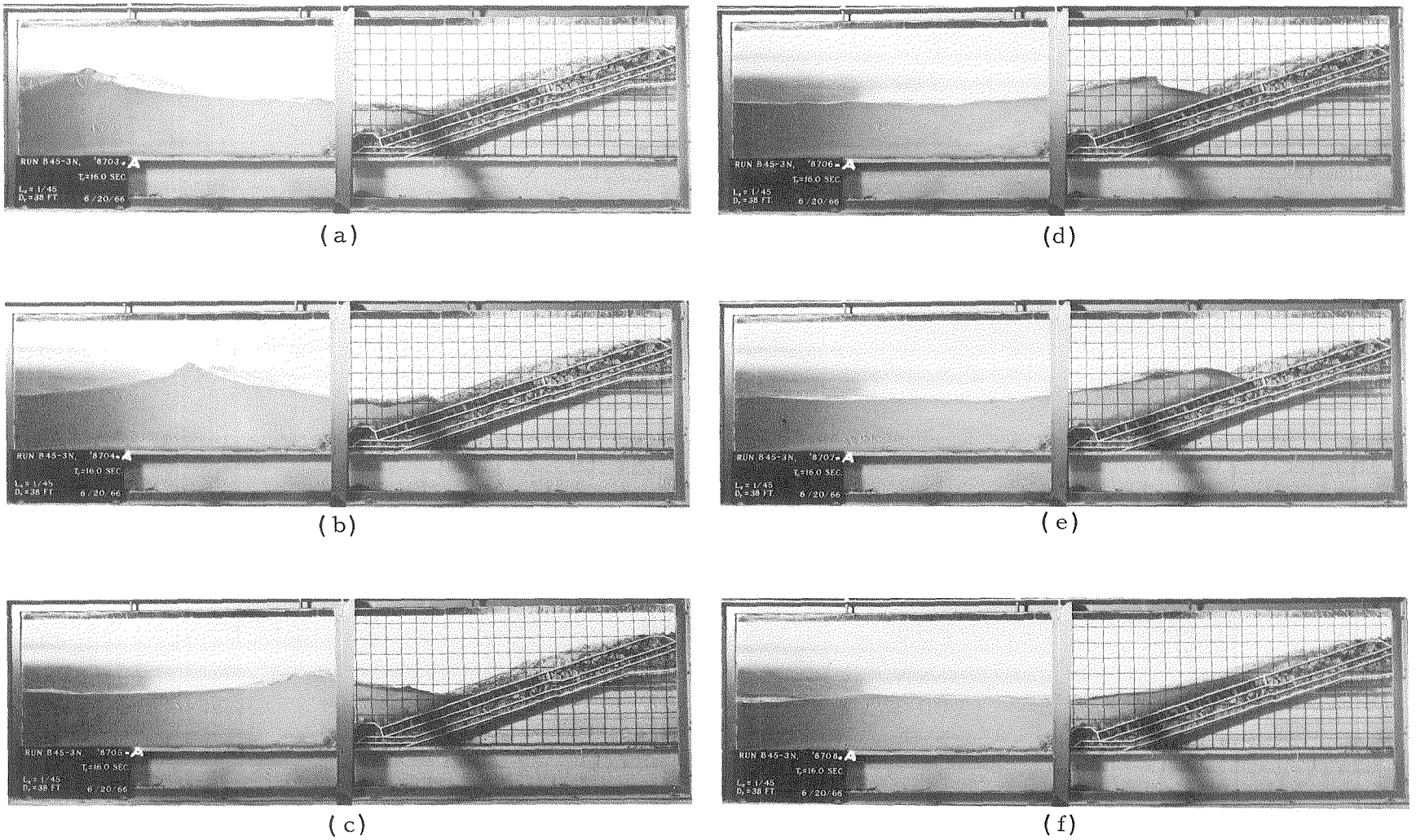

Figure 3.10 Sequence of Wave Advance in 1:45 Scale Model
H = 20.7 ft., R_{elev} = +38.3 ft., T = 16 sec.,
MLLW +8 ft. (grid spacing is equivalent to 10 ft.)

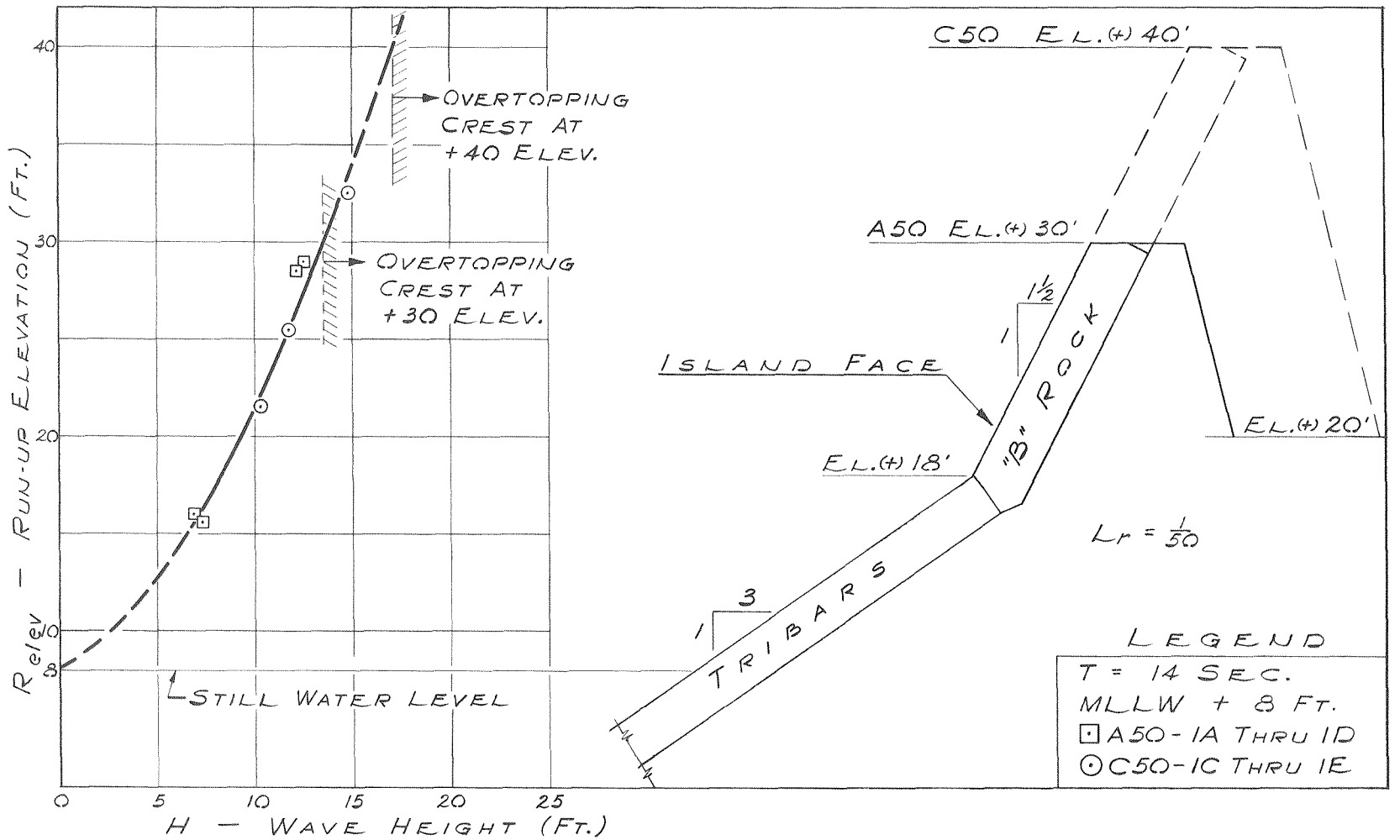

Figure 3.11 Run-Up in 1:50 Scale Model, T = 14 sec., MLLW +8 ft.

run-up to the top row of the tribars. For wave heights greater than this the run-up will be on the cap-rock where the slope is 1-1/2 horizontal to 1 vertical. In Fig. 3.11 it is seen that for a prototype wave height exceeding 13.5 ft. the structure having the original design with a crest elevation of +30 ft. will be overtopped. If the run-up curve shown is extrapolated as shown by the dotted line then the model having a crest height of +40 ft. will be overtopped for prototype waves higher than approximately 17 ft. Therefore, Fig. 3.11 shows that the original design is unacceptable with respect to run-up, and even after increasing the crest elevation to +40 ft., this design is also unacceptable.

For the experiments in which overtopping was experienced (not shown in Fig. 3.11) measurements were made of the rate of flow (see Chapter Two, Section A.4). These data are presented in Table 3.5 where the wave height and the unit discharge expressed in cfs per foot are presented for the prototype. These data are for the original design with crest elevations corresponding to +30 ft., +35 ft., and +40 ft. respectively. Depending upon the rate of flow, the overtopping measurement represents the average overtopping for from 10 to 15 waves impinging upon the structure. More than one wave was used because it was desired to collect the flow for a significant period of time so that a reasonable average of the flow rate could be obtained.

Table 3.5. Prototype Overtopping Unit Discharge in 1:50 Scale Model.

Experiment	Crest elev. (ft)	H (ft)	q (cfs/ft)
A50-1L	+30	23.5	3.45
A50-1M	+30	23.6	2.77
A50-1O	+30	22.9	2.21
A50-1P	+30	22.3	3.52
A50-1Q	+30	17.8	0.254
B50-1B	+35	21.4	1.09
C50-1A	+40	24.2	0.497
C50-1B	+40	24.3	0.25
C50-1F	+40	23.3	1.47

For the model with a crest elevation of +30 ft., the average overtopping unit discharge (to a prototype scale) ranged from approximately .254 cfs/ft. to approximately 3.5 cfs/ft. depending on the incident wave height. This would correspond to a total discharge over the seaward face of the island of from 380 cfs to 5300 cfs. With the crest elevation increased to +35 ft. one overtopping measurement was made and for the prototype the unit discharge was approximately 1.1 cfs/ft. giving a total discharge across the island crest of approximately 1650 cfs. When the crest elevation was increased to +40 the unit discharge varied from approximately .25 cfs/ft. to 1.5 cfs/ft., giving total crest discharges of from 375 cfs to approximately 2300 cfs. Due to the question as to how well one can scale up overtopping from a model to a prototype as well as the scatter of the model data, the exact values of these quantities are perhaps in question. However, the important feature of these results is that the quantity of overtopping in terms of prototype values is unacceptably large.

The results of the run-up measurements in the 1:40 scale model are presented in Fig. 3.12. This figure is for a prototype wave period of 14 sec. and for a tidal elevation of MLLW +8 ft. The results of two series are shown in this figure, that of Series A40-1, and of A40-2, where the structure was rebuilt to the same design. Comparing the run-up shown in Fig. 3.12 to that obtained in the original design (Fig. 3.11), the run-up has been significantly reduced for higher waves by modifying the original design so that the island face had a continuous slope of 3 horizontal to 1 vertical. The maximum run-up for this series was to elevation +38 for a 23-ft. wave, whereas for the same wave height in the original design (composite slope) the structure would be overtopped.

For wave heights less than approximately 8 ft. the run-up for the two cases is identical. For these wave heights the only difference between the two cases presented (Fig. 3.11 and Fig. 3.12) is the model scale. (The period, tidal elevation, slope and elevation to the top of the tribars are the same.) Therefore, for small wave heights, if there is a scale effect it is too small to detect for a 20% change in scale.

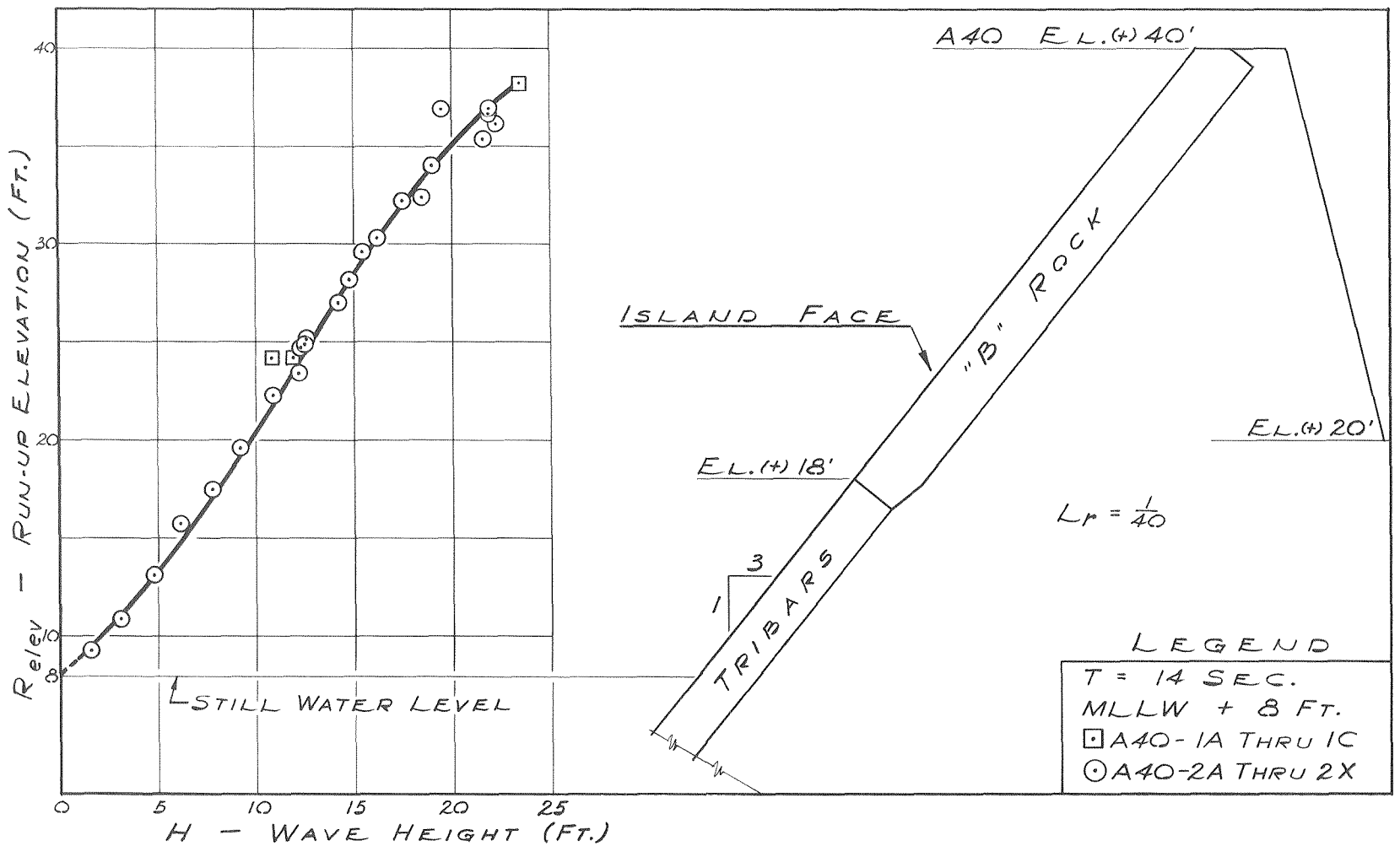

Figure 3.12 Run-Up in 1:40 Scale Model, T = 14 sec., MLLW +8 ft.

Run-up information is presented in Fig. 3.13 for the model having a scale of 1:45 and for the condition of high tide (MLLW +8 ft.). In this figure, the run-up information for the three wave periods (16 sec., 14 sec., and 12 sec.) is shown. The run-up curves presented in Fig. 3.13 show an interesting trend. For a given wave height the run-up decreases as the wave period decreases. Since, for a given depth the wave length L, is proportional to the period T; therefore, for a given wave height and depth the run-up decreases as the wave steepness (H/L) increases. The variation of run-up with relative wave height (H/d) will be discussed later.

In comparing the run-up for the 14-sec. wave in the 1:45 scale model shown in Fig. 3.13 with that shown in Fig. 3.12 for the 1:40 scale model for comparable wave heights it is seen that the run-up is identical for wave heights up to approximately 8 ft. (up to elevation +18 ft.). For larger waves the 1:40 scale model experiences greater run-up. If the scale effects in these tests are small, as they appear to be at low wave heights, then this effect may be explained by the fact that the cap-rock section had deformed significantly at higher waves compared to the cap-rock in the 1:45 scale model. If the deformation led to locally larger slopes in this section, based on the results of the 1:50 scale model this could explain the larger run-up for the 1:40 scale model.

The run-up data obtained in the 1:45 scale model for the condition of low tide and for the same wave periods as those shown in Fig. 3.13 are presented in Fig. 3.14. In this case it is evident that the run-up never reached the elevation of the top of the tribars, i.e., elevation +18 ft. Therefore, for all cases run-up was on the tribar section alone. It is rather difficult to see very much difference between the run-up curves for the three different wave periods, although they are still in the expected sequence, that is, the highest run-up for a given wave height occurs for the wave having the largest wave period (smallest steepness).

The prototype run-up information from the 1:45 scale model which has been presented in Figs. 3.13 and 3.14 has been replotted in Figs.

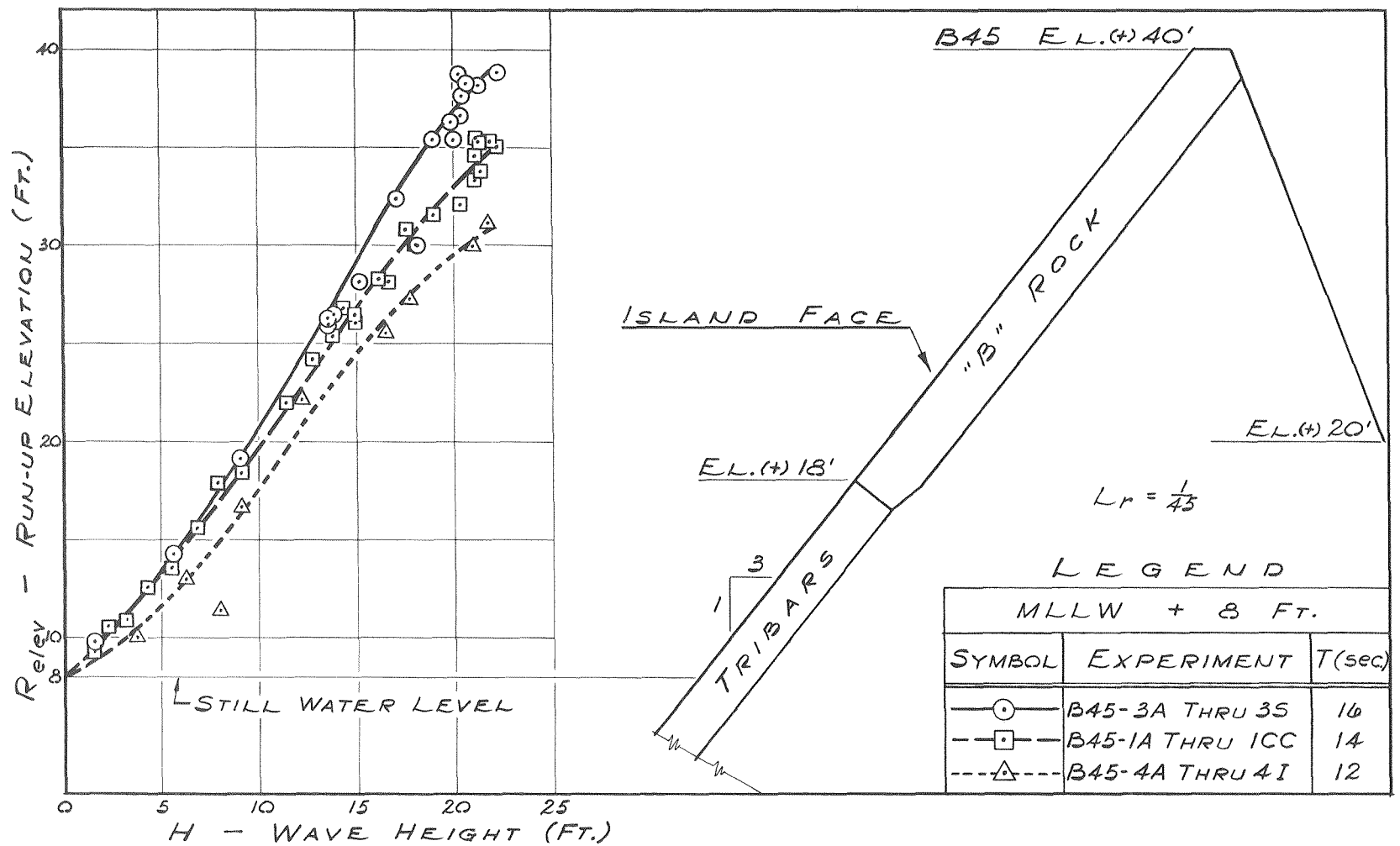

Figure 3.13 Run-Up in 1:45 Scale Model, T = 16 sec., 14 sec., 12 sec., MLLW +8 ft.

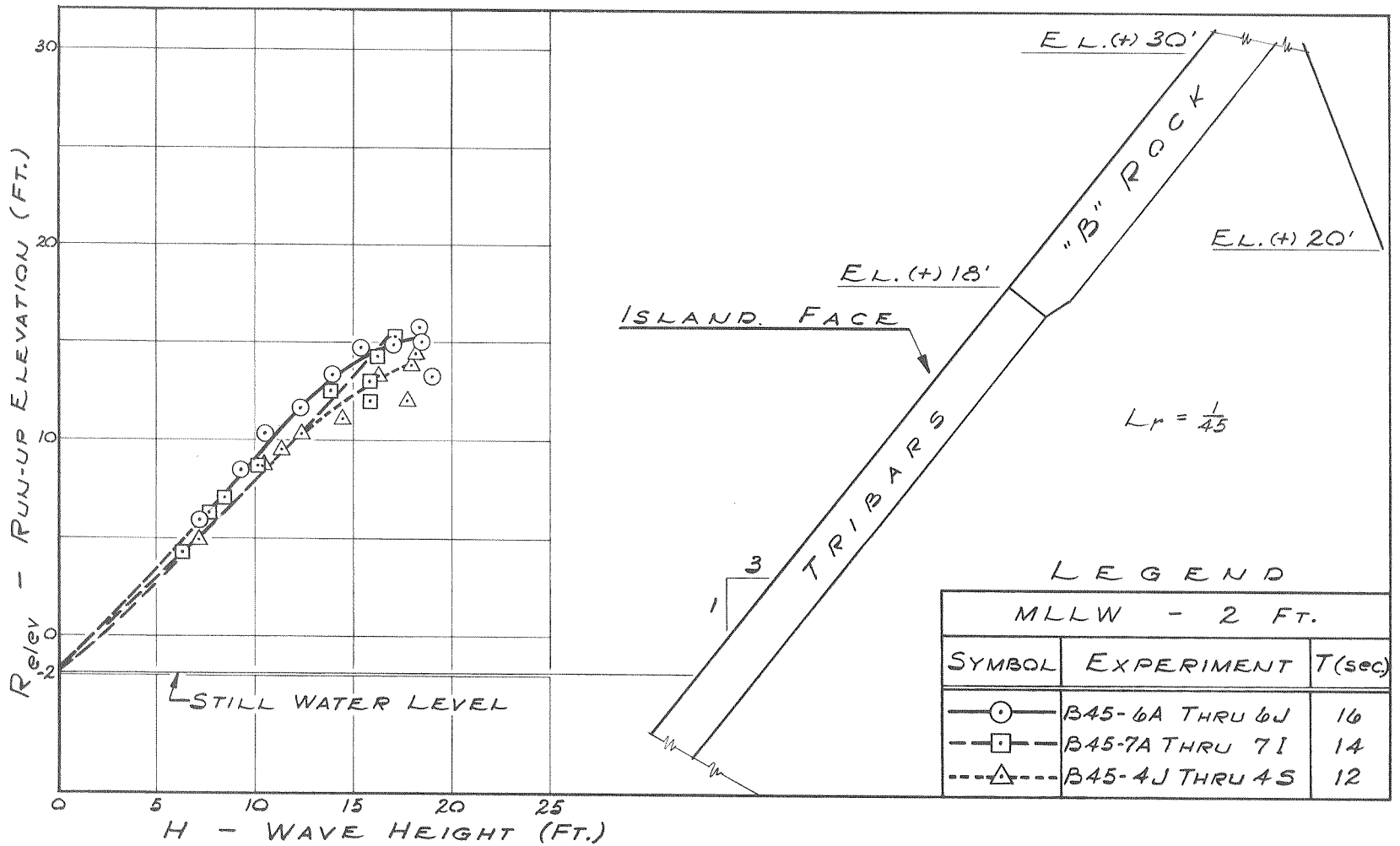

Figure 3.14 Run-Up in 1:45 Scale Model, T = 16 sec., 14 sec., 12 sec., MLLW -2 ft.

3.15 and 3.16 in dimensionless coordinates, i.e., R/H vs. H/d. Fig. 3.15 presents this information for the condition of high tide where run-up is on both the tribar surface as well as the cap-rock section. Three curves are shown, one for each of the periods tested: 16 sec., 14 sec., and 12 sec. These three curves show the same trend as was indicated in Fig. 3.13, i.e., the maximum relative run-up is for the case of the maximum wave period (maximum wave length). In addition, these curves show that for each period there is a definite tendency for the relative run-up to increase with increasing relative wave height, (H/d) reaching a maximum between values of H/d of from 0.4 to 0.5, and then decreasing with increasing relative height. Indicated on this figure are two other curves which define the geometry of the system. The curve at a lower value of H/d indicates the intersection of the tribars and the cap-rock (elevation +18 ft.). The curve shown at larger values of H/d is called the overtopping curve. This curve indicates the elevation +40 ft., the crest of the wave defense, and the region above this curve indicates that the structure has been overtopped. It is interesting to see in Fig. 3.15 that the curve of relative run-up for a wave period of 16 sec. tends to become parallel to the overtopping curve at the large values of H/d. The so-called tribar interface curve is put in as a reference so that one can readily see that the major run-up in this structure at high tide is on the cap-rock section.

Similar relative run-up curves are shown in Fig. 3.16 for the case of low tide (MLLW -2 ft.) and for the same three wave periods (16 sec., 14 sec., and 12 sec.). A similar curve again called the tribar interface curve, is plotted in this figure, showing that the run-up for all three wave periods is on the tribar section. These curves also show the same general trend of decreasing relative run-up with decreasing wave period at a constant value of relative wave height (H/d). However, the separation of the curves is nowhere near as great as for the case of high tide.

The experimental data dealing with run-up which has been presented cover a much greater range of H/d than the data which were used to determine the crest height of the island defense in the original

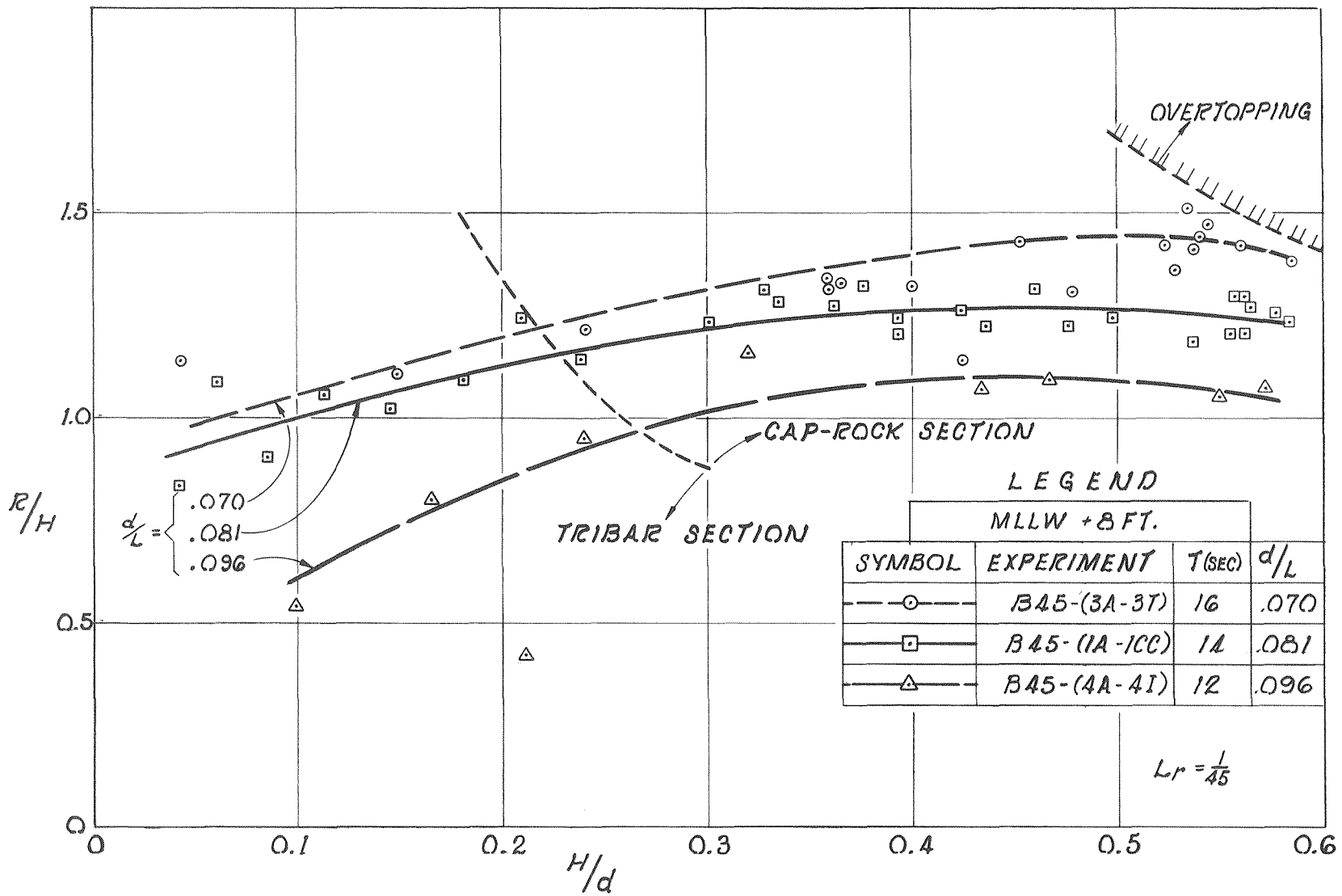

Figure 3.15 Relative Run-Up (R/H) vs. Relative Wave Height (H/d) in 1:45 Scale Model, T = 16 sec., 14 sec., 12 sec., MLLW +8 ft.

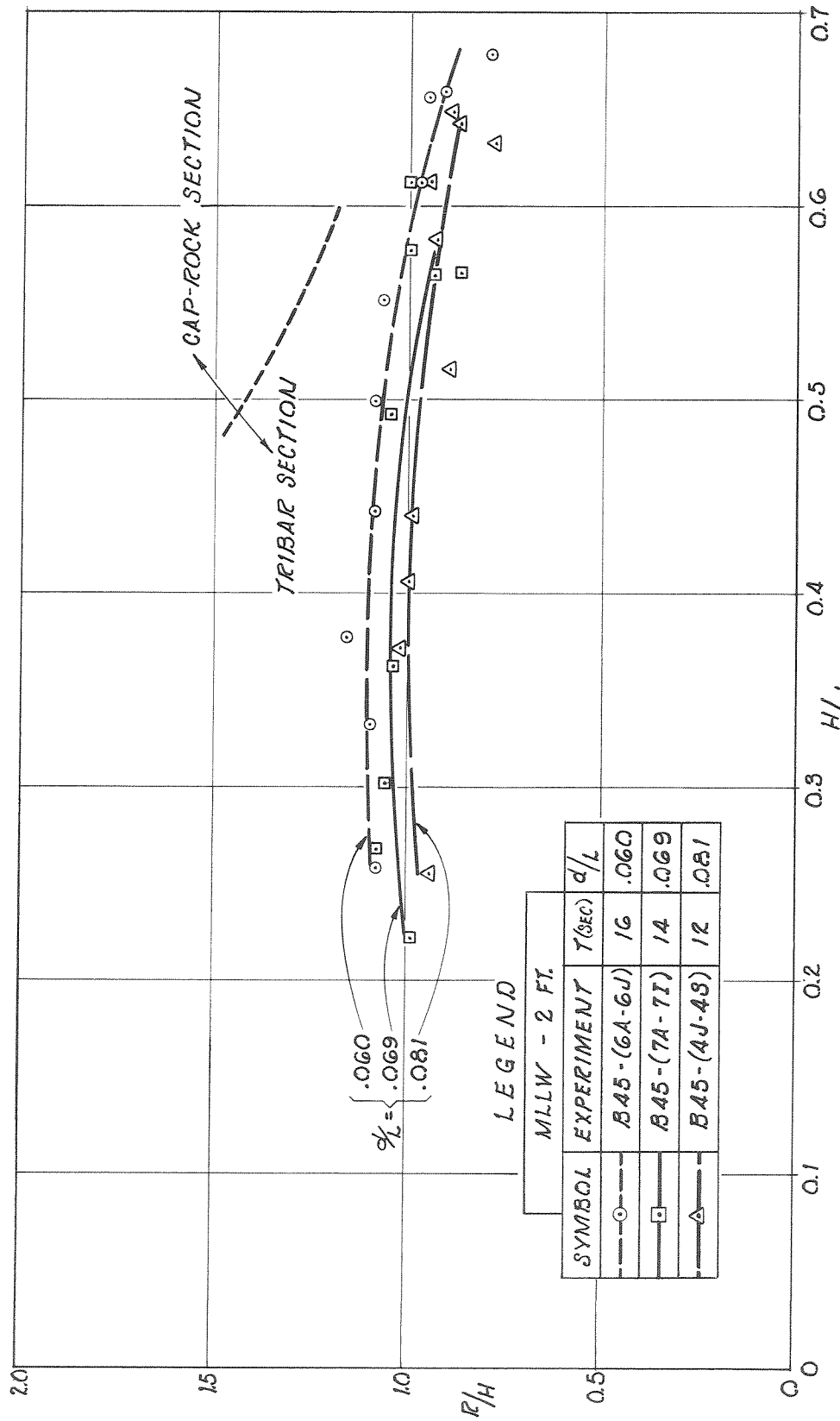

Figure 3.16 Relative Run-Up (R/H) vs. Relative Wave Height (H/d) in 1:45 Scale Model, T = 16 sec., 14 sec., 12 sec., MLLW -2 ft.

design. For instance, for the depth to wave length ratios which are of interest in this study ($\frac{d}{L} < 0.1$), the run-up data of Hudson (4) are for values of H/d less than 0.25 for the two slopes of the island face considered in this investigation.

Photographs were taken of the condition of maximum run-up for most of the experiments conducted, and some of these are shown in Fig. 3.17. Fig. 3.17a shows the condition of overtopping for the original design and Fig. 3.17b shows the case where the crest height was increased to elevation +40 ft. and the island face still with a composite slope. Figs. 3.17c, 3.17d and 3.17g show the condition of maximum run-up for a 14-sec. wave at high tide acting on the structure with modified design, i.e., a continuous slope of 3 horizontal to 1 vertical and a crest elevation of +40 ft. Similar photographs are shown in Fig. 3.17e and 3.17i for the case of the 12-sec. and 16-sec. wave respectively. The condition of maximum run-up for the case with wave attack at low tide is shown in Figs. 3.17f, 3.17h and 3.17j for the 12-sec., 14-sec., and 16-sec. waves, respectively.

Each of Figs. 3.18, 3.19 and 3.20 contains a number of photographs showing the condition of maximum run-up at high tide (elev. +8 ft.) for several wave heights for wave periods of 16 sec., 14 sec., and 12 sec., respectively, in the 1:45 scale model. The photographs show the shape of the "tongue" of water which runs up the slope. Comparison of the shapes of these tongues for the same wave heights at the three periods is difficult because the wave heights are not the same and one is not certain that the photographs were taken at the instant of maximum run-up. Despite this, one can see that for high waves the thickness of the tongue near the base of the structure and the length of the tongue are greatest for the highest period.

As discussed previously, the design wave which was used in the original engineering design of the island was obtained by a hindcasting procedure by the Marine Advisors Incorporated(see Ref. 2 - Appendix D, page 27). Their analysis showed that in a period of 25 years the highest individual wave which could be anticipated at the island is 28 ft. Their report states that this wave is one which "...progresses through

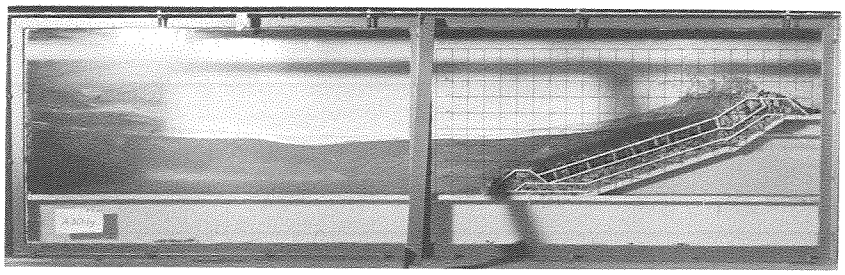

(a)

A50-1G
T = 14 sec.
MLLW +8 ft.
H = 17.7 ft.
Overtopping

(b)

C50-1A
T = 14 sec.
MLLW +8 ft.
H = 24.2 ft.
Overtopping

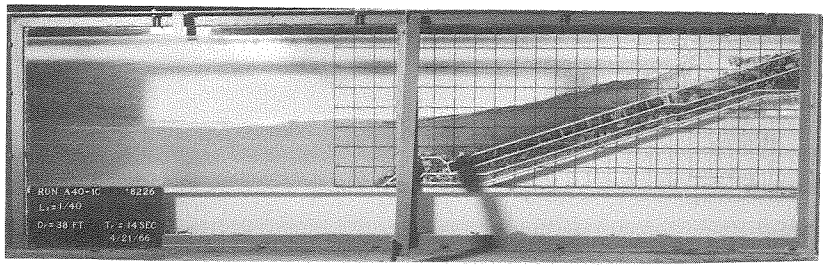

(c)

A40-1C
T = 14 sec.
MLLW +8 ft.
H = 23.5 ft.
R_{elev} = +38.2 ft.

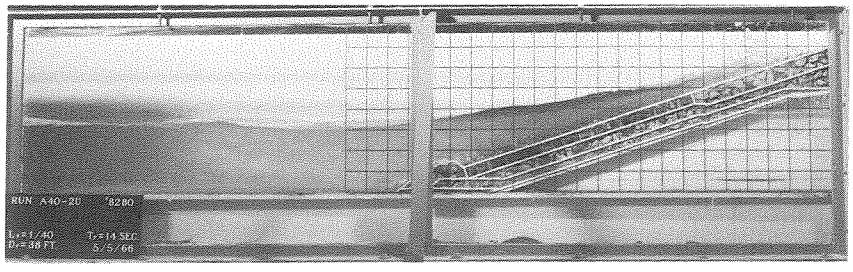

(d)

A40-2U
T = 14 sec.
MLLW +8 ft.
H = 22.3 ft.
R_{elev} = +36.1 ft.

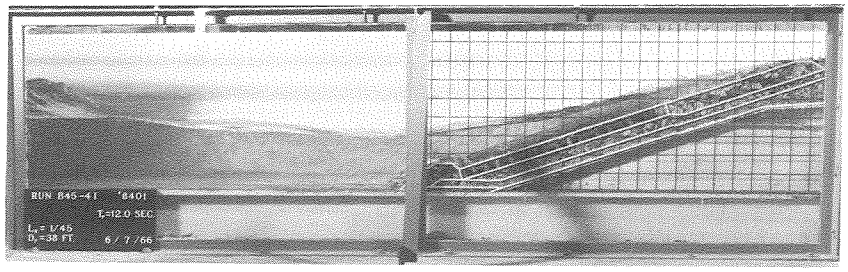

(e)

B45-4I
T = 12 sec.
MLLW +8 ft.
H = 21.8 ft.
R_{elev} +31.2 ft.

Figure 3-17a-e Photographs of Maximum Run-up for Various Models Tested

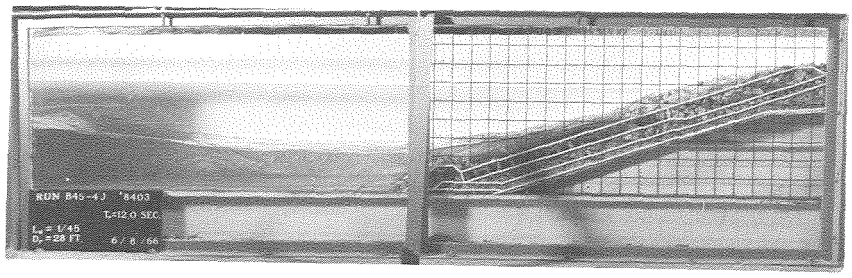

(f)

B45-4J
T = 12 sec.
MLLW -2 ft.
H = 16.3 ft.
R_{elev} = +13.2 ft.

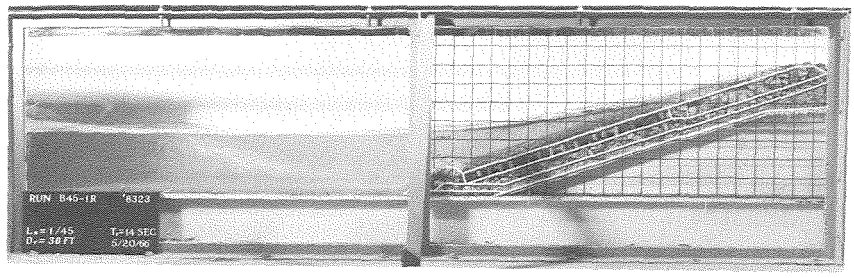

(g)

B45-1R
T = 14 sec.
MLLW +8 ft.
H = 22.1 ft.
R_{elev} = +35.1 ft.

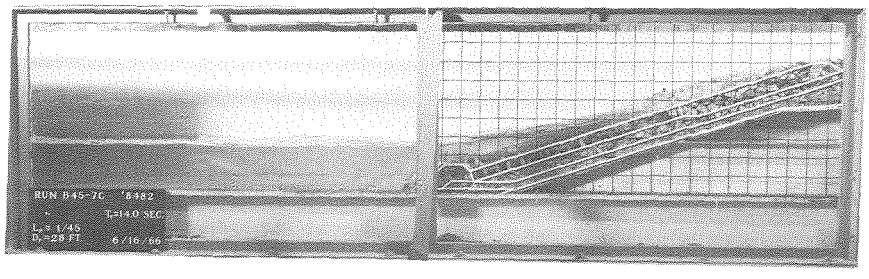

(h)

B45-7C
T = 14 sec.
MLLW -2 ft.
H = 17.2 ft.
R_{elev} = +15.3 ft.

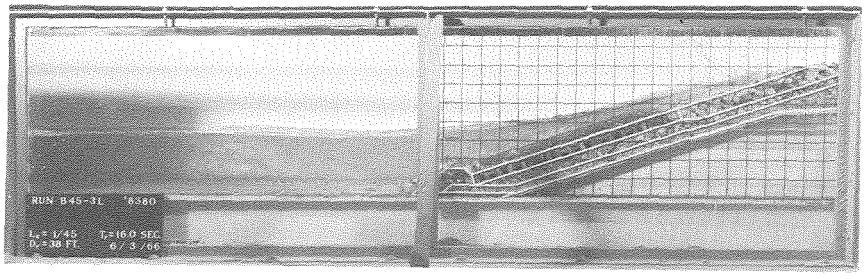

(i)

B45-3L
T = 16 sec.
MLLW +8 ft.
H = 21.3 ft.
R_{elev} = +38.2 ft.

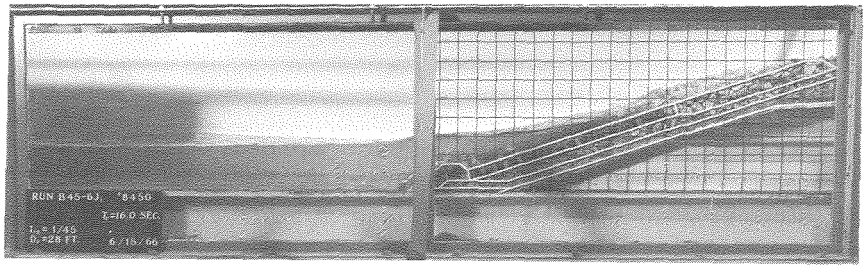

(j)

B45-6J
T = 16 sec.
MLLW -2 ft.
H = 19.0 ft.
R_{elev} = +13.2 ft.

Figure 3.17f-j Photographs of Maximum Run-Up for Various Models Tested

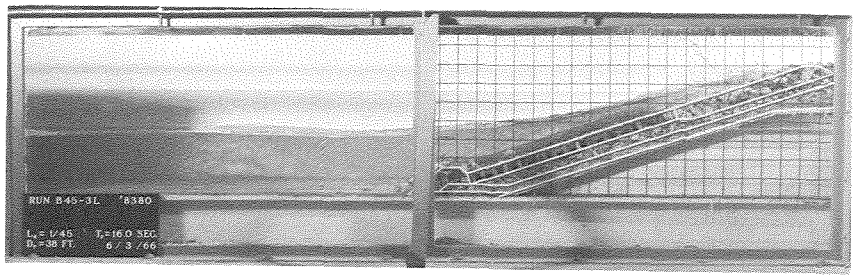

(a)

B45-3L
H = 21.3 ft.
R_{elev} = +38.2 ft.

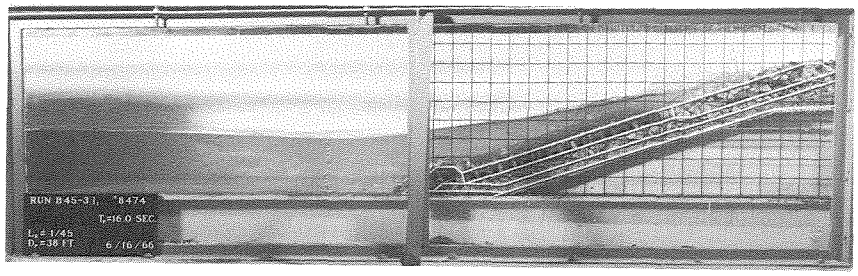

(b)

B45-3I
H = 18.2 ft.
R_{elev} = 30.0 ft.

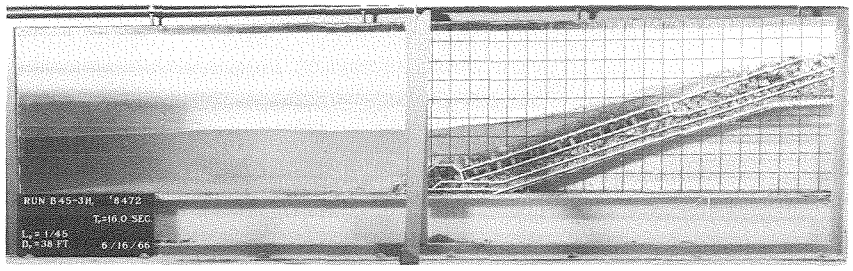

(c)

B45-3H
H = 15.2 ft.
R_{elev} = +28.2 ft.

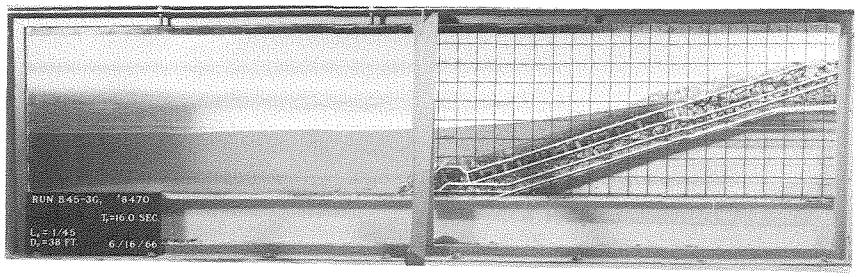

(d)

B45-3G
H = 9.1 ft.
R_{elev} = +19.2 ft.

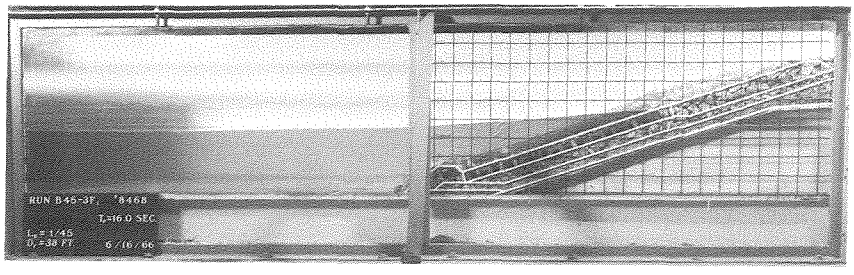

(e)

B45-3F
H = 5.6 ft.
R_{elev} = 14.3 ft.

Figure 3.18 Photographs of Run-Up in 1:45 Scale Model T = 16 sec., MLLW + 8 ft.

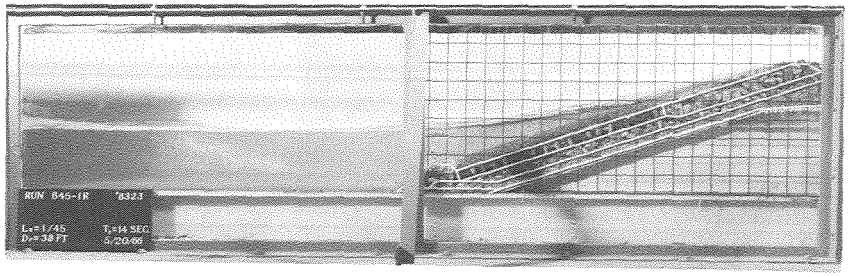

(a)

B45-1R
H = 22.1 ft.
R_{elev} = +35.1 ft.

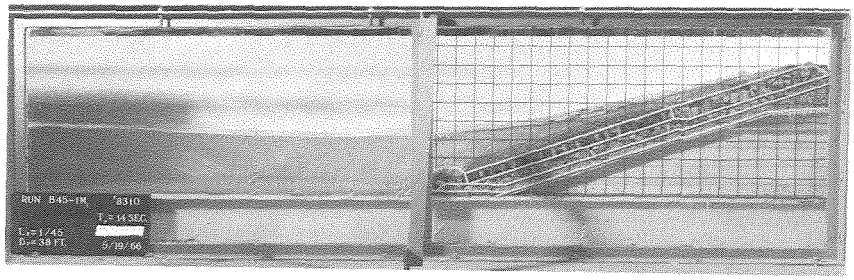

(b)

B45-1M
H = 18.1 ft.
R_{elev} = +30.0 ft.

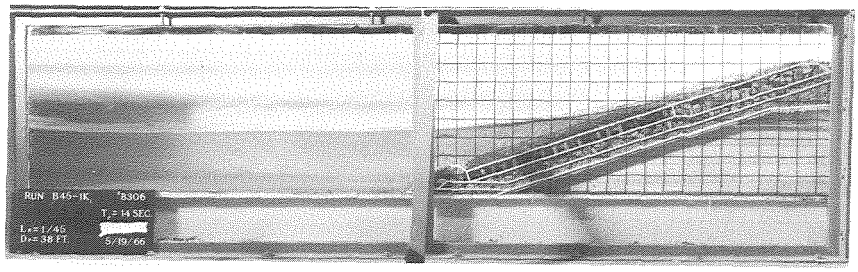

(c)

B45=1K
H = 16.1 ft.
R_{elev} = +28.3 ft.

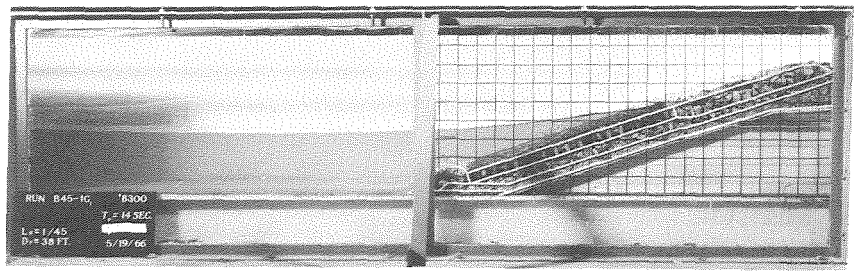

(d)

B45-1G
H = 9.1 ft.
R_{elev} = +18.4 ft.

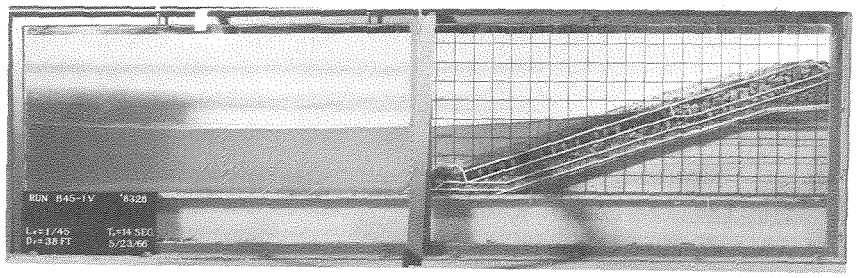

(e)

B45-1V
H = 5.5 ft.
R_{elev} = +13.6 ft.

Figure 3.19 Photographs of Run-Up in 1:45 Scale Model T = 14 sec., MLLW + 8 ft.

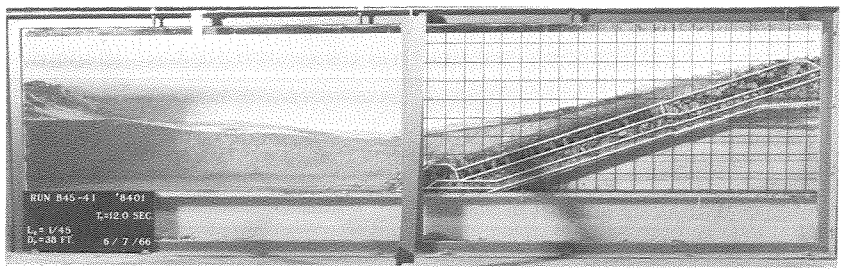

(a)

B45-4I
H = 21.8 ft.
R_{elev} = +31.2 ft.

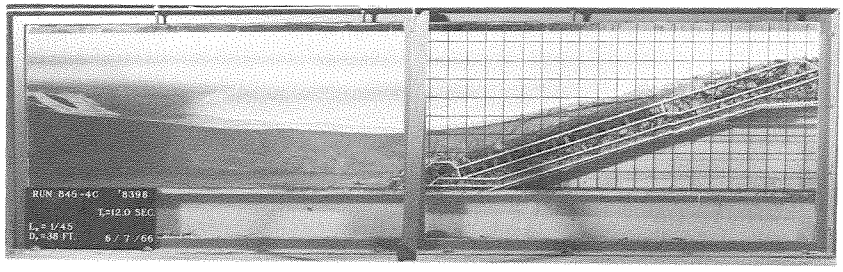

(b)

B45-4C
H = 17.7 ft.
R_{elev} = +27.3 ft.

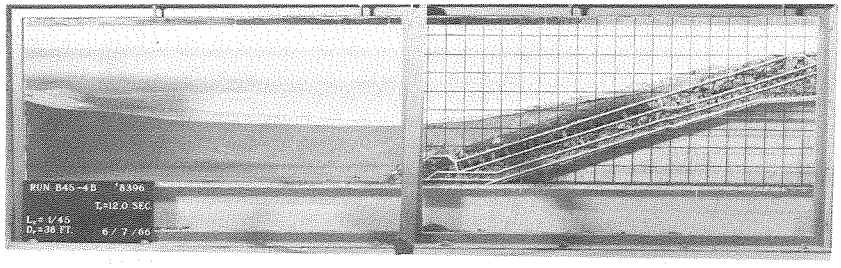

(c)

B45-4B
H = 16.5 ft.
R_{elev} = +25.6 ft.

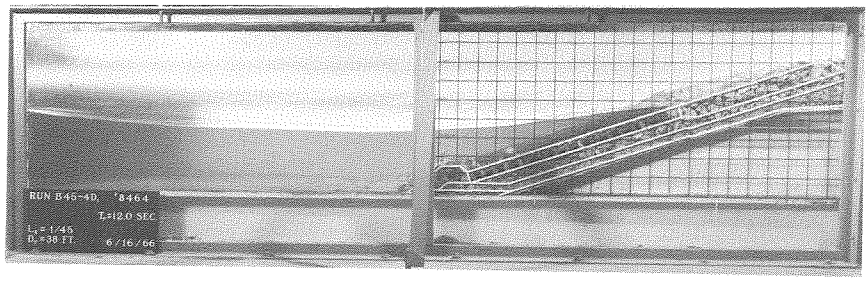

(d)

B45-4D
H = 9.1 ft.
R_{elev} = +16.7 ft.

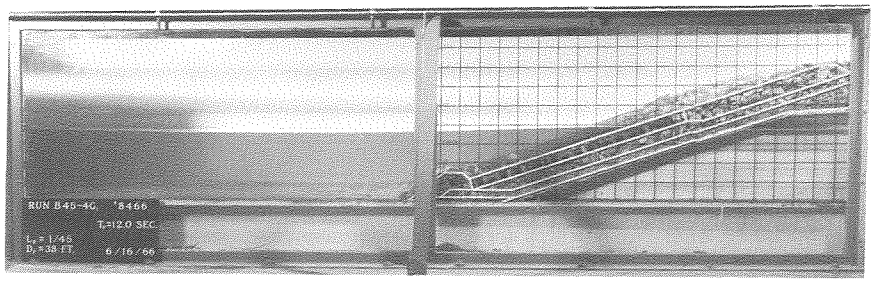

(e)

B45-4G
H = 3.8 ft.
R_{elev} = +10.0 ft.

Figure 3.20 Photographs of Run-Up in 1:45 Scale Model T = 12 sec., MLLW + 8 ft.

the ocean at the island site without the island being present." However, when there is wave reflection, as in the case when the island is present, the wave system cannot be considered to be a progressive wave system. Danel (5) has shown that there is a difference between the highest possible progressive wave and the highest possible standing wave in a particular depth of water. The condition specified for the original design was that the height of the highest possible wave was equal to approximately 0.73 times the depth (Lillevang, Ref. 2 - Appendix B). The envelope of Danel's experimental data indicate that for the case of 100% reflection the maximum possible height of the standing wave is approximately 0.625 times the depth. This difference is due to the influence of reflections upon the breaking characteristics of the wave and hence its maximum possible height.

Since the wave defense acts as a reflecting surface to progressive waves which are incident upon it, offshore of the island there would be a partial standing wave system set up by these reflections. Therefore, the highest possible wave that will impinge upon this structure taking into account reflection will be less than that which would be possible in this location without the island present. Therefore, it is felt that the results of these tests, where the maximum value of H/d attained was less than 0.73, realistically describe the wave environment which would exist in the prototype.

C. THREE-DIMENSIONAL MODEL STUDIES

1. Wave Measuring Techniques

Wave heights were measured in the three-dimensional model in the locations shown in Figs. 2.24a, 2.24b, and 2.24c. As seen in these figures in all tests wave heights were measured at two or three points near the wave machines in a prototype water depth of approximately 60 ft. Wave heights were also measured near the island by a gage located (in prototype dimensions) approximately 3100 ft. down-coast of the island at the 30-ft. contour.

Before proceeding with the testing it was of interest to look in detail at the wave systems on the island centerline and 3100 ft. down-coast of the island. The results of this portion of the investigation for normally incident waves are presented in Fig. 3.21 where the ratio of wave heights to water depth in the vicinity of the 60-ft. contour are plotted as a function of the ratio of the wave height to depth in the vicinity of the 30-ft. contour (near the island site). As in the two-dimensional study, the reflection of the incident wave from the island affects the wave height in the vicinity of the island. By moving the run-up beam shown in Fig. 2.23 out from the island, along the island centerline, it was possible to obtain a wave envelope on the island centerline. The incident wave height and the reflected wave height were then obtained from this envelope in the same manner as that in the two-dimensional tests, i.e., equations (3.10) and (3.11). Therefore, in Fig. 3.21 the relative wave heights plotted in the vicinity of the island are: the incident wave heights on the centerline of the island, and the wave heights measured at the gage located down-coast from the island at the 30-ft. contour where wave heights are not affected by reflection. These values are plotted as a function of the corresponding relative wave heights near the wave machines (see Fig. 2.24a). The information shown is for two wave periods, a prototype wave period of 14 sec. and of 17.5 sec. It is seen from Fig. 3.21 that for the same value of H/d near the 60-ft. contour the H/d obtained at Location A at the 30-ft. contour is approximately the same as that determined from the incident wave height obtained from

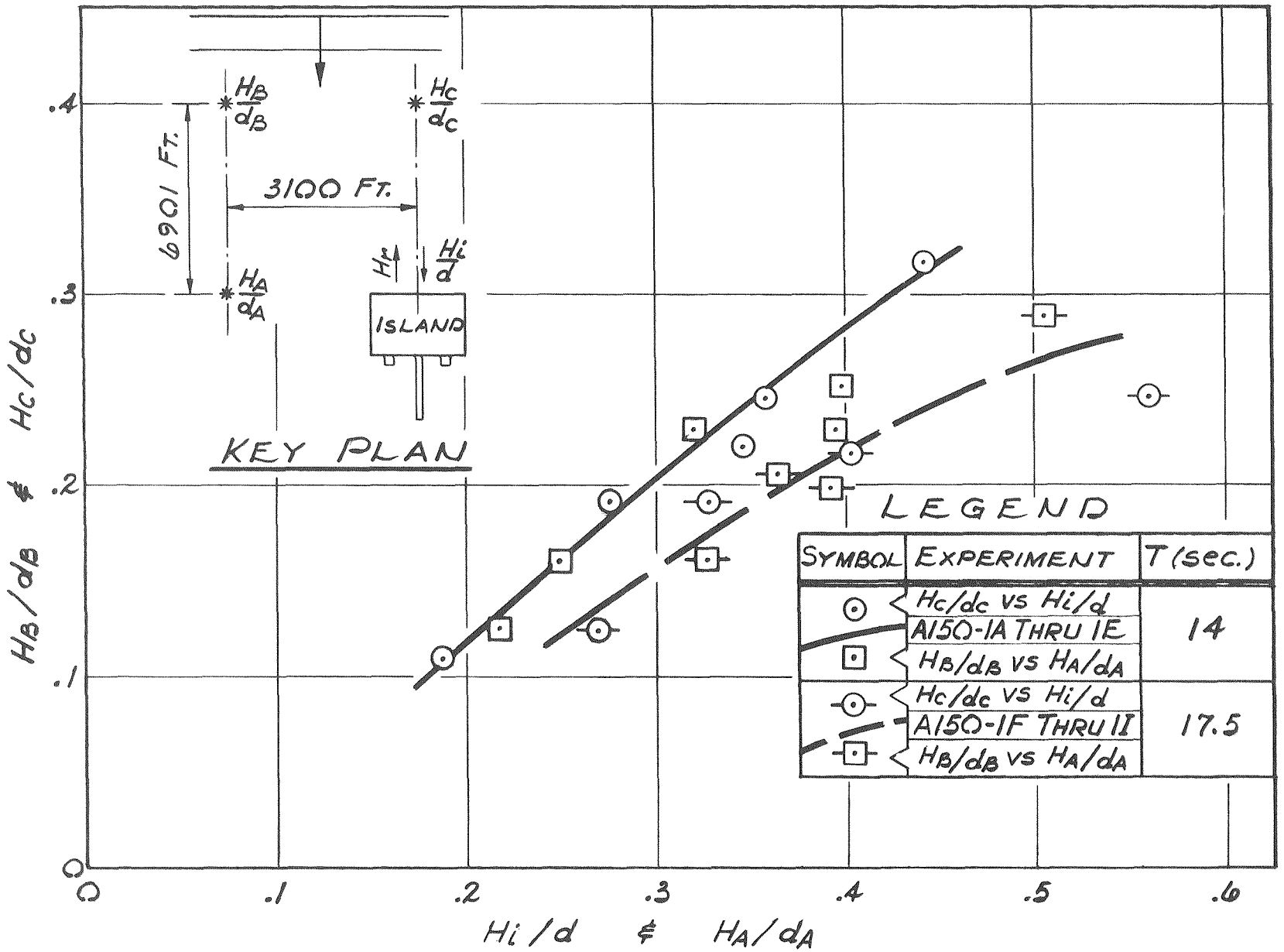

Figure 3.21 A Comparison of Relative Wave Heights Measured on Island Centerline and Down Coast for Wave Direction Azimuth 230°, T = 14 sec., 17.5 sec., MLLW +8 ft.

the wave envelope on the island centerline. The depths used in this figure in normalizing the wave heights are the depths at the gage locations except for the measurement on the island centerline where the depth is the depth of the toe at the defense on the centerline. This figure shows that within experimental error the ratio H/d measured at A was representative of the incident wave height to depth ratio at the seaward face of the island for this case of a normally incident wave. Since the depths at these two locations are essentially the same, this argument also applies to the actual wave heights.

With this information in mind, for the other two incident wave directions used in this study, location A was also used to define the incident wave height in the vicinity of the island. This is considered to be reasonable, since the ocean bottom contours as seen in Figs. 2.24b and 2.24c are approximately parallel to the beach and the bottom is therefore almost plane.

2. Run-Up

Run-up measurements were made in the three-dimensional model using the method described in Chapter Two, Section B.4.b for three different incident wave directions: a normally incident wave (wave direction azimuth at the island of 230^{o}), the oblique design wave (wave direction azimuth at the island of 200^{o}), and for oblique waves from an up-coast direction (wave direction azimuth at the island of 240^{o}). For the case of the normally incident waves and the design wave the run-up was studied for various wave heights at wave periods of 16 sec., 14 sec., and 12 sec. In the case of the up-coast wave only a wave period of 10 sec. was used.

The run-up information obtained is plotted in the form of run-up envelopes, i.e., the maximum run-up elevation reached at 14 locations around the island. The location of these run-up stations is shown in the plan view of the island, Fig. 2.21. These data are presented in Figs. 3.22 through 3.28 as the run-up elevation in feet in the prototype as a function of location on the island perimeter.

The run-up information for the normally incident wave (wave direction azimuth at the island site of 230°) are presented in Figs. 3.22, 3.23 and 3.24 for the 16-sec., 14-sec., and 12-sec. waves, respectively. Plotted on these figures are the comparable run-up elevations which would be predicted from the results of the two-dimensional tests for the same wave height and wave period. There are a number of features of interest in these three figures. As would be expected, the run-up measured on the seaward face of the island (face BC) is much greater than that measured on the other three faces. The minimum run-up is experienced on the shoreward face of the island (face AD). For this case the run-up on the up-coast and down-coast faces of the island (faces CD and BA, respectively) are approximately the same and show the same general decrease in run-up with distance from the seaward corners to the shoreward corners of the island.

Considering the difficulty of the run-up measurements in this 1:150 scale model, one can say that the average run-up experienced on the seaward face of the island (face BC) in the three-dimensional model is reasonably close to that obtained in the two-dimensional model for comparable wave heights. However, due to the influence of the offshore topography or three-dimensional effects in the vicinity of the island, the run-up along the seaward face of the island is not uniform.

At the larger wave heights in most cases the run-up measured in the 1:45 scale model is 10% to 15% greater than that measured in the 1:150 scale model. Since experimental error is also of this order, it is difficult to draw conclusions as to the scale effect from this comparison. However, it seems pertinent that run-up in the three-dimentional model was usually less than in the larger two-dimensional model. This is interpreted to mean that at least some of the difference observed is due to scale effect.

To the authors' best knowledge information pertaining to the exact nature of the effect of model scale upon run-up does not exist. However, at this point in the discussion the results of the two-dimensional tests again should be emphasized. In those tests it was found that the maximum run-up for the 14-sec. wave was to elevation +35 ft. and to

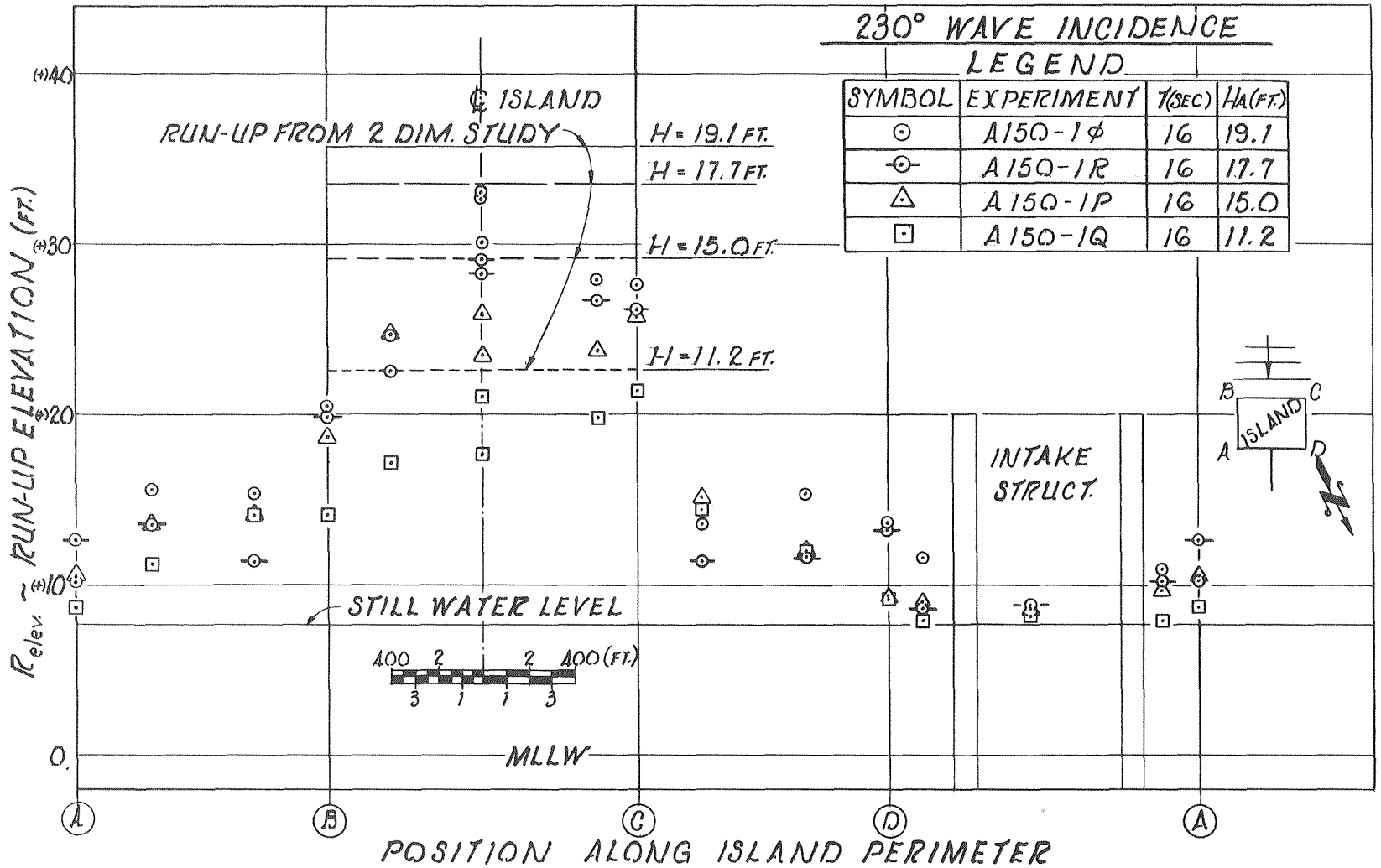

Figure 3.22 Run-Up Envelope in Three-Dimensional Model
Wave Direction at Island Site Azimuth 230°
T = 16 sec., MLLW +8 ft.

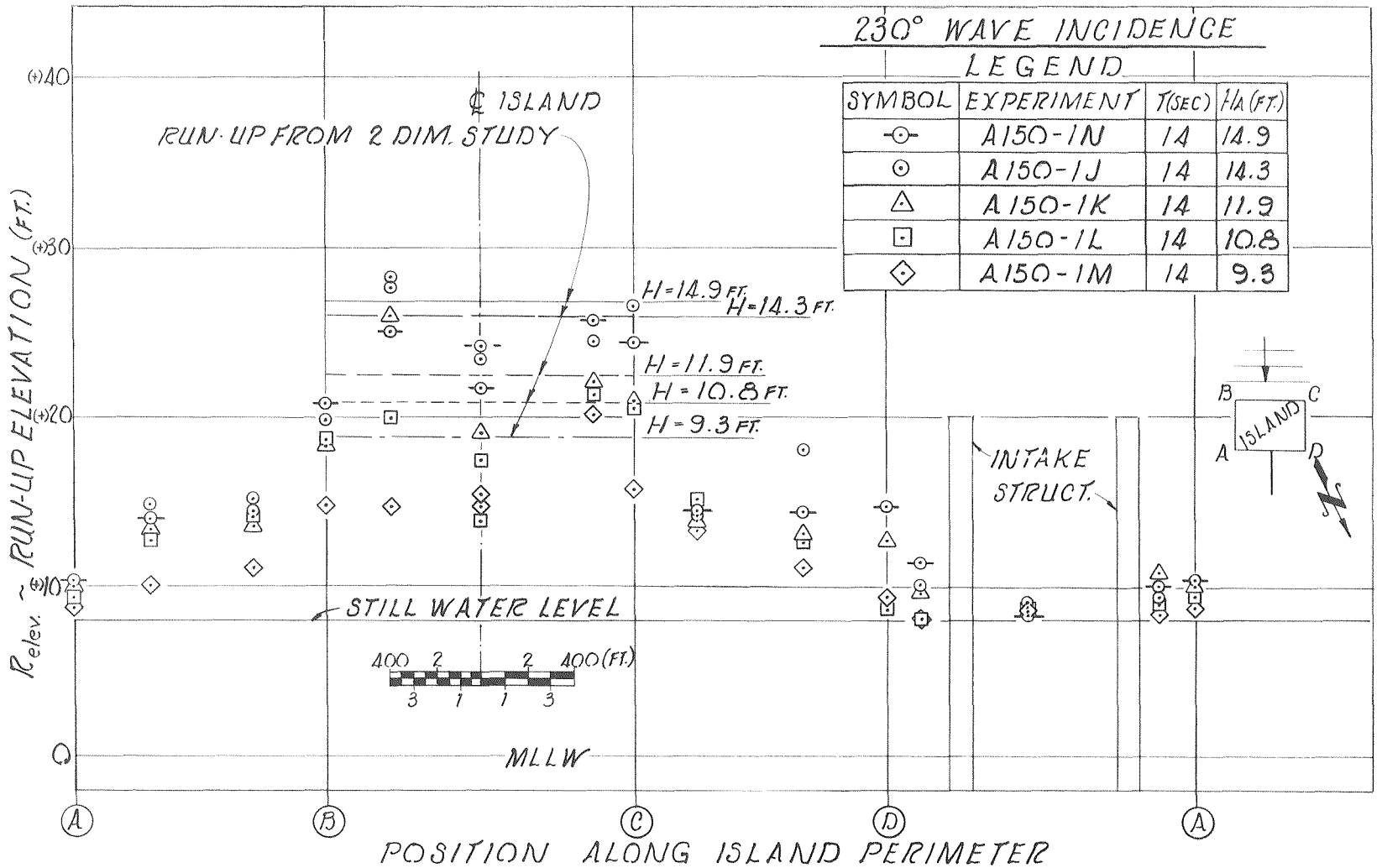

Figure 3.23 Run-Up Envelope in Three Dimensional Model
Wave Direction at Island Site Azimuth 230°
T = 14 sec., MLLW +8 ft.

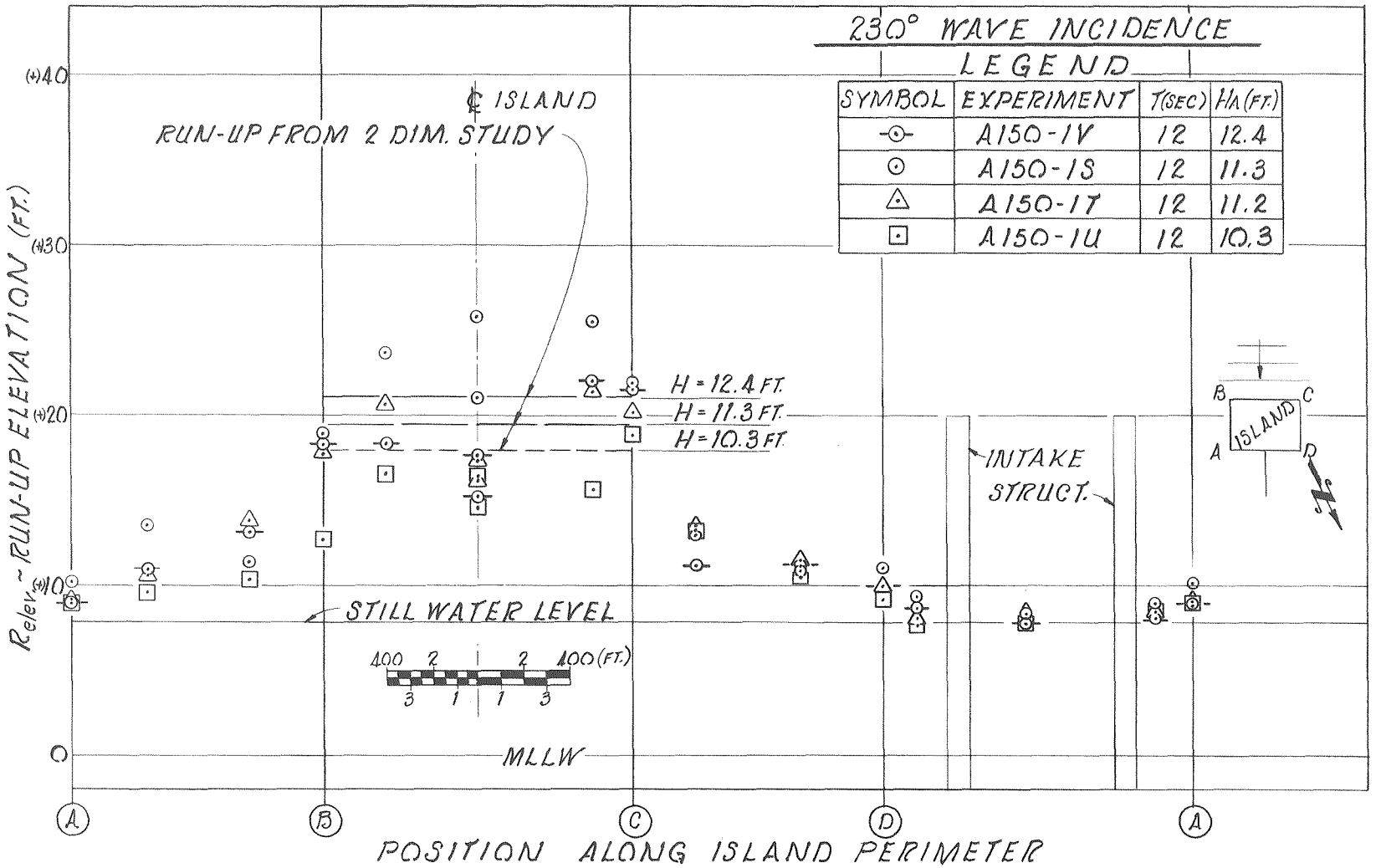

Figure 3.24 Run-Up Envelope in Three-Dimensional Model
Wave Direction at Island Site Azimuth 230°
T = 12 sec., MLLW +8 ft.

elevation +39 ft. for the 16-sec. wave. The 14-sec. wave period is the period associated with the highest one-third waves, and for a hurricane produced wave system it is considered to be more realistic than a wave of 16-sec. period which results from assuming an uncertainty in the period of +15%. Therefore, for the most probable wave (14-sec. period) a freeboard exists of about 5 ft. or approximately 19% of the maximum run-up measured. This is probably sufficient to account for the effects of scale in applying the results of this study to the prototype.

The run-up data for normally incident waves can be compared with the data presented in Figs. 3.25, 3.26, and 3.27 for the case of the design waves having a wave direction at the island of azimuth 200^{o}. In these figures the comparable results from the two-dimensional tests are also included. With only one exception the maximum run-up measured for this wave direction was at island corner B (the first point of wave attack on the island). The seaward face of the island (face BC) and the down-coast face of the island (face BA) experienced the maximum run-up for each of the three wave periods and for all wave heights, as would be expected. The up-coast face (face CD) and the shoreward face (face AD) both experienced essentially the same run-up, significantly less than the other two faces. The run-up generally tends to decrease on the seaward face of the island with distance from corner B to corner C. In all cases on the seaward face of the island the average run-up is significantly less than the run-up which was experienced at a comparable wave height and wave period in the two-dimensional model. Comparing Figs. 3.22 through 3.24 to Figs. 3.25 through 3.27 one can conclude that for the case of oblique incidence the run-up is somewhat less than for the case of a normally incident wave, with the exception of the corner first attacked by the wave (corner B). For this corner it appears that the run-up is approximately the same as that experienced at the center of the island face with the normally incident wave.

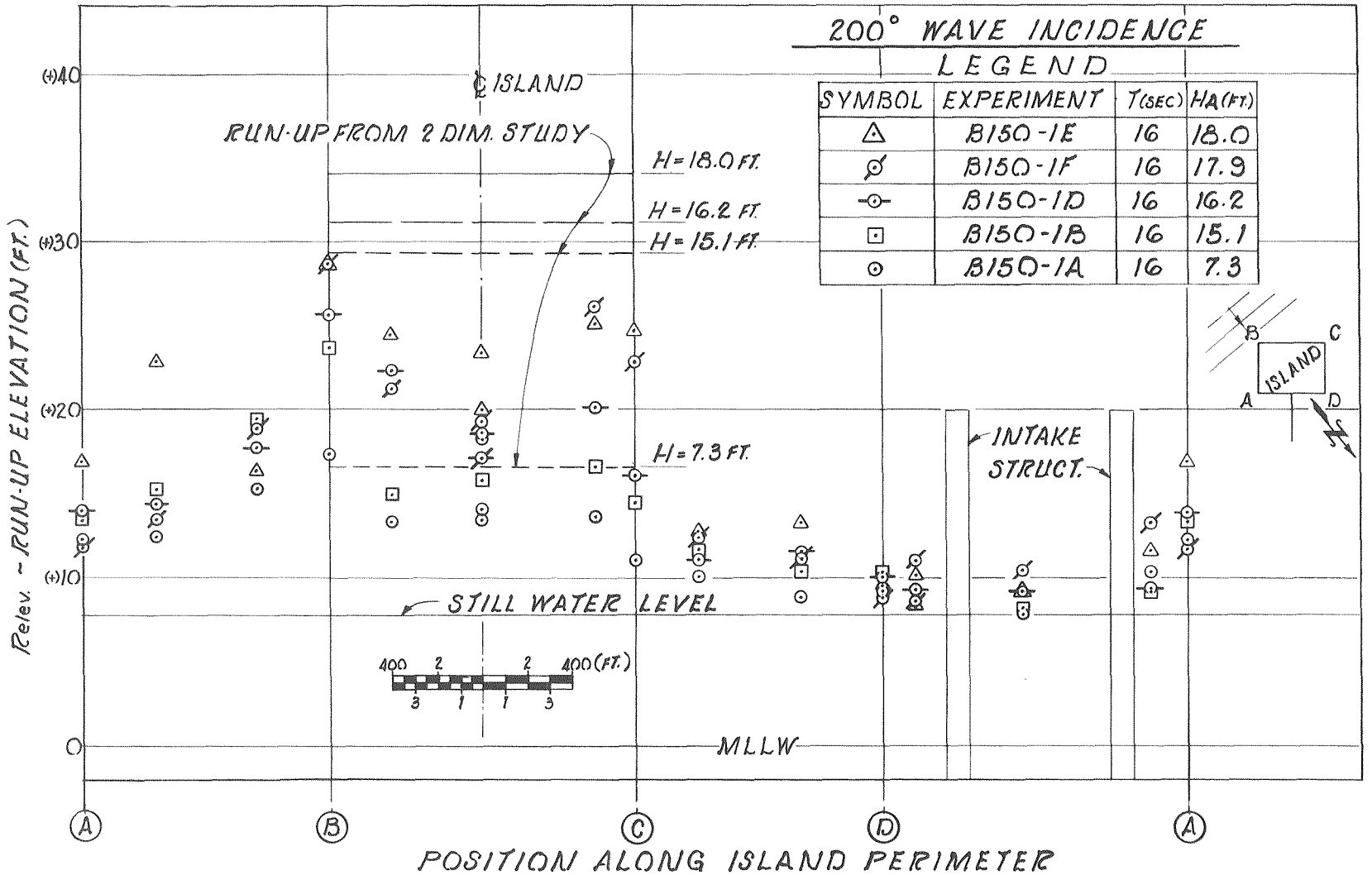

Figure 3.25 Run-Up Envelope in Three-Dimensional Model
Wave Direction at Island Site Azimuth 200°
T = 16 sec., MLLW +8 ft.

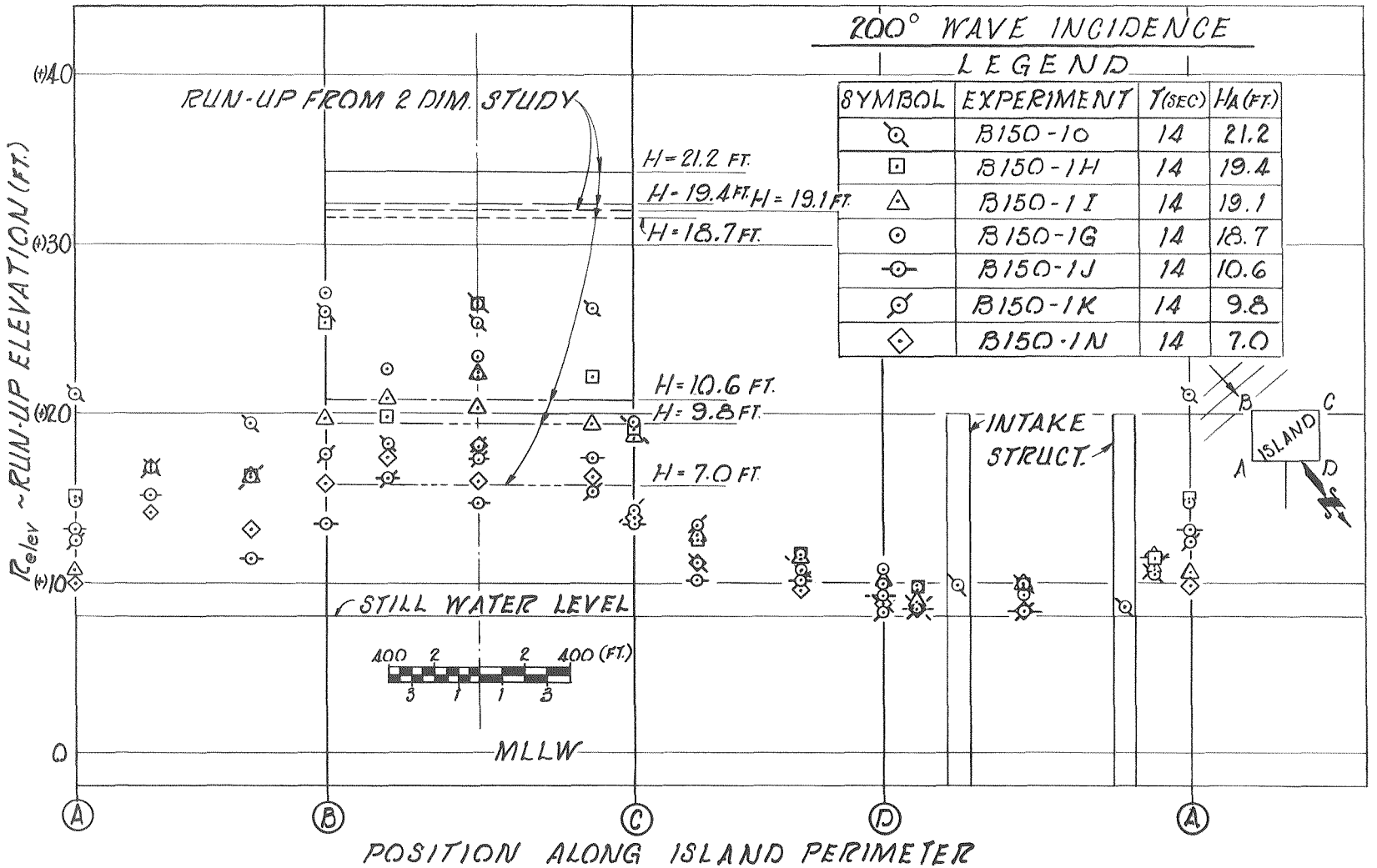

Figure 3.26 Run-Up Envelope in Three-Dimensional Model
Wave Direction at Island Site Azimuth 200°
T = 14 sec., MLLW +8 ft.

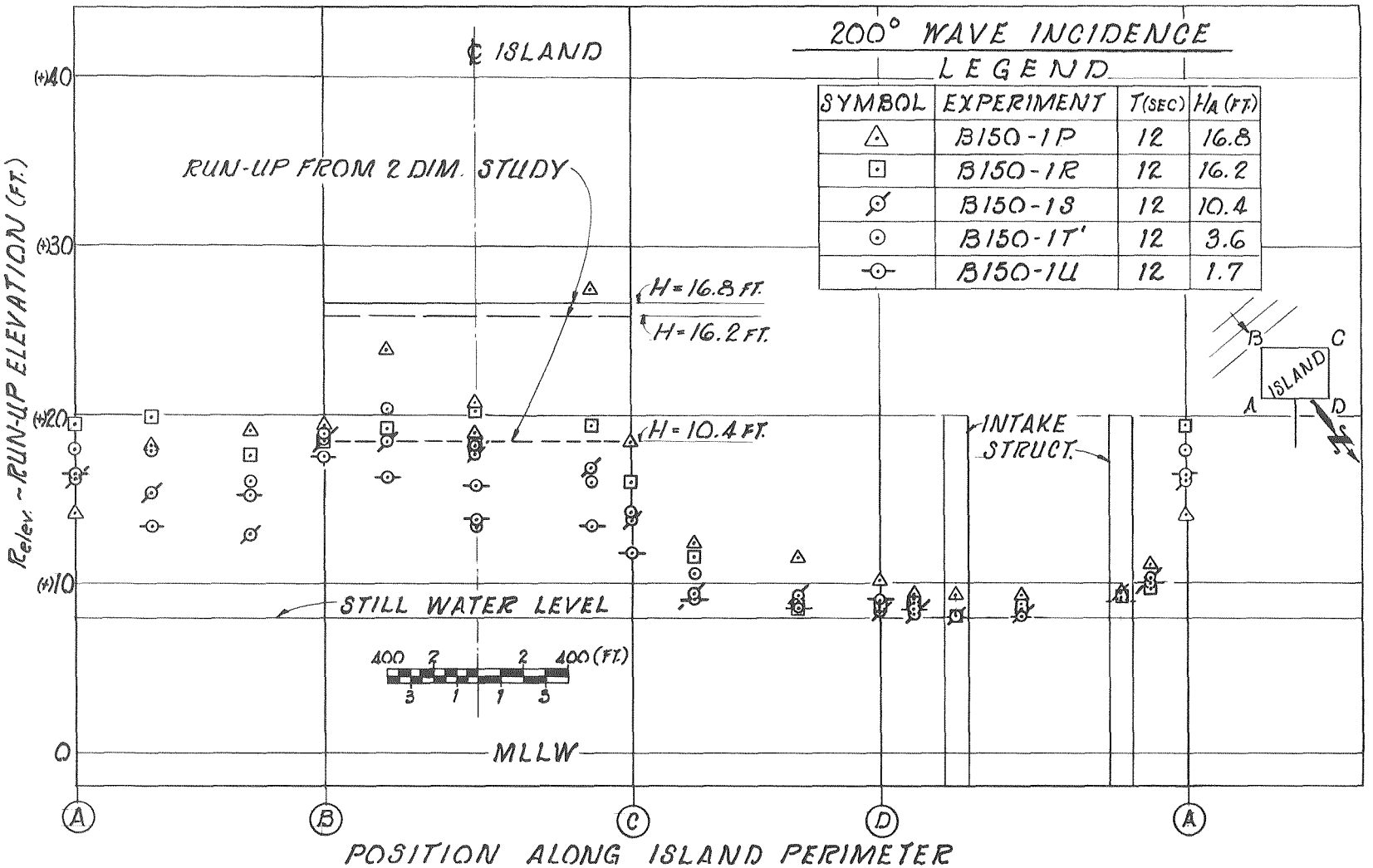

Figure 3.27 Run-Up Envelope in Three-Dimensional Model
Wave Direction at Island Site Azimuth 200°
T = 12 sec., MLLW +8 ft.

In view of the above results, one can say with assurance that the worst case of run-up on the seaward face of the island is for the case of a normally incident wave. In addition, the run-up on the seaward corner of the island (corner B) for the obliquely incident wave is no worse than the run-up on the seaward face of the island (face BC) for the normally incident wave.

The run-up envelope for the oblique wave coming from up-coast (wave direction at the island site of azimuth 240^{o})is presented in Fig. 3.28. Since two-dimensional model tests were not run at a prototype wave period of 10 seconds, there are no two-dimensional results shown in this figure. The trend of the results, however, are essentially the same as those shown on the other figures dealing with the three-dimensional run-up problem. The maximum run-up again occurred on the seaward face of the island (face BC) while in this case the run-up on the up-coast face (face CD) is somewhat greater than that on either the down-coast face (face AB) or the shoreward face (face AD). As would be expected, the maximum run-up is at corner C, the up-coast seaward corner, with a general decrease of run-up with distance from corner C to corner B and from corner C to corner D. The run-up on the shoreward face is again the minimum run-up experienced.

Photographs are presented in Figs. 3.29 through 3.33 showing, where possible, the condition of maximum run-up on the seaward face of the island (face BC) and the wave condition in the vicinity of the shoreward face (face AD). The wave height, wave period, and tide condition for each set of photographs is given in the figure. Vertical scales can be seen in each photograph located at the corners of the island. Each white or dark band on the scales is 10 ft. wide (to a prototype scale).

3. Wave Patterns

The wave patterns on and near the beach in the vicinity of the island were photographed in the three-dimensional model. Plan-view photographs were taken from the tower above the model and oblique views were taken from the floor of the laboratory. The photographs

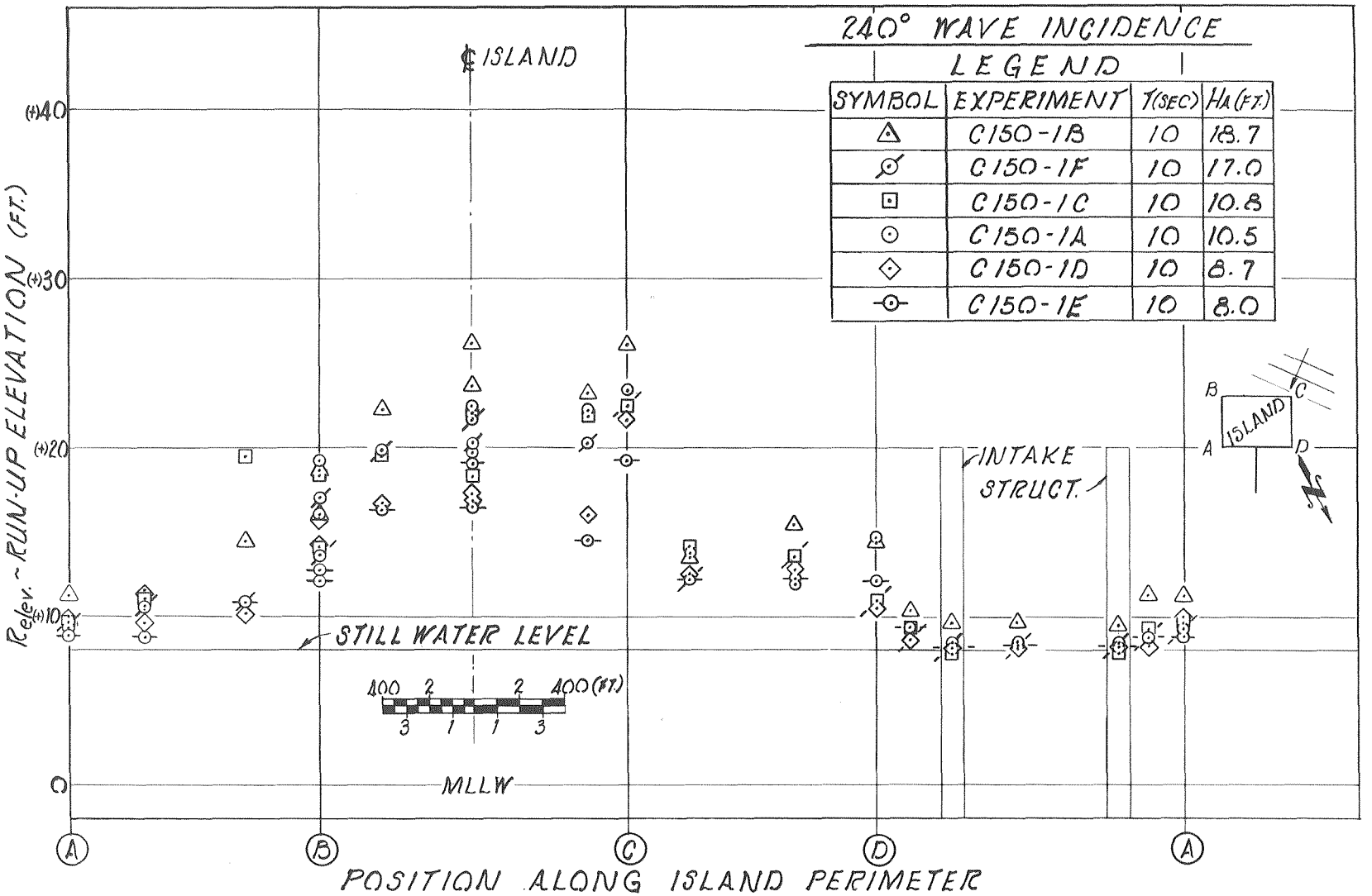

Figure 3.28 Run-Up Envelope in Three-Dimensional Model
Wave Direction at Island Site Azimuth 240°
T = 10 sec., MLLW + 8 ft.

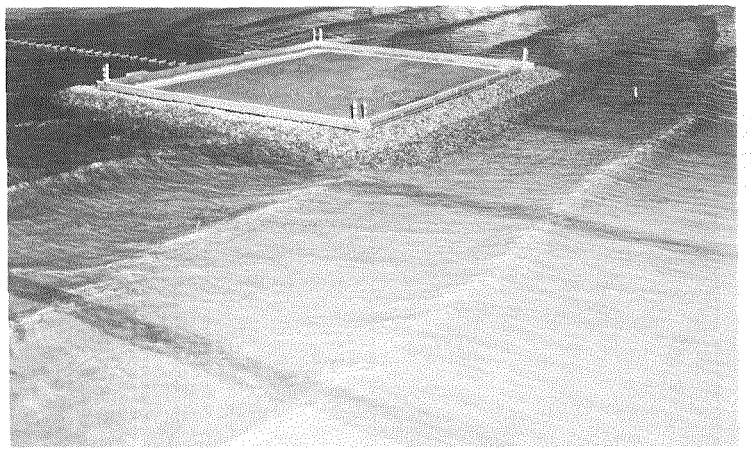

Figure 3.29a Photographs of Wave Attack on Seaward and Shoreward Faces of Island; Wave Direction at Island Site of Azimuth 230° (A150-1Y, T = 16 sec., H_A = 17.7 ft., MLLW + 8 ft.)

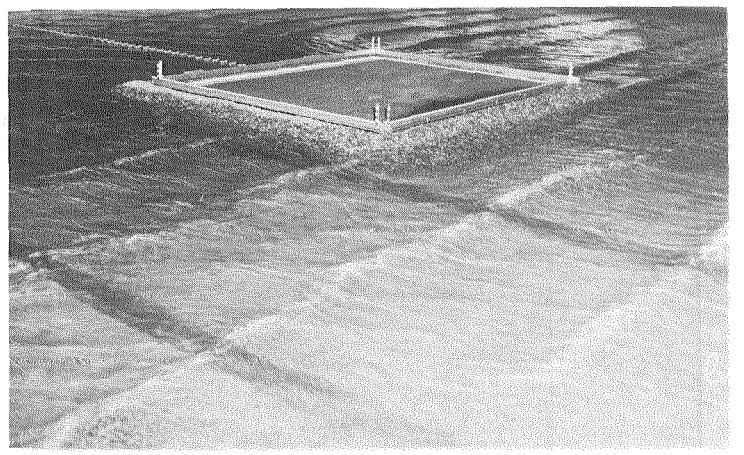

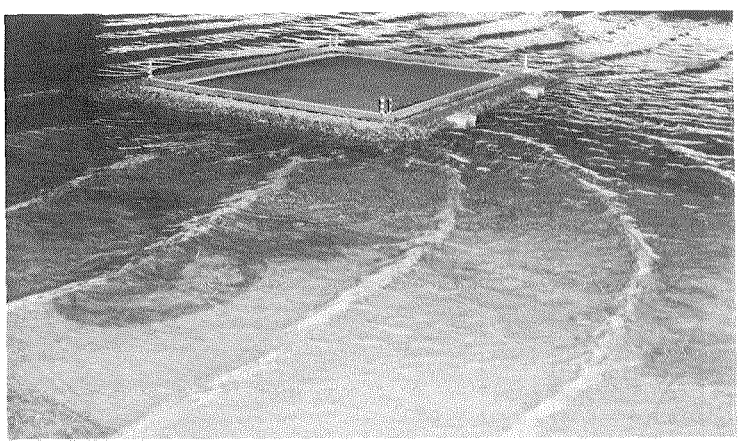

Figure 3.29b Photographs of Wave Attack on Seaward and Shoreward Faces of Island; Wave Direction at Island Site of Azimuth 230° (A150-1X, T = 14 sec., H_A = 14.9 ft., MLLW + 8 ft.)

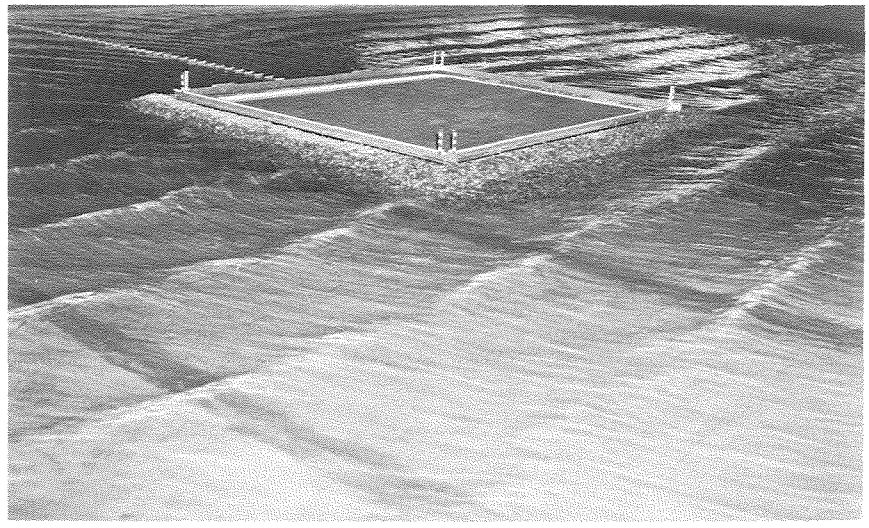

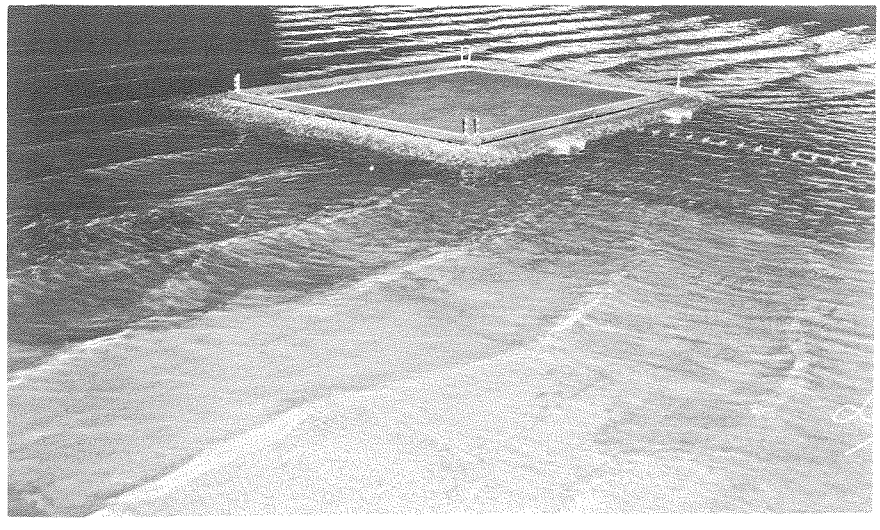

Figure 3.29c Photographs of Wave Attack on Seaward and Shoreward Faces of Island; Wave Direction at Island Site of Azimuth 230° (A150-1W, T = 12 sec., H_A = 11.3 ft., MLLW +8 ft.)

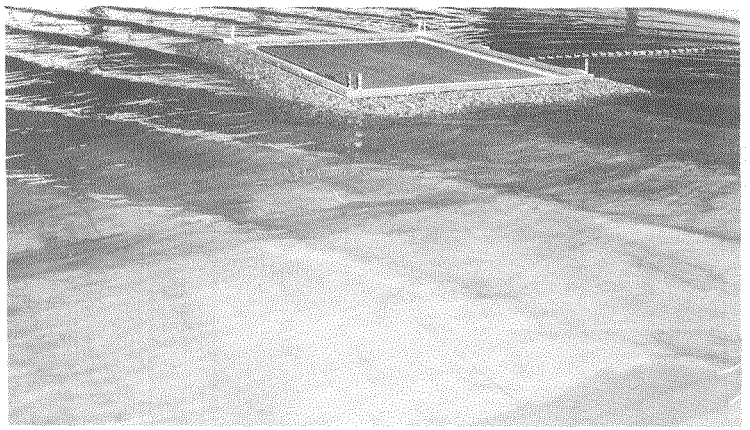

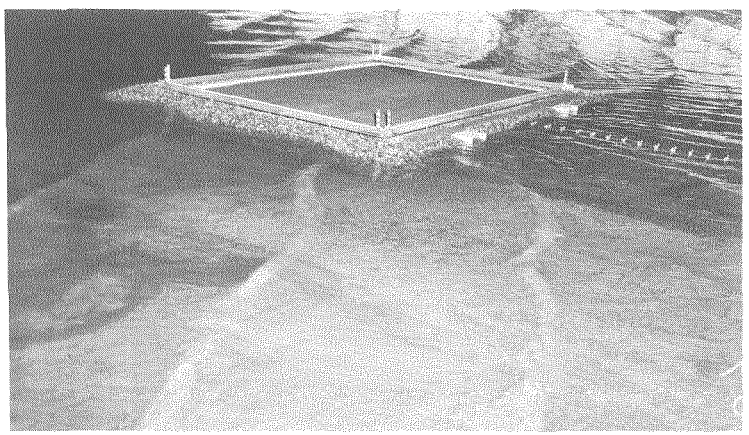

Figure 3.30a Photographs of Wave Attack on Seaward and Shoreward Faces of Island; Wave Direction at Island Site of Azimuth 200° (B150-1Y, T = 16 sec., H_A = 16.2 ft., MLLW + 8 ft.)

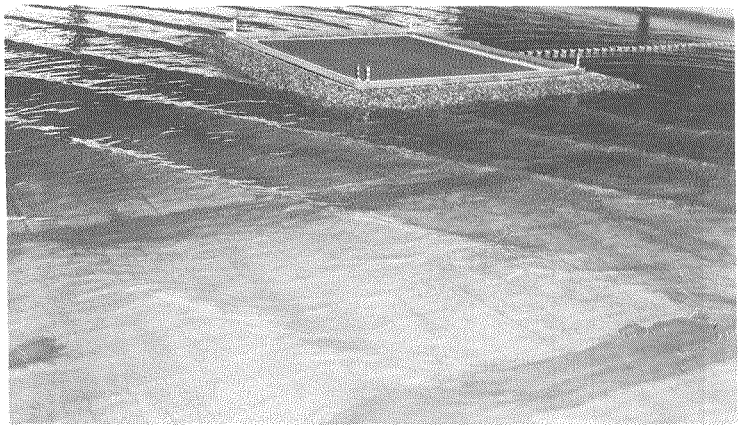

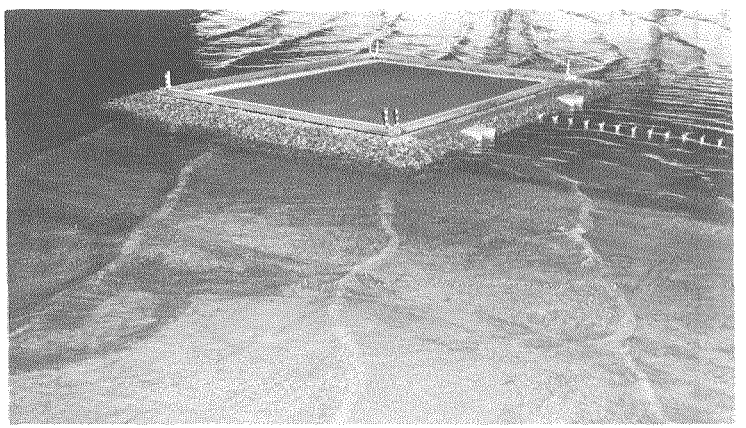

Figure 3.30b Photographs of Wave Attack on Seaward and Shoreward Faces of Island; Wave Direction at Island Site of Azimuth 200° (B150-1Z, T = 16 sec., H_A = 5.0 ft., MLLW - 2 ft.)

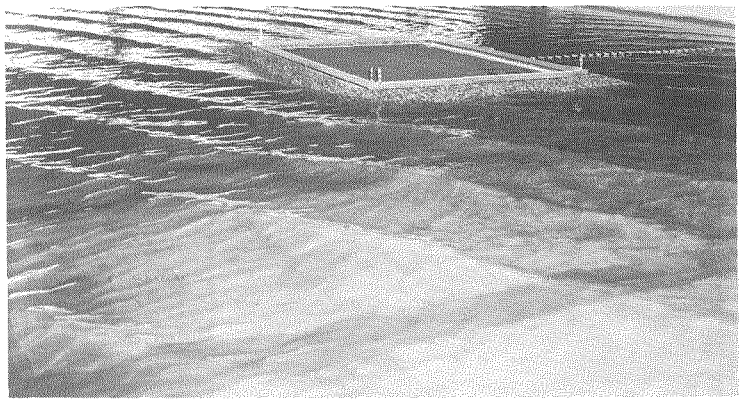

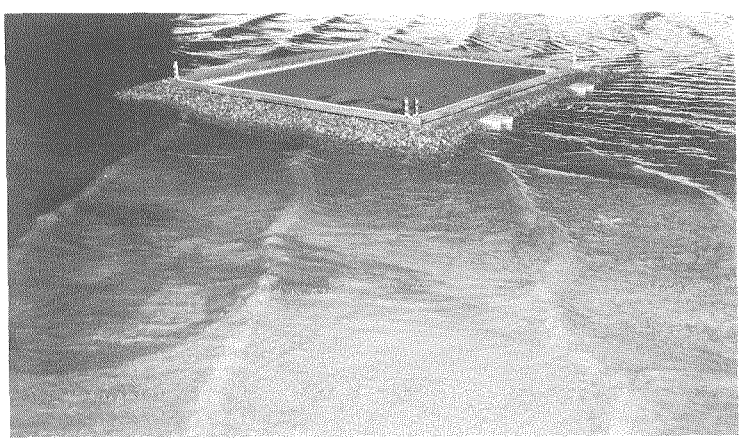

Figure 3.31a Photographs of Wave Attack on Seaward and Shoreward Faces of Island; Wave Direction at Island Site of Azimuth 200° (B150-1X, T = 14 sec., H_A = 8.7 ft., MLLW + 8 ft.)

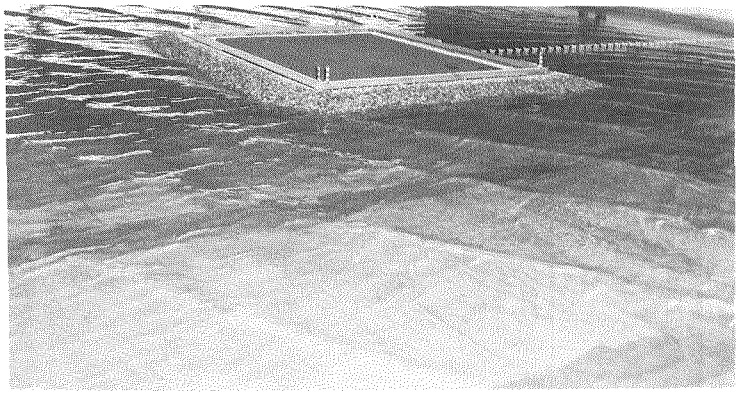

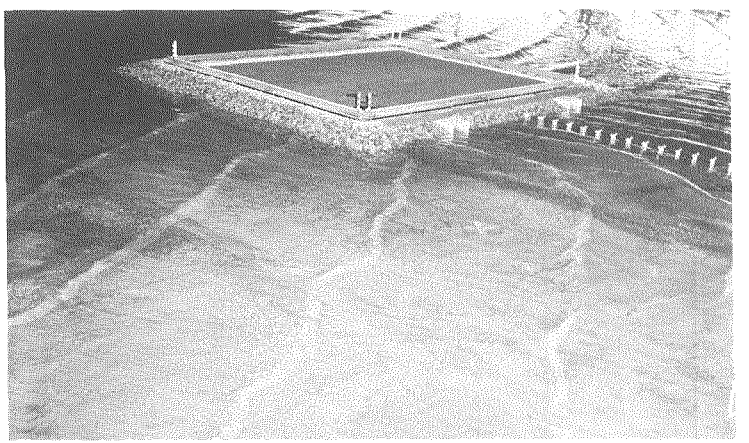

Figure 3.31b Photographs of Wave Attack on Seaward and Shoreward Faces of Island; Wave Direction at Island Site of Azimuth 200° (B150-1AA, T = 14 sec., H_A = 10.5 ft., MLLW - 2 ft.)

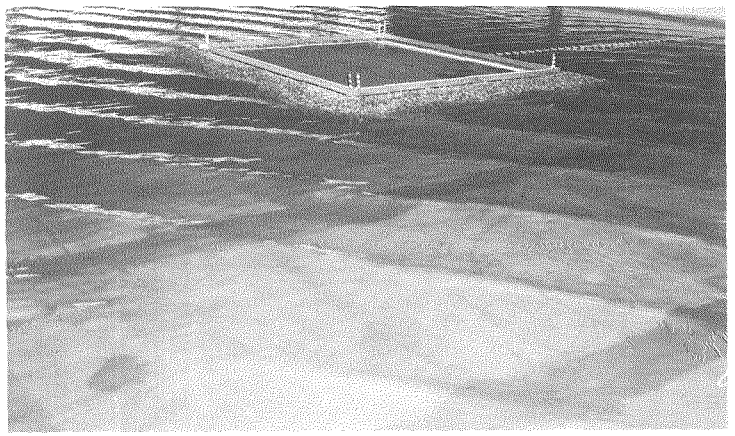

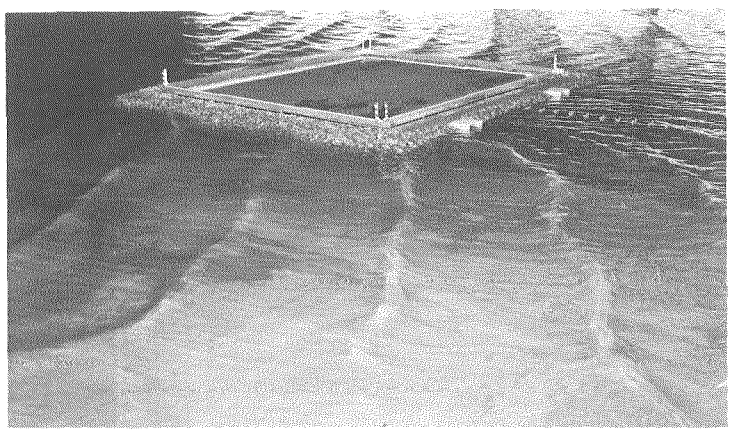

Figure 3.32a Photographs of Wave Attack on Seaward and Shoreward Faces of Island; Wave Direction at Island Site of Azimuth 200° (B150-1W, T = 12 sec., H_A = 16.2 ft., MLLW + 8 ft.)

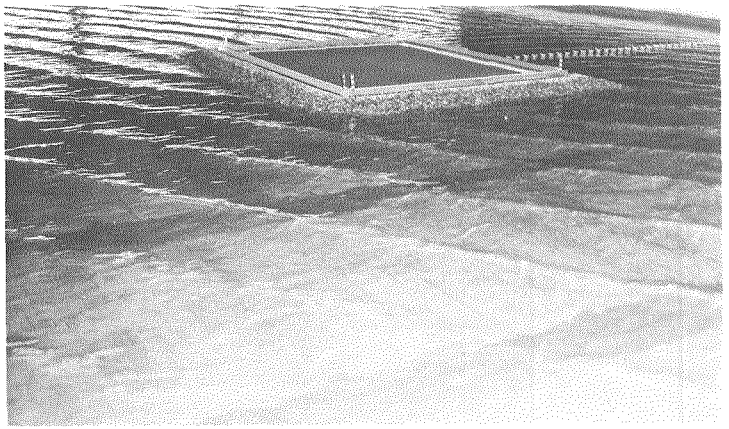

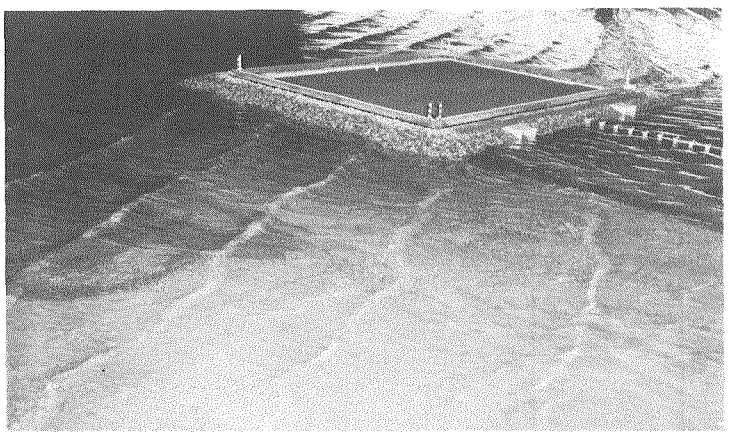

Figure 3.32b Photographs of Wave Attack on Seaward and Shoreward Faces of Island; Wave Direction at Island Site of Azimuth 200° (B150-1BB, T = 12 sec., H_A = 10.4 ft., MLLW - 2 ft.)

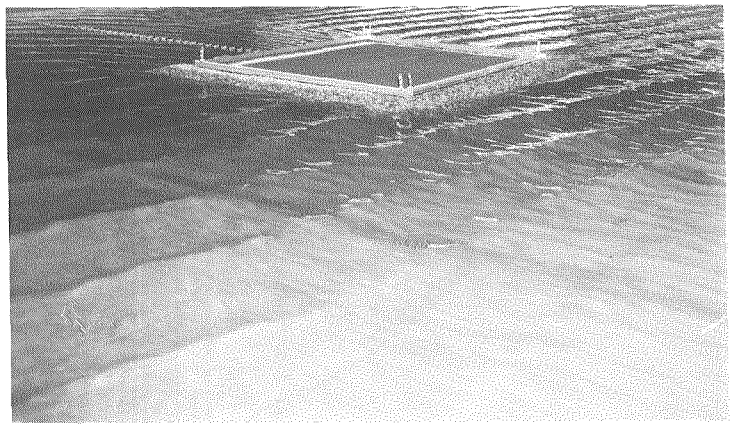

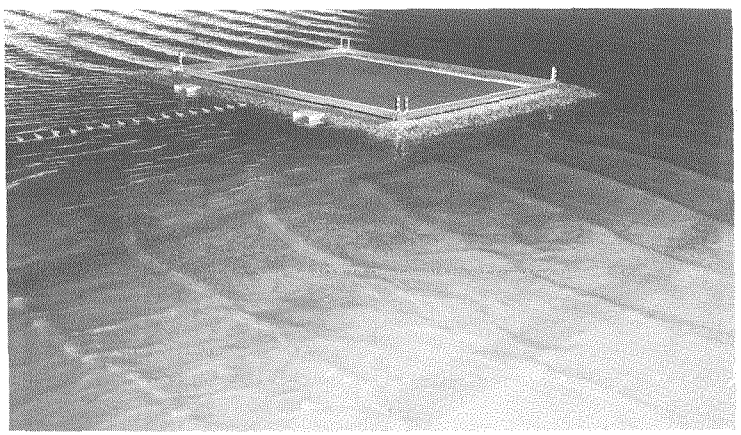

Figure 3.33a Photographs of Wave Attack on Seaward and Shoreward Faces of Island; Wave Direction at Island Site of Azimuth 240° (C150-1H, T = 10 sec., H_A = 17.0 ft., MLLW + 8 ft.)

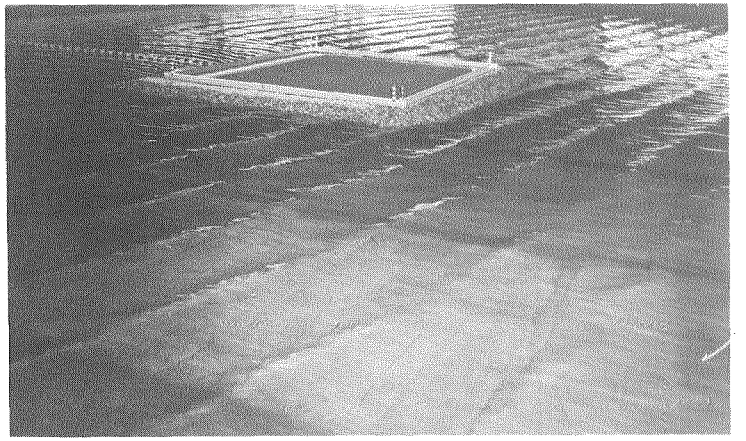

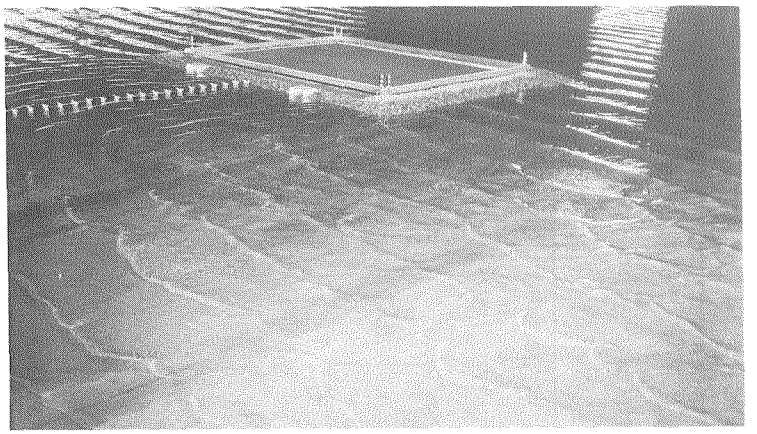

Figure 3.33b Photographs of Wave Attack on Seaward and Shoreward Faces of Island; Wave Direction at Island Site of Azimuth 240° (150-1I, T = 10 sec., H_A = 9.8 ft., MLLW - 2 ft.)

presented herein which show the wave patterns are listed in Table 3.6 for each of the three wave directions. For ease in interpreting the vertical photographs a scale in prototype feet has been placed on each photograph parallel to the beach. In addition small "crosses" have been painted on the bottom at the intersections of a number of the coordinates shown in Figs. 2.24, and these can be found in the plan-view photographs. The vertical pictures show very clearly the diffraction pattern in the lee of the island and that near the shoreward face of the island there is very little wave activity. The oblique photographs were taken especially to show the wave patterns near the beach. For the normally incident waves, pictures were taken only at the high tide, that is, tide stage elevation MLLW +8 ft. For waves with oblique incidence photographs were taken at the tide stages +8 ft. and -2 ft. For normally incident waves and for waves having a direction in the vicinity of the island of azimuth 200^{o} photographs were taken for wave periods corresponding to 12 sec., 14 sec. and 16 sec. in the prototype. For waves with a direction of azimuth 240^{o} near the island only waves with 10-sec. period were simulated.

4. Observations on and near Beach

The principal observations on and near the beach were made photographically and are contained in the photographs listed in Table 3.6. As shown by these photographs the waves diffracting around the north side of the island intersected with those diffracting around the south end of the island. Intersections of the Mach type were usually produced when these two diffracted waves intersected near the beach. At the point where the two waves intersected the waves became higher and moved faster than those in the vicinity of the intersection. This was usually accompanied by a strong breaking of the wave and the formation of the typical "Y" Mach intersection. These intersections also usually occurred in the lee of the island where the littoral current was very small or reversed in direction from that away from the shadow of the island.

Table 3.6. Photographs Showing Wave Patterns.

Fig. No.	Experiment	Wave Period T, (sec)	Wave Ht H (ft)	Tide Stage ft MLLW	Vertical View	Oblique View
	A. Waves Normally Incident on Island (Az. 230 deg.).					
3.34	A150-1W	12	11.3	+8	*	
3.35	A150-1X	14	14.9	+8	*	
3.36	A150-1X	14	14.9	+8		*
3.37	A150-1W	12	11.3	+8		*
3.38	A150-1Y	16	17.7	+8	*	
3.39	A150-1Y	16	17.7	+8		*
	B. Waves at Island Site Az. 200 deg.					
3.40	B150-1W	12	16.2	+8	*	
3.41	B150-1BB	12	10.4	-2	*	
3.42	B150-1W	12	16.2	+8		*
3.43	B150-1BB	12	10.4	-2		*
3.44	B150-1X	14	18.7	+8	*	
3.45	B150-1Y	16	16.2	+8	*	
3.46	B150-1AA	14	10.5	-2	*	
3.47	B150-1Y	16	16.2	+8		*
3.48	B150-1AA	14	10.5	-2		*
3.49	B150-1Z	16	15.0	-2	*	
3.50	B150-1Z	16	15.0	-2		*
	C. Waves at Island Site Az. 240 deg.					
3.51	C150-1G	10	10.5	+8	*	
3.52	C150-1H	10	17.0	+8	*	
3.53	C150-1I	10	9.8	-2	*	
3.54	C150-1G	10	10.5	+8		*
3.55	C150-1I	10	9.8	-2		*

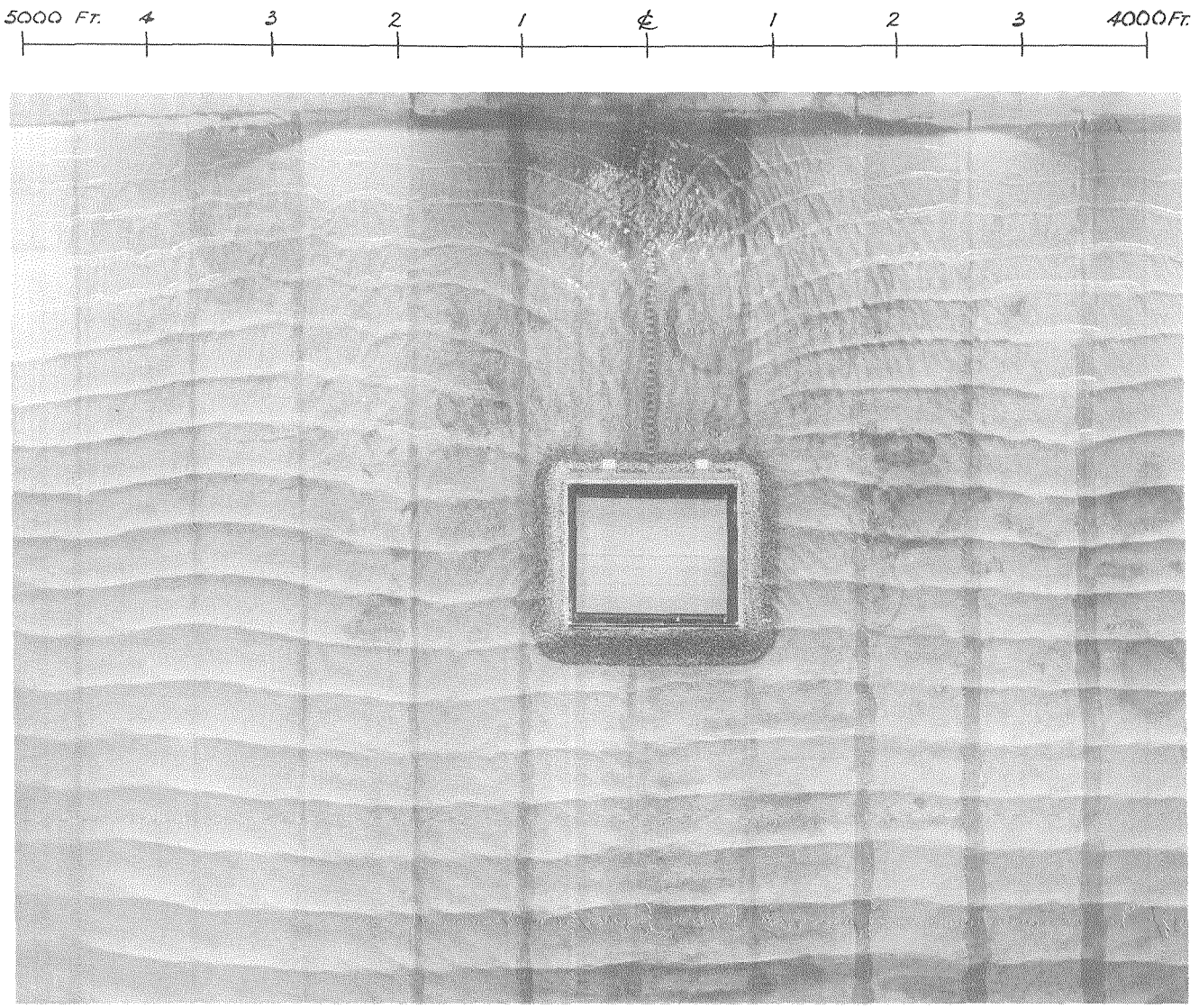

Figure 3.34 Plan View Photograph of Three-Dimensional Model, Azimuth 230° (A150-1W, T = 12 sec., H_A = 11.3 ft., MLLW +8 ft.)

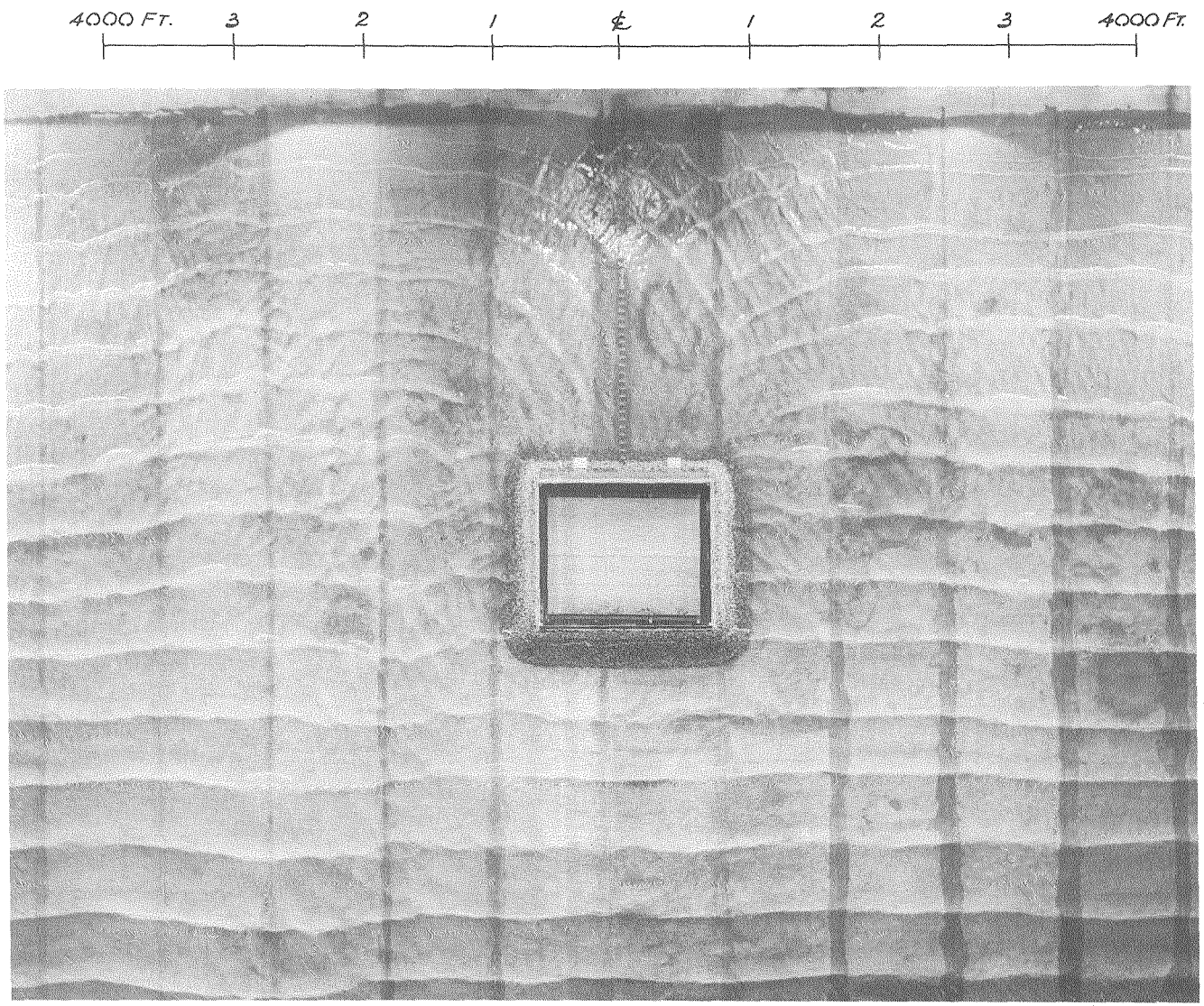

Figure 3.35 Plan View Photograph of Three-Dimensional Model, Azimuth 230° (A150-1X, T = 14 sec., H_A = 14.9 ft., MLLW + 8 ft.)

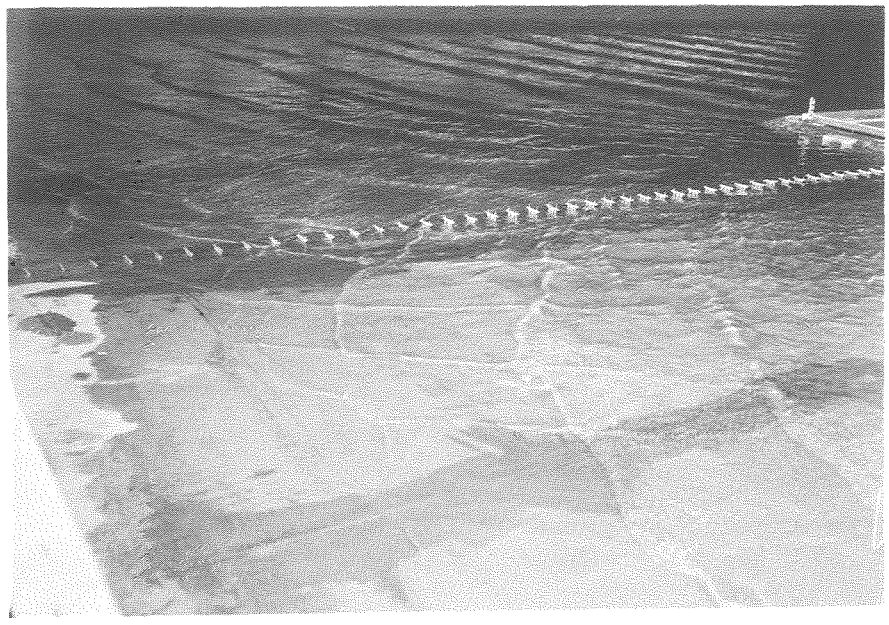

Figure 3.36 Oblique View of Wave Pattern near Beach, Azimuth 230° (A150-1X, T = 14 sec., H_A = 14.9 ft., MLLW +8 ft.)

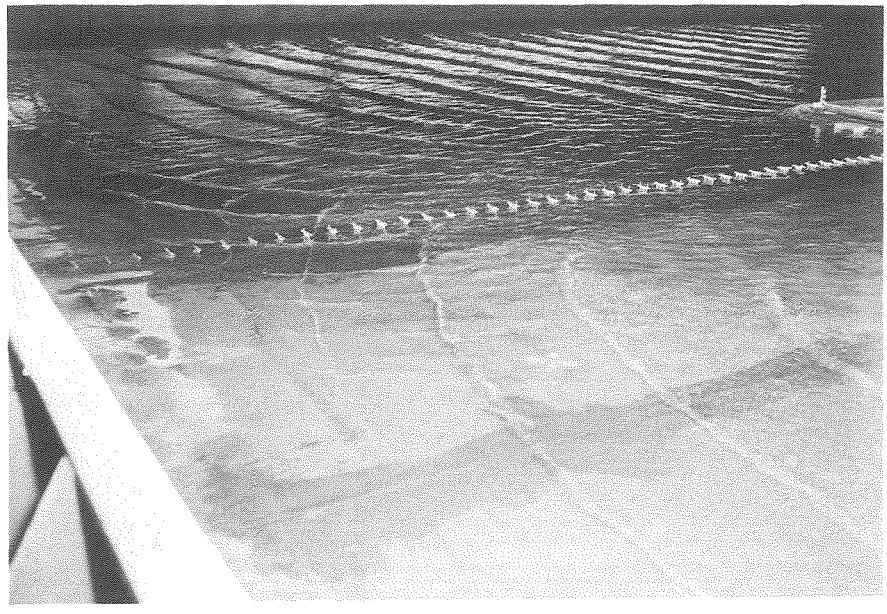

Figure 3.37 Oblique View of Wave Pattern near Beach, Azimuth 230° (A150-1W, T = 12 sec., H_A = 11.3 ft., MLLW +8 ft.)

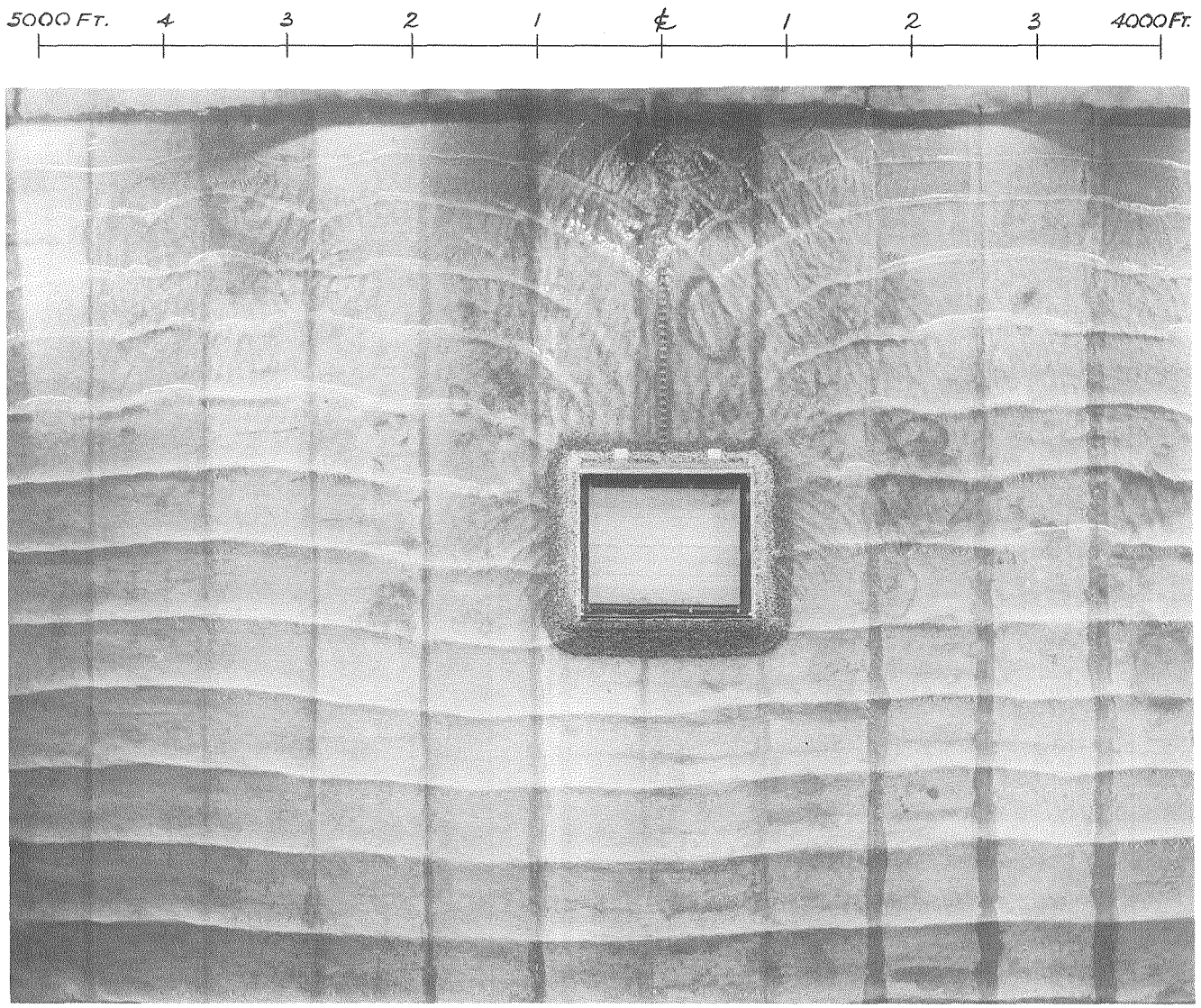

Figure 3.38 Plan View Photograph of Three-Dimensional Model, Azimuth 230° (A150-1Y, T = 16 sec., H_A = 17.7 ft., MLLW + 8 ft.)

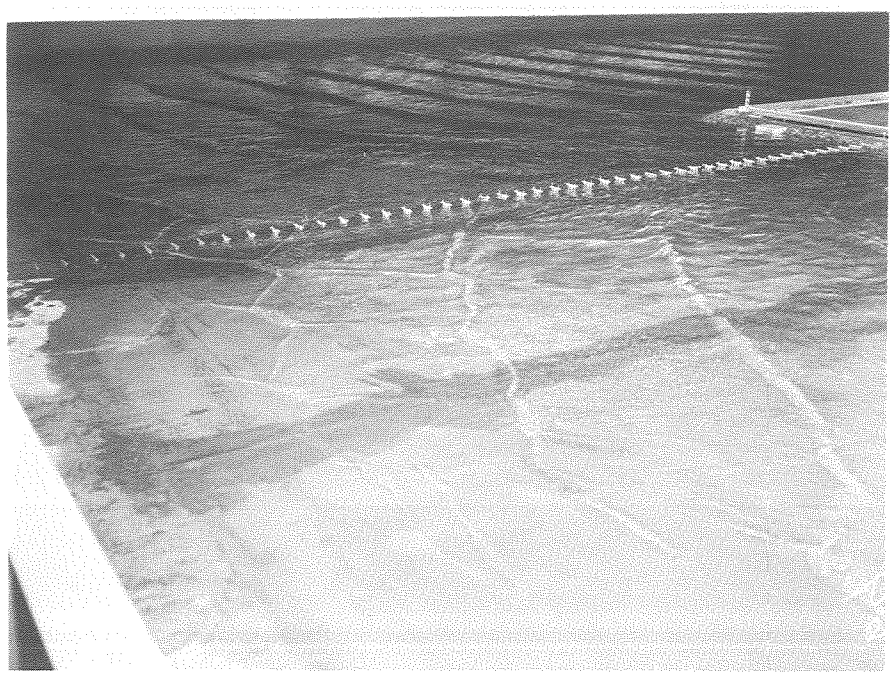

Figure 3.39 Oblique View of Wave Pattern near Beach, Azimuth 230° (A150-1Y, T = 16 sec., H_A = 17.7 ft., MLLW +8 ft.)

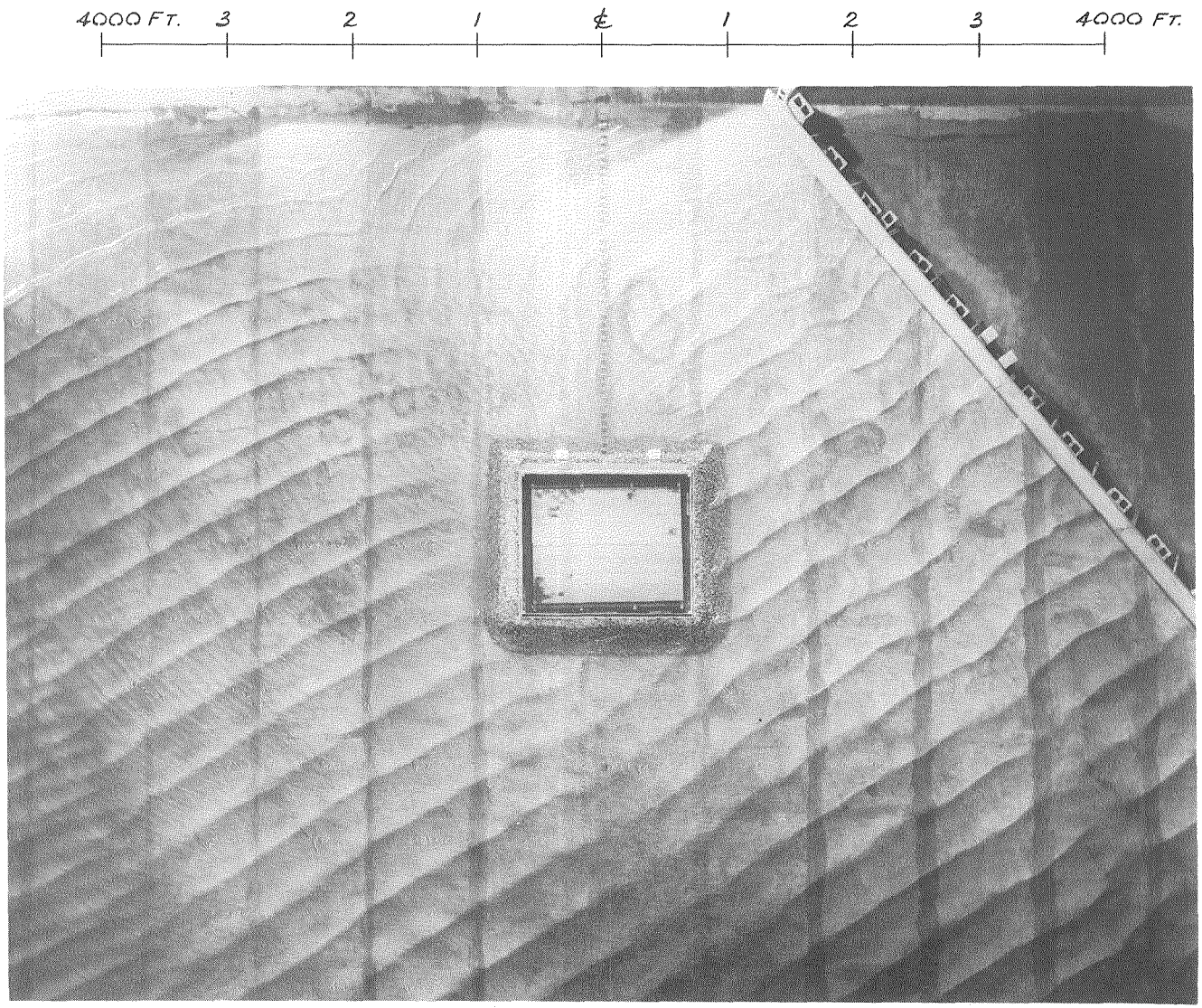

Figure 3.40 Plan View Photograph of Three-Dimensional Model, Azimuth 200° (B150-1W, T = 12 sec., H_A = 16.2 ft., MLLW +8 ft.)

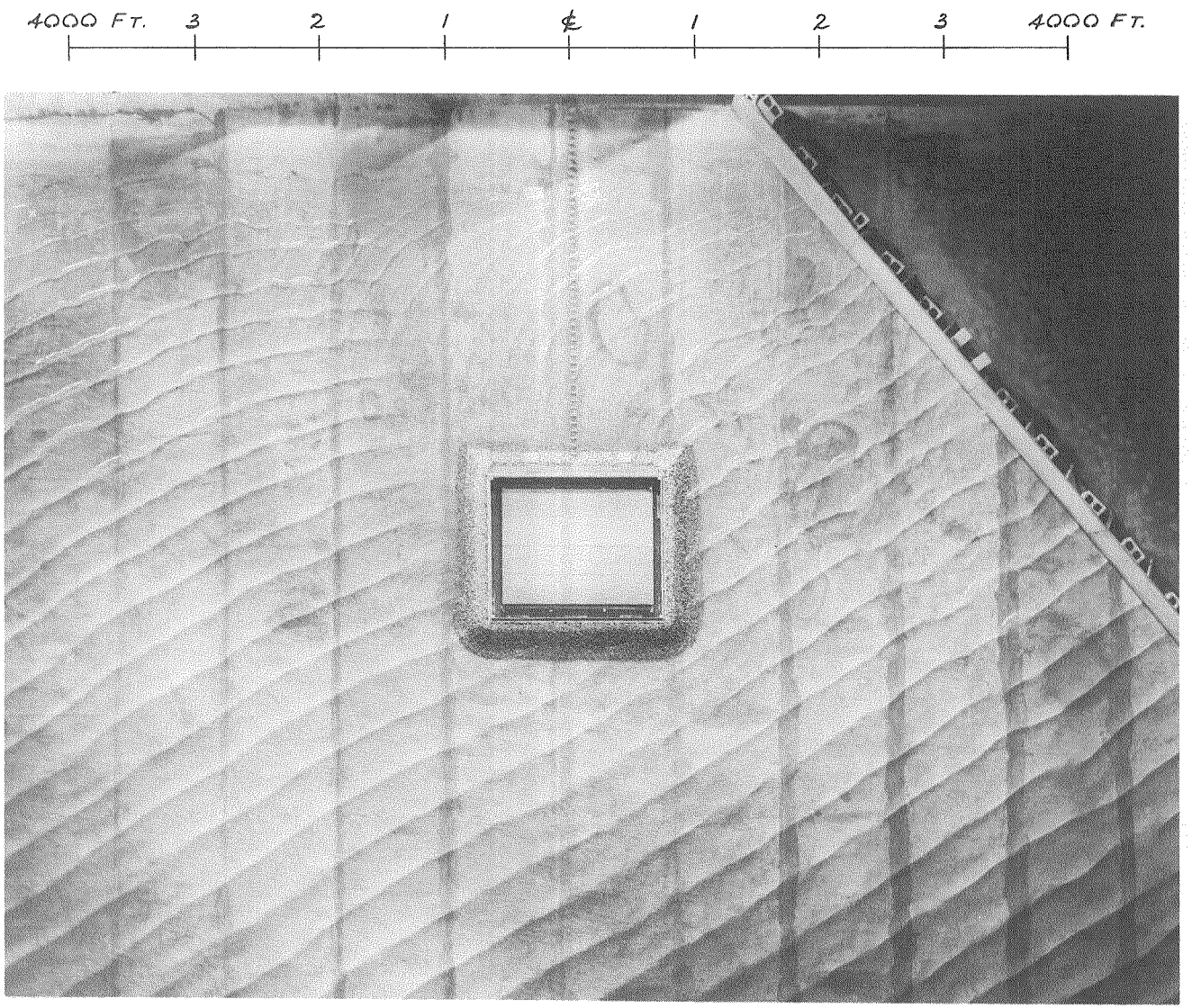

Figure 3.41 Plan View Photograph of Three-Dimensional Model, Azimuth 200° (B150-1BB, T = 12 sec., H_A = 10.4 ft., MLLW -2 ft.)

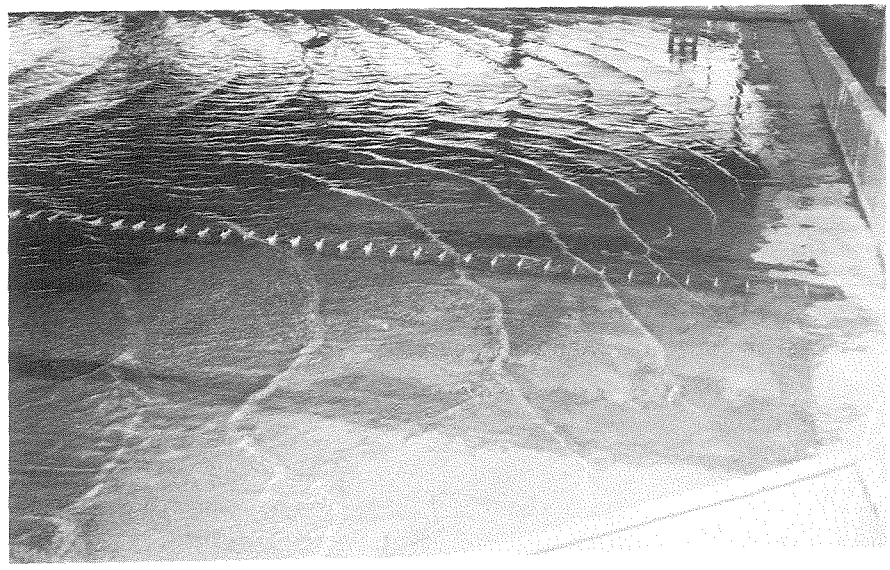

Figure 3.42 Oblique View of Wave Pattern near Beach, Azimuth 200° (B150-1W, T = 12 sec., H_A = 16.2 ft., MLLW +8 ft.)

Figure 3.43 Oblique View of Wave Pattern near Beach, Azimuth 200° (B150-1BB, T = 12 sec., H_A = 10.4 ft., MLLW -2 ft.)

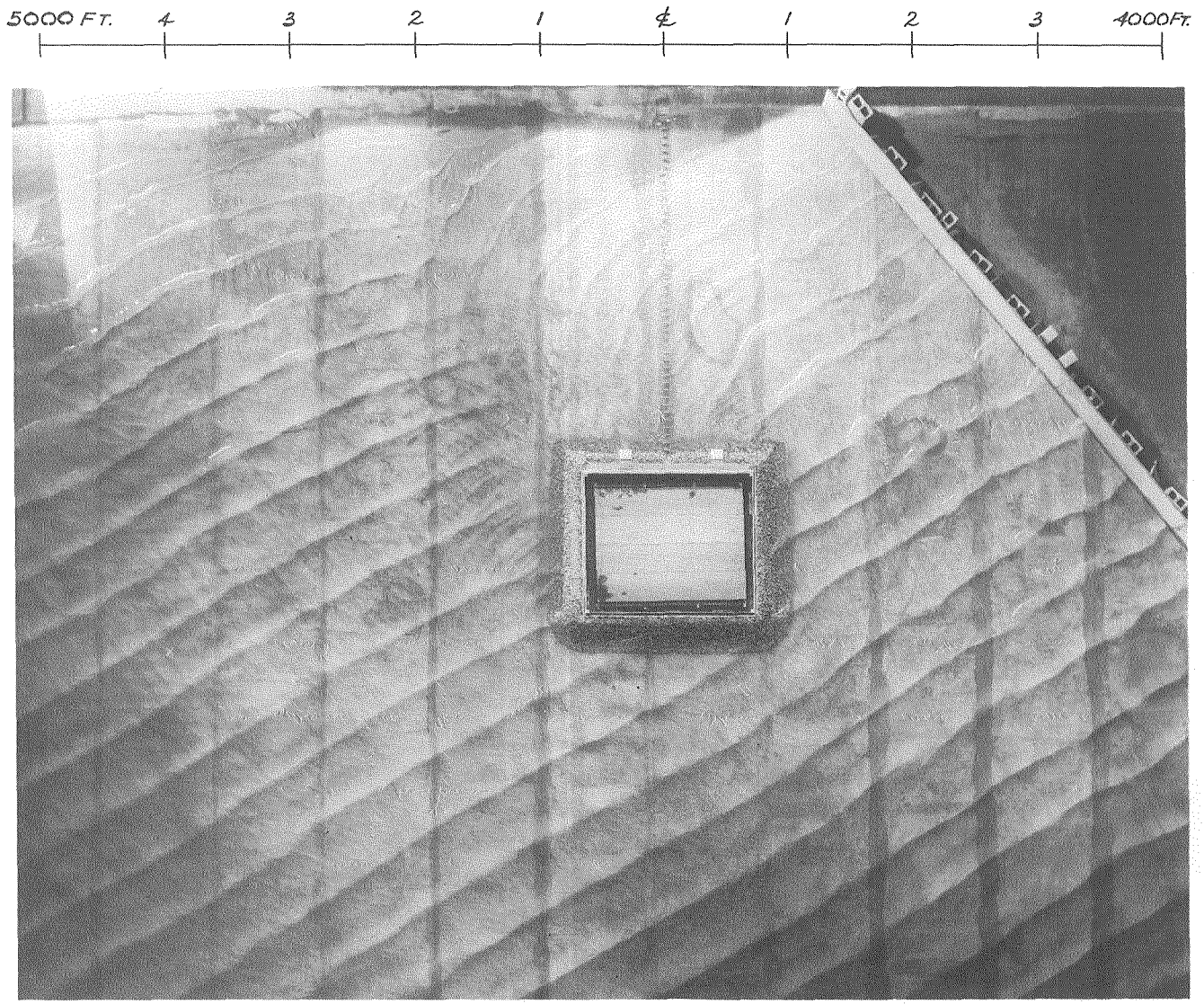

Figure 3.44 Plan View Photograph of Three-Dimensional Model, Azimuth 200° (B150-1X, T = 14 sec., H_A = 18.7 ft., MLLW +8 ft.)

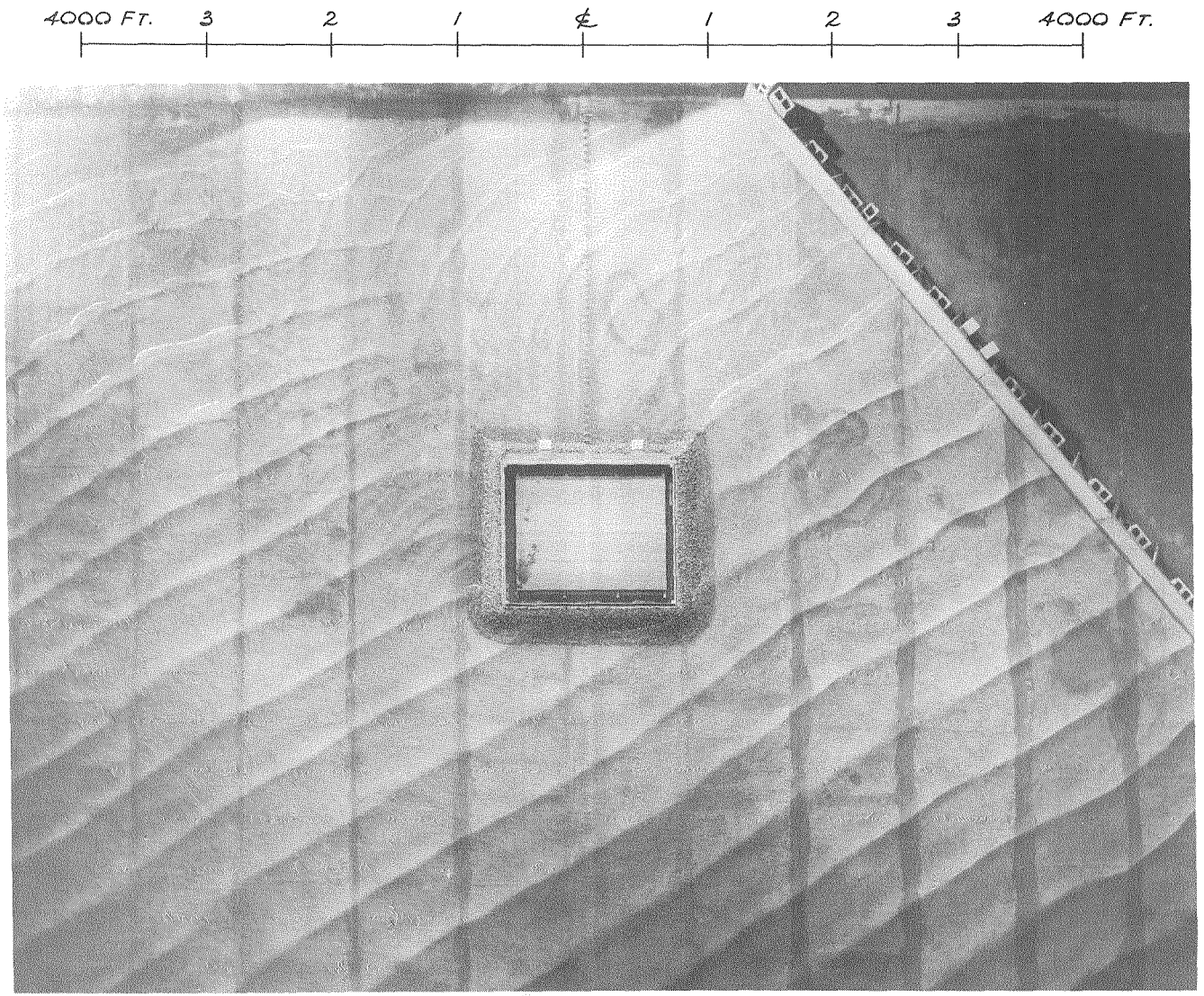

Figure 3.45 Plan View Photograph of Three-Dimensional Model, Azimuth 200° (B150-1Y, T = 16 sec., H_A = 16.2 ft., MLLW +8 ft.)

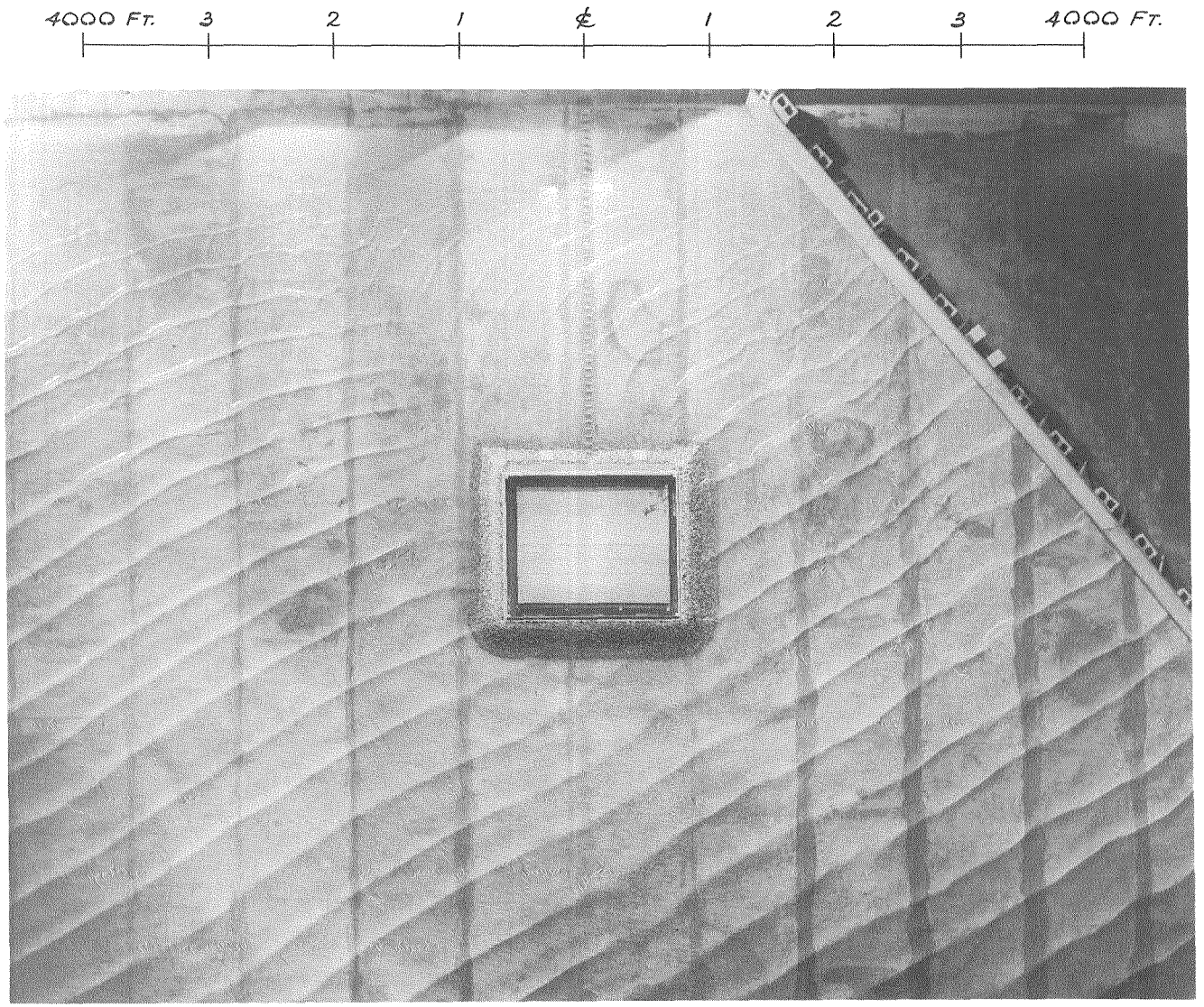

Figure 3.46 Plan View Photograph of Three-Dimensional Model, Azimuth 200° (B150-1AA, T = 14 sec., H_A = 10.5 ft., MLLW -2 ft.)

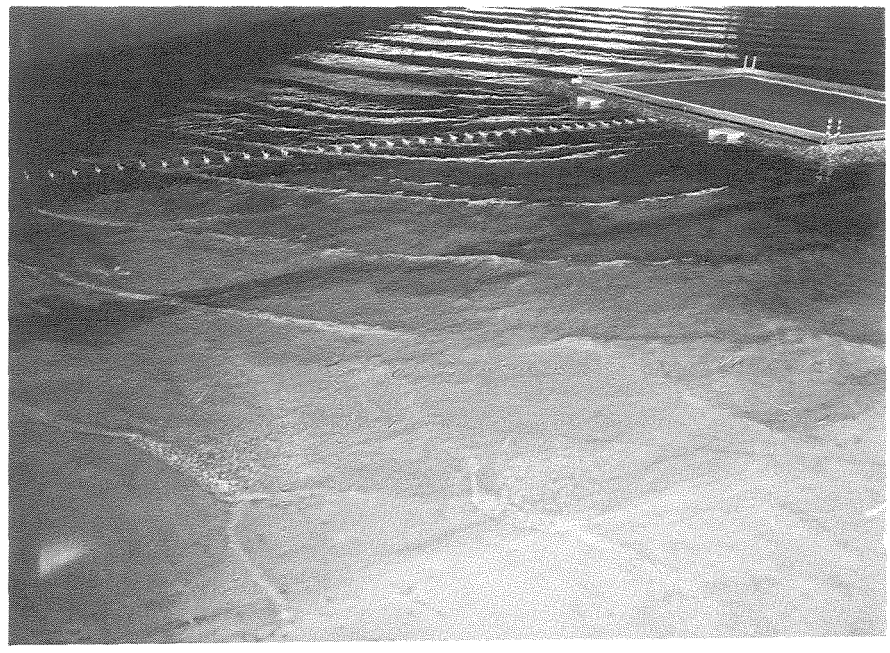

Figure 3.47 Oblique View of Wave Pattern near Beach, Azimuth 200° (B150-1Y, T = 16 sec., H_A = 16.2 ft., MLLW +8 ft.)

Figure 3.48 Oblique View of Wave Pattern near Beach, Azimuth 200° (B150-1AA, T = 14 sec., H_A = 10.5 ft., MLLW -2 ft.)

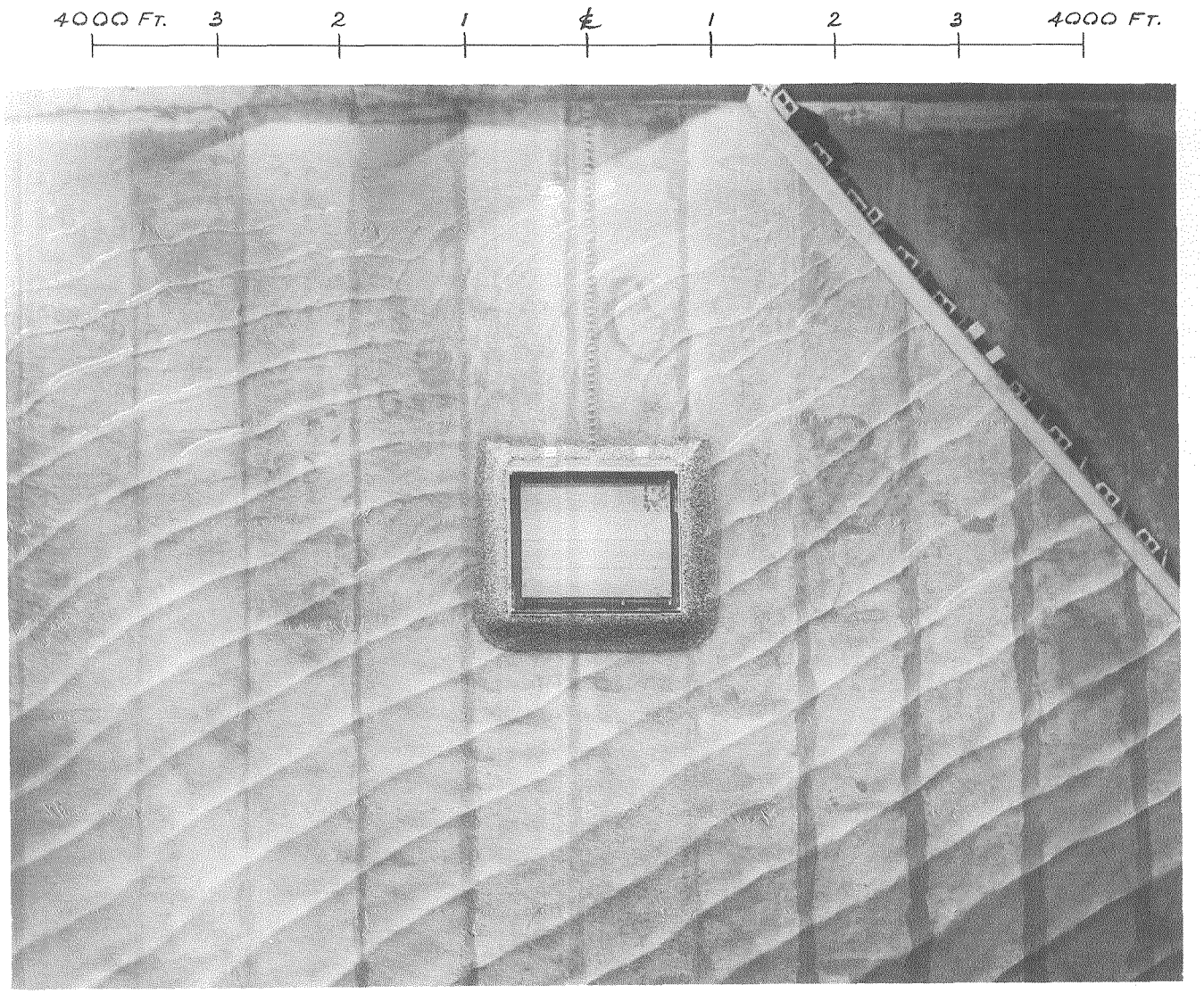

Figure 3.49 Plan View Photograph of Three-Dimensional Model, Azimuth 200° (B150-1Z, T = 16 sec., H_A = 15.0 ft., MLLW -2 ft.)

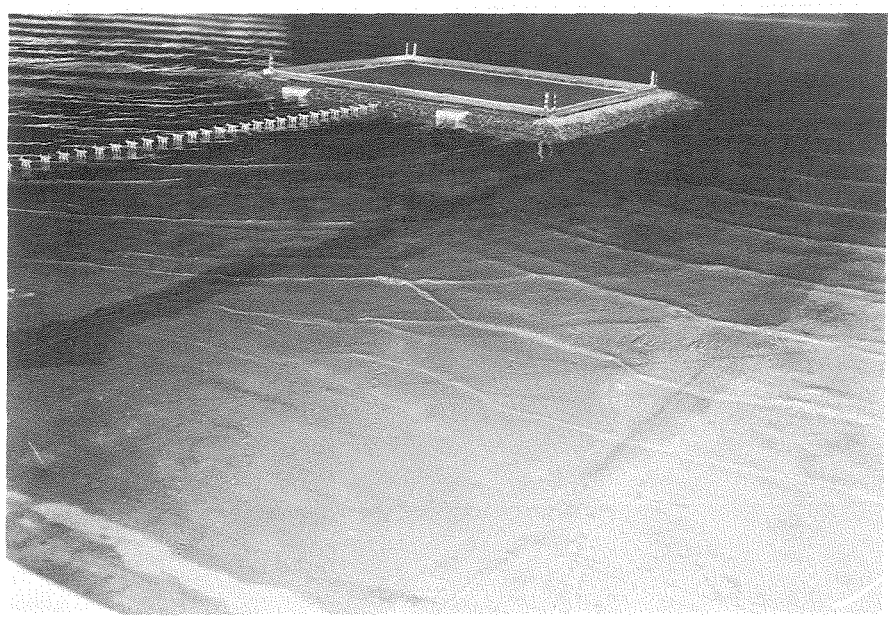

Figure 3.50 Oblique View of Wave Pattern near Beach, Azimuth 200° (B150-1Z, T = 16 sec., H_A = 15.0 ft., MLLW -2 ft.)

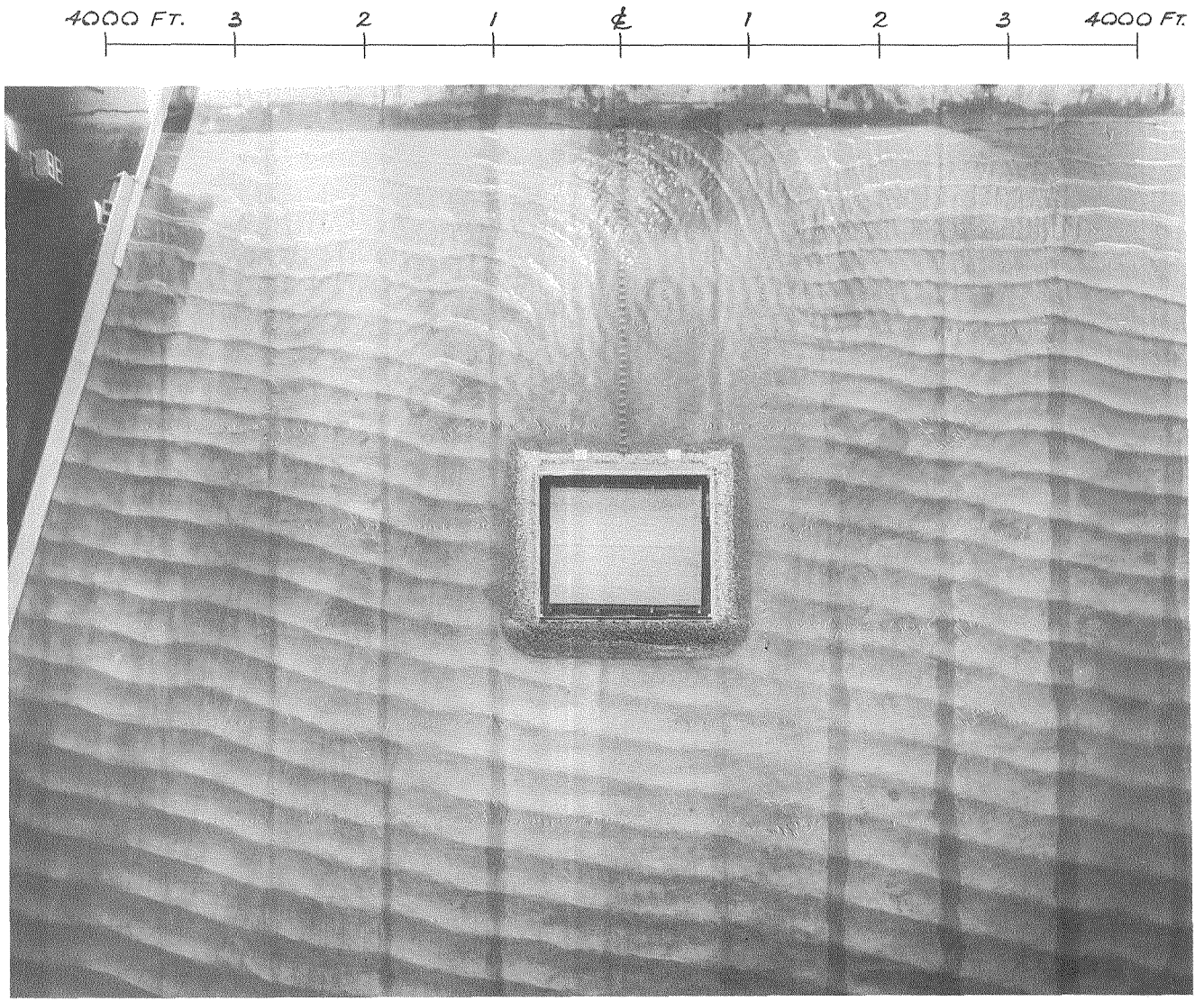

Figure 3.51 Plan View Photograph of Three-Dimensional Model, Azimuth 240° (C150-1G, T = 10 sec., H_A = 10.5 ft., MLLW +8 ft.)

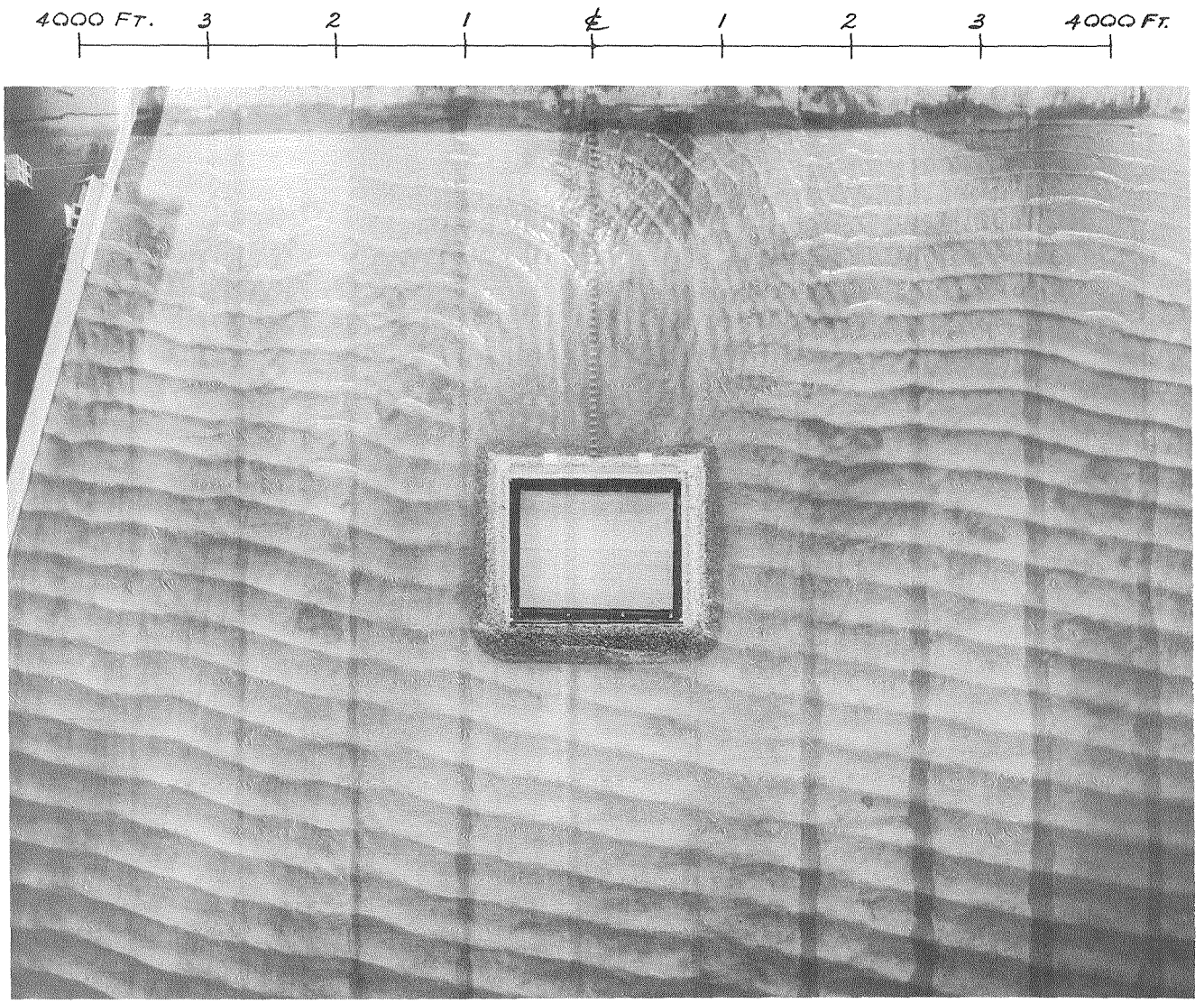

Figure 3.52 Plan View Photograph of Three-Dimensional Model, Azimuth 240° (C150-1H, T = 10 sec., H_A = 17 ft., MLLW +8 ft.)

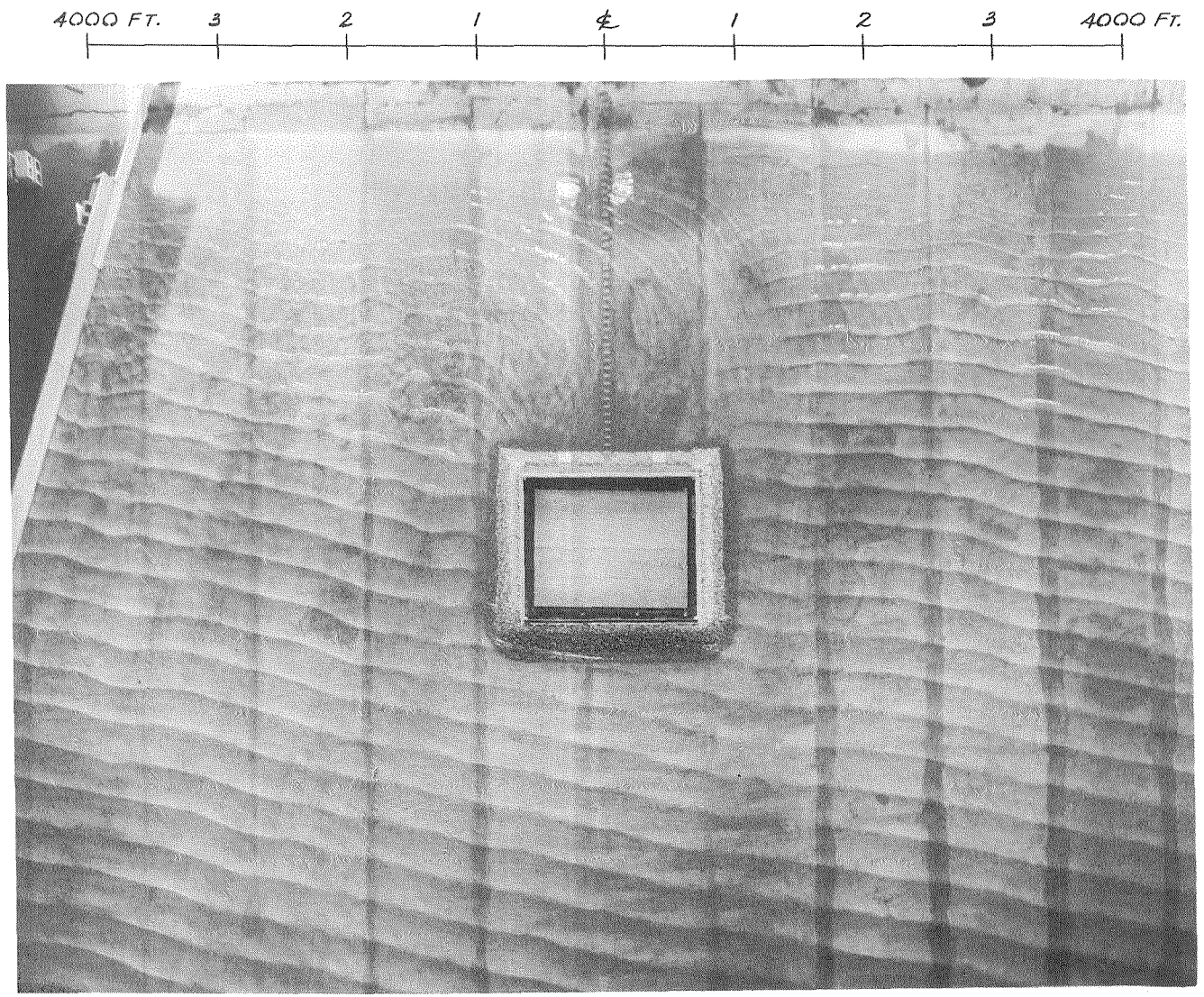

Figure 3.53 Plan View Photograph of Three-Dimensional Model, Azimuth 240° (C150-1I, T = 10 sec., H_A = 9.8 ft., MLLW -2 ft.)

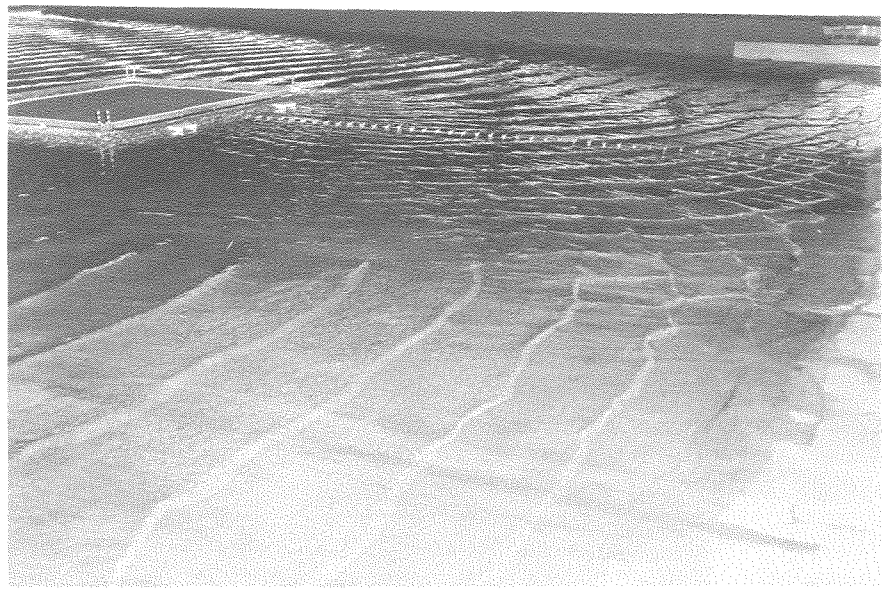

Figure 3.54 Oblique View of Wave Pattern near Beach, Azimuth 240° (C150-1G, T = 10 sec., H_A = 10.5 ft., MLLW + 8 ft.)

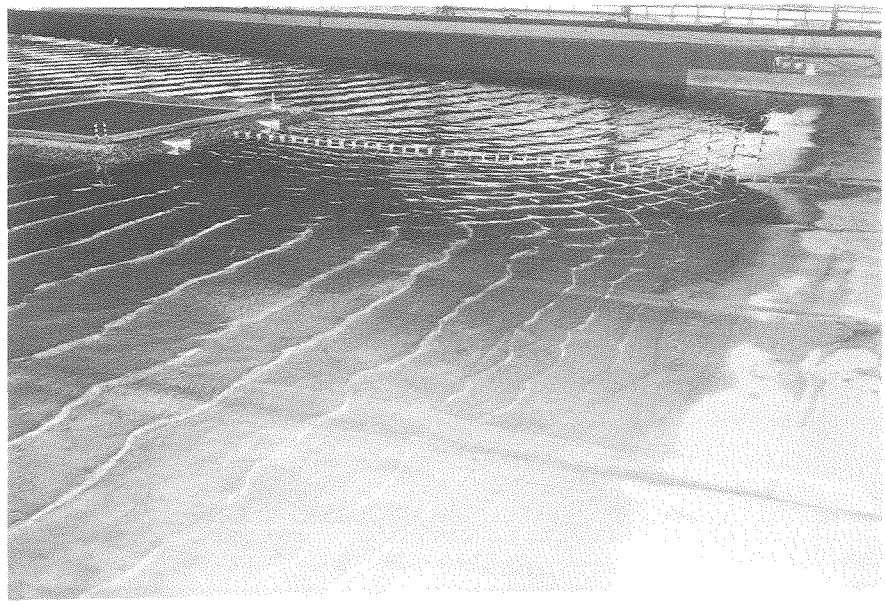

Figure 3.55 Oblique View of Wave Pattern near Beach, Azimuth 240° (C150-1I, T = 10 sec., H_A = 9.8 ft., MLLW -2 ft.)

Several schemes were tried for observing littoral currents. One of these was to put ground coal on the beach and to follow its motion. Another was to observe the currents by following bubbles which are usually present on the water surface. A third method was to drop crystals of dye into the water and to observe the current direction by dye dissolved from the crystals. The use of coal as an indicator of littoral drift was not found very satisfactory because small irregularities in the beach, not representative of the prototype conditions, could interfere with the drift. The dye worked very well but most of the time the observations were made by merely following bubbles on the surface of the water.

Observations of the littoral currents produced by normally incident waves showed that the currents were toward the causeway of the island in the reach extending approximately 2000 feet on each side of the island causeway. Plan view photographs Figs. 3.34, 3.35 and 3.38 show that this includes the zone in which the strong Mach intersections occur. Close-up views of such Mach intersections on the beach are seen very clearly in Figs. 3.36, 3.37 and 3.39.

Observations of littoral currents in the model at high tide for the conditions of wave directions near the island of azimuth 200^{o} showed that for high waves there was very little current or a southerly current between points 750 ft. and 1600 ft. north of the island causeway. The current in the reach from 1600 ft. to 2400 ft. north of the causeway alternated in direction. For lower waves this shadow was about the same length but was displaced to the north. The vertical photographs Figs. 3.40 and 3.44 taken for this wave direction and presented herein show that the reaches of slack current occur where the diffracted waves from the two sides of the island intersect. The wave intersections at low tide occur closer to the causeway than they do at high tide or in other words the wave shadow moves southward as the tide stage lowers. This may be seen by comparing the plan view photographs of Figs. 3.40, 3.44 and 3.45 for high tide with Figs. 3.41, 3.46 and 3.49 for low tide. No observations of littoral currents were made for low tide.

The photographs of the model with wave direction at the island site of azimuth 240° are shown in Figs. 3.51 through 3.55. Observations at high tide showed that between points 1000 ft. and 2400 ft. south of the island causeway the littoral currents were to the north and opposite to those on the rest of the beach. The plan view photographs Figs. 3.51 and 3.52 for this wave direction show that the strong Mach intersections occurred in this reach of beach. At low tide the wave intersections on the beach are closer to the causeway than they are at high tide, that is, the intersections move northward as the tide stage lowers. This can be seen by comparing Figs. 3.51 and 3.52 with 3.53.

In summary it can be said that the wave shadow of the island on and near the beach occurred in the region where the waves which diffract around the sides of the island intersect. In this region there was a tendency for the currents to be opposite to the currents on the beach away from the shadow region. Near the ends of the shadow zones the littoral currents tend to alternate in direction. For obliquely incident waves the intersections occur closer to the causeway at low tide than they do at high tide.

5. Wave Heights at Island Causeway

Maximum wave heights at the causeway for high tide were observed in the model with waves obliquely incident on the island. As already explained, these observations were made with a point gage on a tripod. No such observations were made for the normally incident waves. For the condition of normal incidence the highest water surface occurred at the Mach intersection which may be seen in Figs. 3.36, 3.37, and 3.39. Fig. 3.56 is a graph showing maximum water surface elevation along the causeway for high tide with waves approaching the island from azimuth 200°. Fig. 3.57 shows similar data for waves approaching the island from azimuth 240°. As these figures show the water rises to its highest elevation at points about 1700 ft. from the island face and about 1000 ft. from the beach. The highest rise of the water surface was to elevation +18 ft. and occurred with waves with heights in the vicinity of the island of about 21 ft. Since

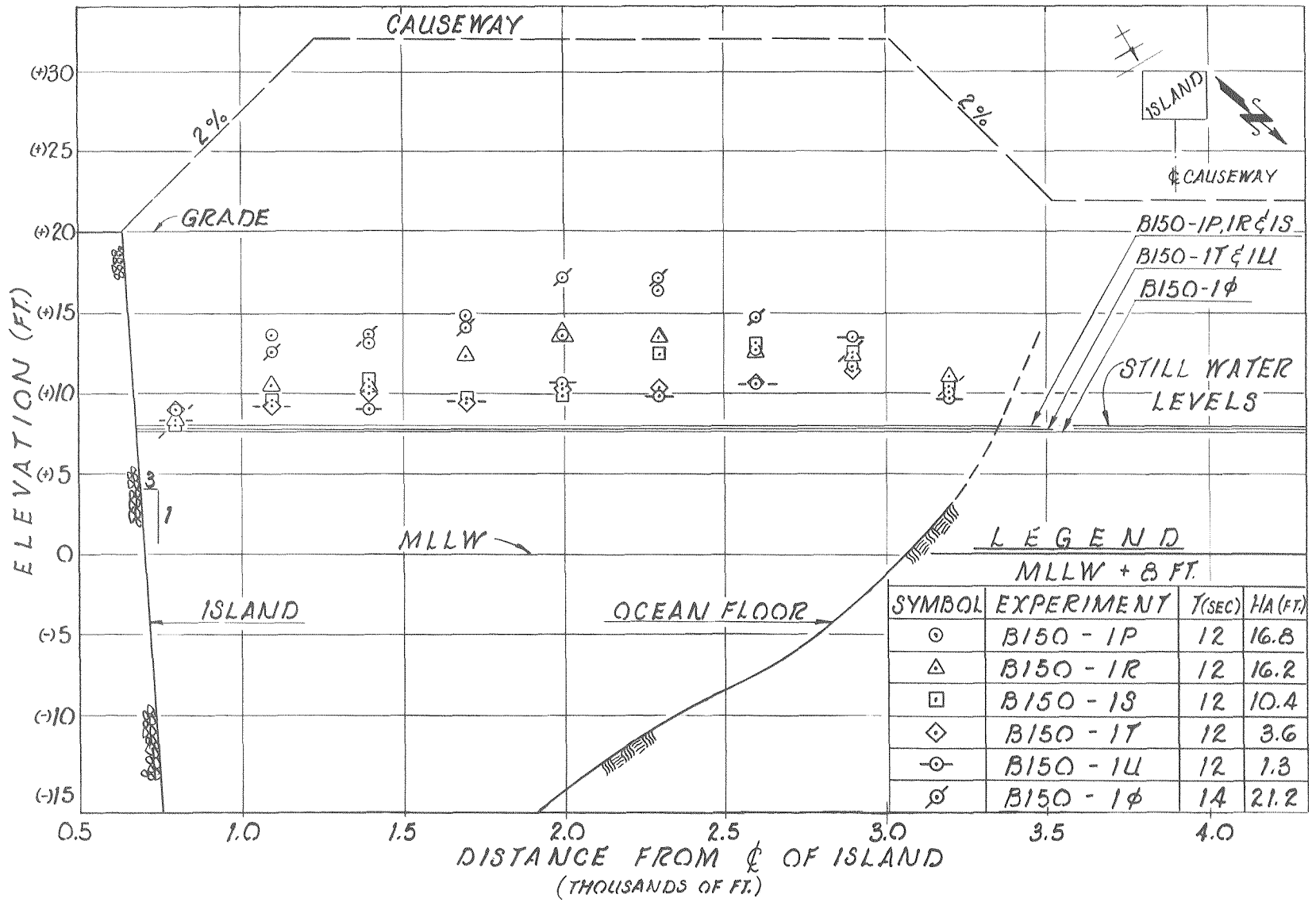

Figure 3.56 Maximum Wave Elevations along Centerline of Causeway, Island Wave Incidence Azimuth 200°
T = 12 sec., 14 sec., MLLW + 8 ft.

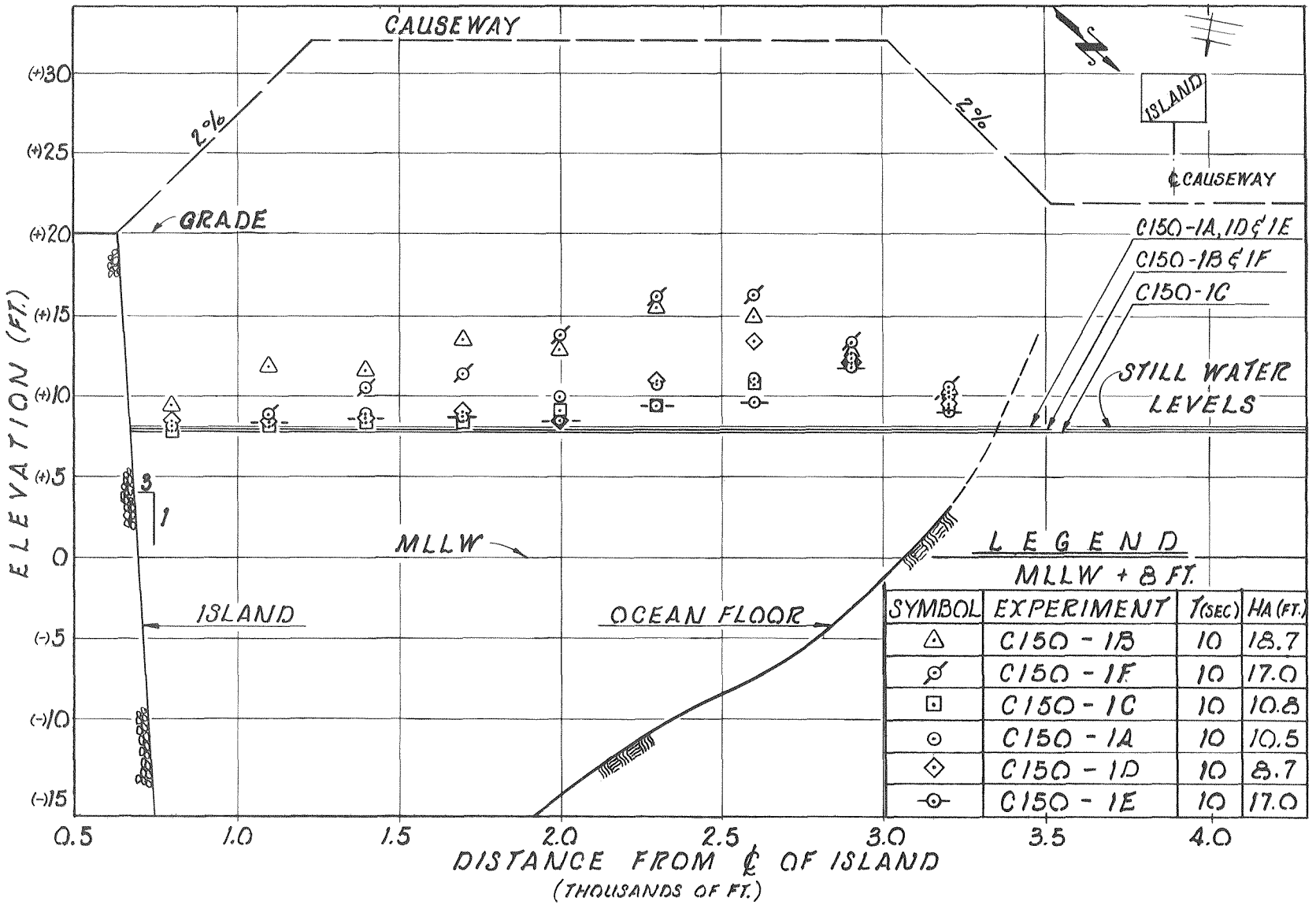

Figure 3.57 Maximum Wave Elevations along Centerline of Causeway, Island Wave Incidence Azimuth 240° T = 10 sec., MLLW +8 ft.

this is about the highest wave that can be produced in the three-dimensional model and since the design wave is 28 ft. high these results do not give the maximum water surface elevation for the design condition. These data can be used as a guide in estimating the water surface elevation for design conditions. However they are probably subject to an appreciable scale effect which reduces their reliability. It is believed that because of scale effect wave heights and hence water surface elevations at the causeway determined from the model are smaller than would actually exist in the prototype.

CHAPTER FOUR

CONCLUSIONS

The following major conclusions may be drawn from this study:

1. The design for the island face resulting from the laboratory studies is shown in Fig. 3.2d. The slope of the face is 3 horizontal to 1 vertical and the crest is at elevation MLLW +40 ft. The armor units consist of 13.8-ton tribars, toe-rock and cap-rock "B", ranging in weight from 2.9 to 7.3 tons and cover rock "C-1" ranging in weight from 0.7 to 2.9 tons. The armor units were stable under the attack of the normally incident design waves and the crest was not overtopped by these waves.
   This design was developed through tests with the 1:45 scale model and is referred to below as the 1:45 scale model.

2. Tribars of 13.8 tons tested in the 1:45 scale model having a continuous slope of 3 horizontal to 1 vertical are considered to be stable. Only slight movement of a very small fraction of the tribars was observed throughout testing.

3. Some movement of the toe rock and the cap-rock was observed in the 1:45 scale model and also in the 1:50 scale model in which the equivalent weight of the rock was the greatest. The rocks used were obviously not as stable as were the tribars. Therefore, in order to obtain uniform stability for the three sections of the wave defense: the toe rock section, the tribar section, and the cap-rock section, the weight of the rock should be increased. The amount of increase in weight of the rock is dependent upon the importance that the design engineer places on eliminating small movements in these rock sections.

4. The region of greatest vulnerability of the island face is at the tribar-cap-rock interface. Good interlocking of the cap-rock and the tribars is extremely important to the stability of the armor units near this interface.

5. The original design, which for the 1:50 scale model had a tribar weight corresponding to 18.9 tons in the prototype was considered to be a stable configuration. However, this design with a crest elevation of +30 ft. experienced significant overtopping for the highest waves produced. For the same composite slope of the island face but with the crest elevation increased to +40 ft. some overtopping was experienced.

6. For the model having a scale of 1:40 and a face of continuous slope of 3 horizontal to 1 vertical the prototype tribar weight of 9.7 tons was found to be unstable. With a crest elevation to +40 ft. overtopping in this structure was eliminated.

7. The maximum run-up observed in the 1:45 scale model was to elevation +39 ft. for the 16-sec. wave, to +35 ft. for the 14-sec. wave, and to +31 ft. for the 12-sec. wave. The 14-sec. wave is considered to be more realistic for a hurricane produced wave system than the 16-sec. wave. Therefore, for the most probable wave a freeboard of 5 ft. exists (19% of the maximum run-up measured).

8. The relative run-up (R/H) was found to be strongly dependent upon the variation of the ratio of wave height to depth (H/d) as well as to the ratio of depth to wave length (d/L).

9. Due to the influence of the structure on the wave system the maximum wave possible in the vicinity of the island is less than that which would be present if the island were not there. The highest waves attained were 24.4 ft. compared to the design wave at MLLW +8 ft. with the island not present.

10. The value of the stability factor, k_D in Hudson's formula, for the condition of incipient failure was found to be approximately 26.2 which confirms the value of 27 recommended in the literature.

11. Within experimental error, the run-up measured in the three-dimensional model on the seaward face of the island for the case of normal wave incidence was usually about 10% less than the run-up measured in the two-dimensional model for comparable wave heights.

12. The maximum run-up observed in the three-dimensional model occurred on the seaward face of the island for the case of normal wave incidence.

13. For the case of oblique wave incidence the maximum run-up was observed to be at the corner first attacked by the waves, and the run-up at this position was comparable to the maximum run-up observed on the seaward face of the island for the case of normally incident waves. In these cases of obliquely incident waves the run-up decreased with distance from this corner of first wave attack; therefore, the average run-up on the seaward face of the island for oblique wave incidence was less than that observed for normal wave incidence.

14. The run-up observed on the shoreward face of the island is of the order of one tenth that observed on the seaward face of the island.

15. The wave shadow of the island on the beach includes the reaches of beach where waves diffracting around the sides of the island intersect.

16. Observations of littoral currents at high tide in the three-dimensional model show that:

    1) for normally incident waves the current is toward the island causeway in the reaches extending approximately 2000 ft. each side of the causeway.

2) For waves which are incident on the seaward face of the island with the azimuth direction of 200 deg. the currents are absent or in the southerly direction and opposite to the general current in the reach lying between approximately 350 and 1600 ft. north of the causeway. In the reach from 1600 to 2400 ft. north of the causeway the currents alternated in direction.

3) For waves which are incident on the seaward face of the island with the azimuth direction of 240 deg. the current is in the northerly direction and opposite to the general current in the reach extending from approximately 1000 to 2400 ft. south of the causeway.

17. Plan view photographs of the three-dimensional model with obliquely incident waves show a tendency for the reaches of reversal in current, that is the wave shadow, to occur closer to the causeway as the tide lowers.

18. The maximum elevations of the water surface at the causeway determined from the model are shown in Figs. 3.56 and 3.57 for obliquely incident waves which are lower than the design wave. Due to scale effects these elevations are thought to be lower than would be experienced in the prototype for the wave height conditions simulated in the model.

ACKNOWLEDGMENTS

The authors wish to acknowledge the invaluable cooperation of the staff of the Bechtel Corporation in carrying out the work at the Azusa Laboratory. Particular acknowledgment is due Everett Spector, who was the Project Test Engineer on the test work and was responsible for the speed with which the study progressed. Lee Erwin was in charge of the modifications of the laboratory facility and the construction of the models. The authors also wish to thank William H. Wilson, Assistant Project Manager, for his hearty support of the work.

During the course of the study a number of personnel of the Bechtel Corporation assisted in both the experimental phases of the study and the reduction of the data. The later phases of the two-dimensional study including photography were conducted by Donald R. Jorgenson. Richard B. Fallgren, James F. O'Sullivan, and Les B. St. Royal participated in various phases of the data reduction. Mas Kosaka and Herbert L. Rogers assisted in various phases of the experiments in the two-dimensional and three-dimensional models. Particular mention should be given to M. Elliott Seymour and Charles J. Dun who participated in the experimental program from its inception, assisting in all phases of the experimental work and the data reduction, and drafting all of the figures presented in this report. Without the enthusiastic cooperation of these people the work could not have been carried out in the short time available, nor would it have been of the high quality that it is.

The cooperation of Omar J. Lillevang, Consulting Engineer, in assisting in the planning of the test program is appreciated. Donald Tuttle of Lillevang's office assisted in the data reduction during a portion of the test program.

Finally, the authors wish to acknowledge the indispensable assistance and cooperation of the staff of the W. M. Keck Laboratory of Hydraulics and Water Resources. Elton F. Daly contributed vitally to the work in designing and constructing special apparatus and coming to the rescue when apparatus broke down. Robert L. Greenway assisted in the construction and maintenance of much of the equipment used. Robert W. Wilson refurbished and maintained a great deal of the electronic equipment. Carl Eastvedt was responsible for the high quality of the photographs shown in this report. Last but not least, particular acknowledgment should be given to Patricia Rankin for her assistance in many of the administrative details involved in this study as well as the final typing of this report.

BIBLIOGRAPHY

1. Palmer, Robert Q., "Component for Rubble-Mound Breakwaters," U. S. Patent No. 2,909,037, 10-20-59, Cl 61-4.

2. Engineering and Economic Feasibility Study,

   Phase III:

   For a Combination Nuclear Power and Desalting Plant, Rep. TID-22330 (Vol. II), Dec. 1965, by Bechtel Corp.

   Appendix B: Wave Defense for an Artificial Island at Sunset Beach, Orange County, California, by Omar J. Lillevang, Consulting Engineer, Oct. 25, 1965.

   Appendix D: Oceanographic Factors Pertinent to the MWD Combined Desalination and Power Plant Feasibility and Site Study by Marine Advisors, Inc., Oct. 1965.

3. Hudson, R. Y., "Design of Tribar and Tetrapod Cover Layers for Rubble-Mound Breakwaters," U. S. Army Corps of Engineers, Waterways Experiment Station, Misc. Paper No. 2-296, Jan. 1959.

4. Hudson, R. Y., "Design of Quarry-Stone Cover Layers for Rubble-Mound Breakwaters," U. S. Army Corps of Engineers, Waterways Experiment Station, Research Report No. 2-2, July 1958.

5. Danel, P., "On the Limiting Clapotis," Gravity Wave Symposium, National Bureau of Standards, Circular 521, November, 1952.